CHEMICAL REVIEWS

pubs.acs.org/CR

Review

Mechanically-Guided 3D Assembly for Architected Flexible Electronics

Published as part of the Chemical Reviews virtual special issue "Wearable Devices".

Renheng Bo,[§] Shiwei Xu,[§] Youzhou Yang,[§] and Yihui Zhang*

Cite This: *Chem. Rev.* 2023, 123, 11137−11189

Read Online

ACCESS | Metrics & More | Article Recommendations

ABSTRACT: Architected flexible electronic devices with rationally designed 3D geometries have found essential applications in biology, medicine, therapeutics, sensing/imaging, energy, robotics, and daily healthcare. Mechanically-guided 3D assembly methods, exploiting mechanics principles of materials and structures to transform planar electronic devices fabricated using mature semiconductor techniques into 3D architected ones, are promising routes to such architected flexible electronic devices. Here, we comprehensively review mechanically-guided 3D assembly methods for architected flexible electronics. Mainstream methods of mechanically-guided 3D assembly are classified and discussed on the basis of their fundamental deformation modes (i.e., rolling, folding, curving, and buckling). Diverse 3D interconnects and device forms are then summarized, which correspond to the two key components of an architected flexible electronic device. Afterward, structure-induced functionalities are highlighted to provide guidelines for function-driven structural designs of flexible electronics, followed by a collective summary of their resulting applications. Finally, conclusions and outlooks are given, covering routes to achieve extreme deformations and dimensions, inverse design methods, and encapsulation strategies of architected 3D flexible electronics, as well as perspectives on future applications.

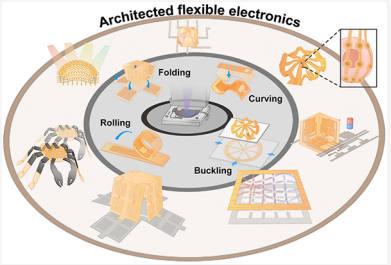

CONTENTS

Received: May 22, 2023
Published: September 7, 2023

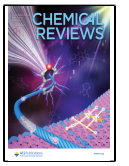

1. INTRODUCTION

The pioneering work on bendable polymer transistors[1] in the 1990s marked the arrival of the stretchable electronics era.[2] Evolving from conventional rigid forms of electronic devices, stretchable electronics represent a new generation of device forms, featuring capabilities of withstanding extreme deformations involving high degrees of stretching, compression, bending, and twisting, while maintaining excellent electrical performances. Over the past two decades, advances in stretchable electronics have drastically transformed the landscape of today's functional devices and led to the current prosperities of the field of flexible and stretchable electronics. Owing to their outstanding deformability, flexible and stretchable electronics have found numerous practical applications, spanning many different aspects of daily life and industry, such as long-term healthcare,[3−5] diagnosis and therapeutics,[6,7] sports protection[8−10] and athletic analysis,[11−13] nondestructive testing of large equipment,[14] robotics,[15−19] cosmetics,[20,21] Internet of things,[22,23] among others. Commercialization of flexible/stretchable electronics is also under way, represented by a series of startups, such as MC10 (Medidata), iRhythm, VitalConnect, Chero, LifeSignals, BioIntelliSense, Sibel Health, c3nano, and Sonica.

The specific terms "stretchable electronics" and "flexible electronics" were gradually nominated over the history. In this review, to avoid confusion, we define "stretchable electronics" as electronics devices that can not only withstand large degrees of bending and twisting but also high levels of stretch. "Flexible electronics" are defined as electronic devices with low bending/twisting rigidities, such that they can bear large degrees of bending and twisting, without specific restrictions on the stretchability. In general, two distinct routes have been exploited to develop flexible and stretchable electronics, including chemical engineering routes[2,24−30] that concentrate to improve electrical performances of organic electronic materials, and structural engineering routes[2,31,32] that focus on creating novel architectures of high-performance inorganic electronic materials to render the flexibility and stretchability. There are plenty of literature reviews[2,32−35] addressing different aspects of stretchable and flexible electronics through both chemical and structural perspectives. Here, this review focuses on flexible/stretchable electronics achieved by means of structural engineering.

Structurally engineered flexible/stretchable electronics were originated from observations of the spontaneous formation of wavy metal thin films on elastomer substrates (i.e., polydimethylsiloxane (PDMS)).[36] The development of stretchable single-crystal Si architectures[31] (i.e., "wavy" Si) pioneered the structural engineering of flexible/stretchable electronics. Early flexible/stretchable electronics were mostly in the forms of wavy architectures and "island-bridge" designs.[37−40] Serpentine designs were later introduced to offer an ultrahigh stretchability, without evidence reduction of the density of functional elements.[41−45] Other structural design concepts, such as kirigami,[46−52] spiral,[53−61] and fractal designs,[62−67] were also proposed to render high levels of stretchability for a limited prescribed space of the structural layout. Based on these design concepts, various planar flexible/stretchable electronic devices were fabricated, achieving applications in diverse areas, such as daily healthcare,[3,11,12,68] robotic machines,[69−75] multifunctional sensors,[73−75] solar cells,[76−78] and biomedical devices.[6,7,79] Despite the significant progress achieved to endow high degrees of stretchability and flexibility in electronic devices, most of these devices are still restricted in planar forms, leaving the gap of geometric shapes and structural functionalities between flexible/stretchable electronics and natural species unfilled. Consequently, it is essential to develop 3D architected flexible electronics that can better conform to complexly shaped biological objects and/or mimic 3D structural forms of natural species to realize more unique functionalities than planar counterparts.

The appearance of 3D forms in flexible electronics naturally conformed to the logic of industrial upgrading, also marked by the establishment of many different 3D manufacturing approaches, including direct ones (e.g., printing techniques,[80−84] photolithographic methods,[85−87] molding[88−90]) and indirect ones (e.g., various mechanically-guided assembly methods[91−107]). Printing and photolithographic methods can form a wide range of 3D structures in almost arbitrary

https://doi.org/10.1021/acs.chemrev.3c00335
Chem. Rev. 2023, 123, 11137−11189

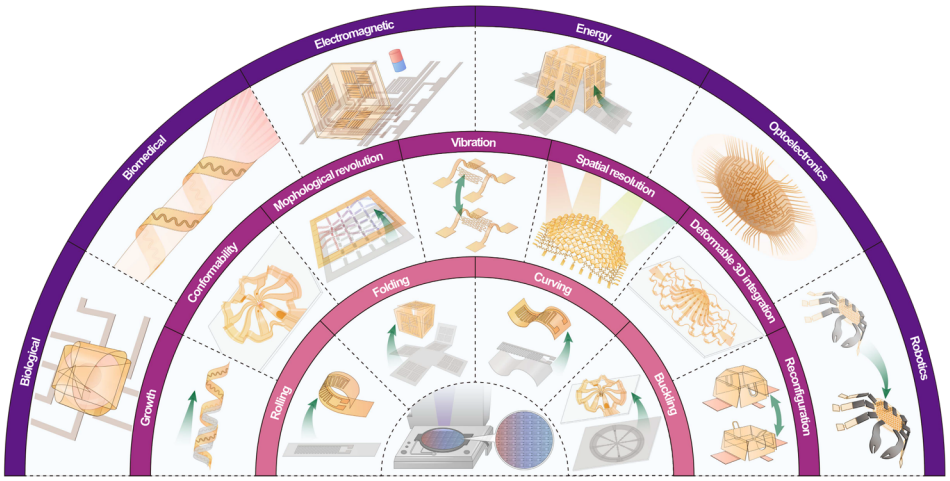

Figure 1. Overview of mechanically-guided 3D assembly methods for architected flexible electronics. Inner circle: mechanically-guided 3D methods (i.e., rolling, folding, curving induced, and bucking-guided assembly approaches) that can transform devices manufactured by mature planar semiconductor techniques into architected 3D structures; Middle circle: a variety of structure-induced functionalities of architected flexible electronics manufactured using mechanically-guided 3D assembly methods; Outer circle: applications of architected flexible electronics spanning biological devices, biomedical devices, electromagnetic devices, energy devices, optoelectronic devices, and robots.

geometrical shapes, with feature dimensions ranging from centimeter scales down to micro- and nanoscales.[83,84,87] However, it is challenging to simultaneously manufacture 3D architectures and integrated circuits using 3D printing and photolithographic methods because they both suffer from limitations of applicable materials (e.g., not applicable to crystalline semiconductors). While molding methods are not restricted to the accessible types of inks, their achievable structures are constrained to dissolvable or meltable polymeric and metallic materials. Additionally, multiple postmolding procedures are often required to fabricate 3D functional devices.[80,88,90] Mechanically-guided 3D assembly methods bypass the difficulties faced by direct manufacturing approaches, through exploiting mechanics principles of materials and structures (e.g., residual stress,[94,108−110] capillary force,[111−114] actuation force,[115−119] compressive buckling,[103,104,120,121] and the rest[119,122,123]) to transform planar electronic devices fabricated using mature semiconductor techniques (Figure 1, central panel) into 3D architected ones. Such indirect manufacturing approaches feature broad applicable materials (including high-performance single-crystal semiconductors),[103] postassembly deformability (e.g., structural multistability and shape morphing),[16,17,123,124] and comparable dimensions with direct ones (i.e., from tens of centimeters down to few hundreds of nanometers).[104,106,107] These characteristics make mechanically-guided assembly a promising route to 3D flexible electronics with a diversity of structure-induced functionalities (Figure 1, third circle), thereby enabling many previously hard-to-achieve applications (Figure 1, outer circle), including single-cell monitoring,[125,126] growing biosensors,[79] 3D conformal electronics for organoid culture,[127,128] photodetectors with spatial resolution, eyeball cameras,[39,101,129,130] electronic fliers,[22,131] robotics with extreme dimensions and multiple locomotion modes,[16,17] among others.[132−135] Although mechanically-guided assembly approaches do not offer the same high-level of geometrical complexity of resulting 3D architectures when comparing to direct manufacturing methods, significant efforts have been devoted to strengthen their assembly capabilities from different perspectives, spanning materials engineering (e.g., growth of heterogeneous materials),[91,92,136,137] structural designs (e.g., precursors designs),[16,103,138] controlled loadings (e.g., magnitudes, directions, applied regions)[116,124,137,139] and so on.

The review provides a comprehensive overview of the field of mechanically-guided 3D assembly for architected flexible electronics. Different from the existing reviews on 3D assembly methods,[35,104−107,140,141] the present review is constructed centering on a unique topic in the field—the structure-induced functionalities. We begin with summarizing existing methods of mechanically-guided 3D assembly based on their distinct deformation modes (Figure 1, second circle) (i.e., rolling, folding, curving, and buckling) (Section 2). Then, the 3D flexible electronic devices are dissected by two different classes of key structural components, and their various geometric forms are discussed separately in Section 3 (for interconnects) and Section 4 (for device forms), followed by their structure-induced functionalities (Section 5). A broad picture presenting diverse applications of 3D flexible electronics is provided in Section 6, covering biological devices, biomedical devices, electromagnetic devices, optoelectronic devices, energy devices, and robotics. Finally, conclusions and perspectives are given in Section 7, addressing current challenges and future directions of mechanically-guided 3D assembly methods and their resulting flexible electronics.

2. MECHANICALLY-GUIDED 3D ASSEMBLY

Mechanically-guided 3D assembly methods exploit controlled mechanical deformations to transform planar electronic devices into 3D ones with various geometric configurations. Based on loading schemes and deformation characteristics, mechanically-guided 3D assembly methods are classified into rolling assembly,[15−17,91−94,108,109,115−119,123,136,137,141−164] folding assembly,[95−98,110−114,122,125,134,165−185] curving-induced assembly,[39,99−102,129,130,135,186−208] and buckling-guided assembly.[16,17,103,104,106,120,121,124,132,138,139,209−244] This section provides an overview of these four assembly approaches, emphasizing their distinct design principles.

https://doi.org/10.1021/acs.chemrev.3c00335
Chem. Rev. 2023, 123, 11137−11189

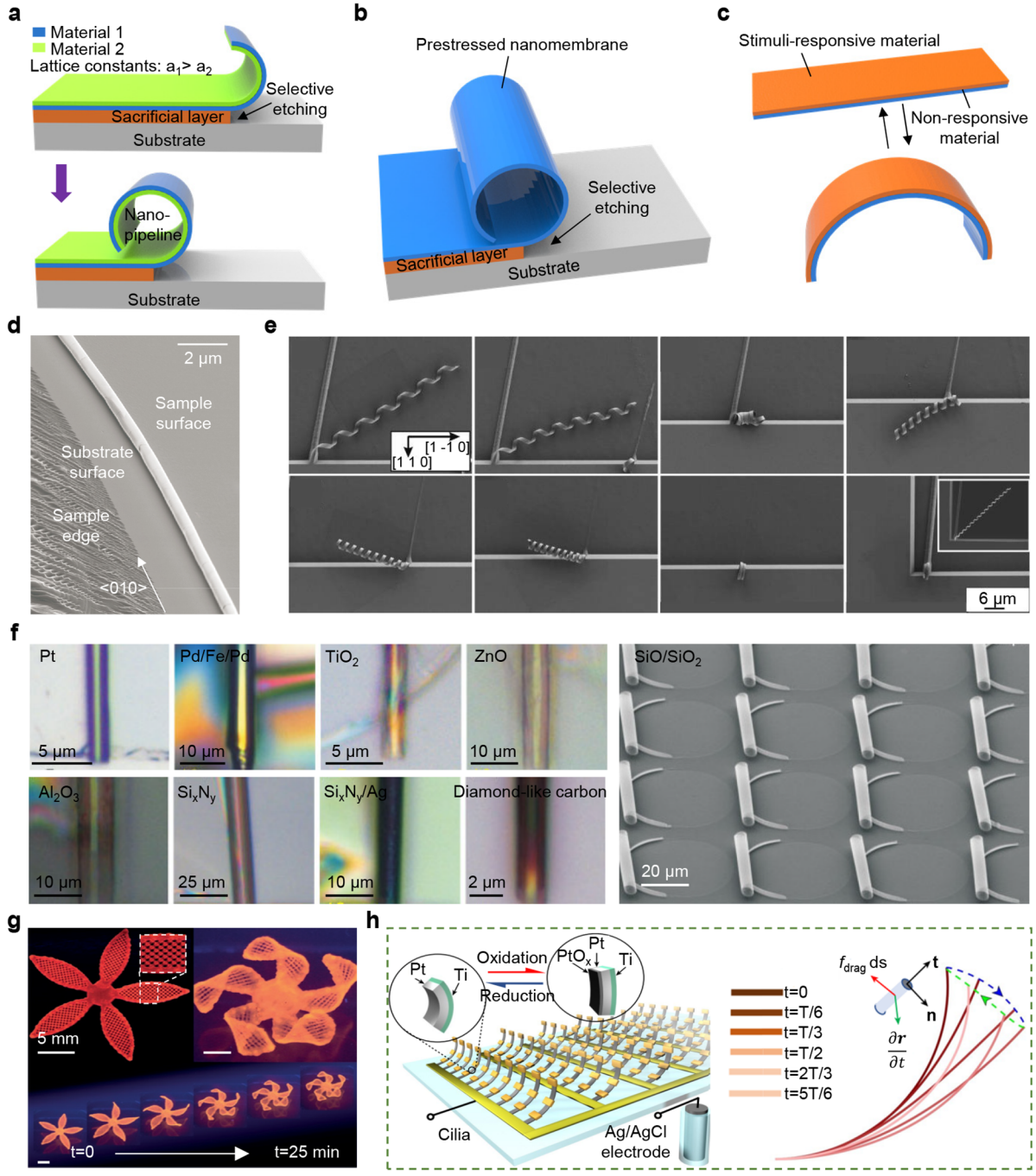

Figure 2. Assembly based on rolling deformations. (a,b) Representative residual stress-induced rolling of heteroepitaxial crystalline bilayers (a) and nonepitaxially deposited nanomembranes (b). (c) Self-actuated rolling through use of stimuli-responsive materials. (d) SEM image of a rolled SiGe nanotube (530 nm in diameter). Reproduced with permission from ref 91. Copyright 2001 Springer Nature. (e) SEM images of rolled SiGe/Si/Cr helices with different widths and orientations. Reproduced with permission from ref 137. Copyright 2006 American Chemical Society. (f) Rolled tubes of heterogeneously layered structures using different materials (i.e., Pt, Pd/Fe/Pd, TiO_2, ZnO, Al_2O_3, Si_xN_y, Si_xN_y/Ag, diamond-like carbon, and SiO/SiO_2). Reproduced with permission from ref 108. Copyright 2008 Wiley. (g) Complex 3D hydrogel "flowers" formed by swelling-induced rolling. Reproduced with permission from ref 115. Copyright 2016 Springer Nature. (h) Artificial cilia formed by residual stress-induced rolling. Reproduced with permission from ref 123. Copyright 2022 Springer Nature.

2.1. Rolling Assembly

Through engineered strain mismatches in heterogeneous structures, rolling assembly approaches typically rely on bending deformations to form 3D architectures, such as tubes, helices, and others. Based on the mechanisms to generate strain mismatches, rolling assembly approaches are divided into two different subfamilies, i.e., residual-stress-induced rolling assembly and responsive-material-induced rolling assembly (Figure 2a−c). In this review, responsive materials denote materials that response to different types of physical (e.g., heating, illumination)[16,17,109,117,118,162,163] and chemical (e.g., redox reactions) stimuli.[119,123,158]

https://doi.org/10.1021/acs.chemrev.3c00335
Chem. Rev. 2023, 123, 11137−11189

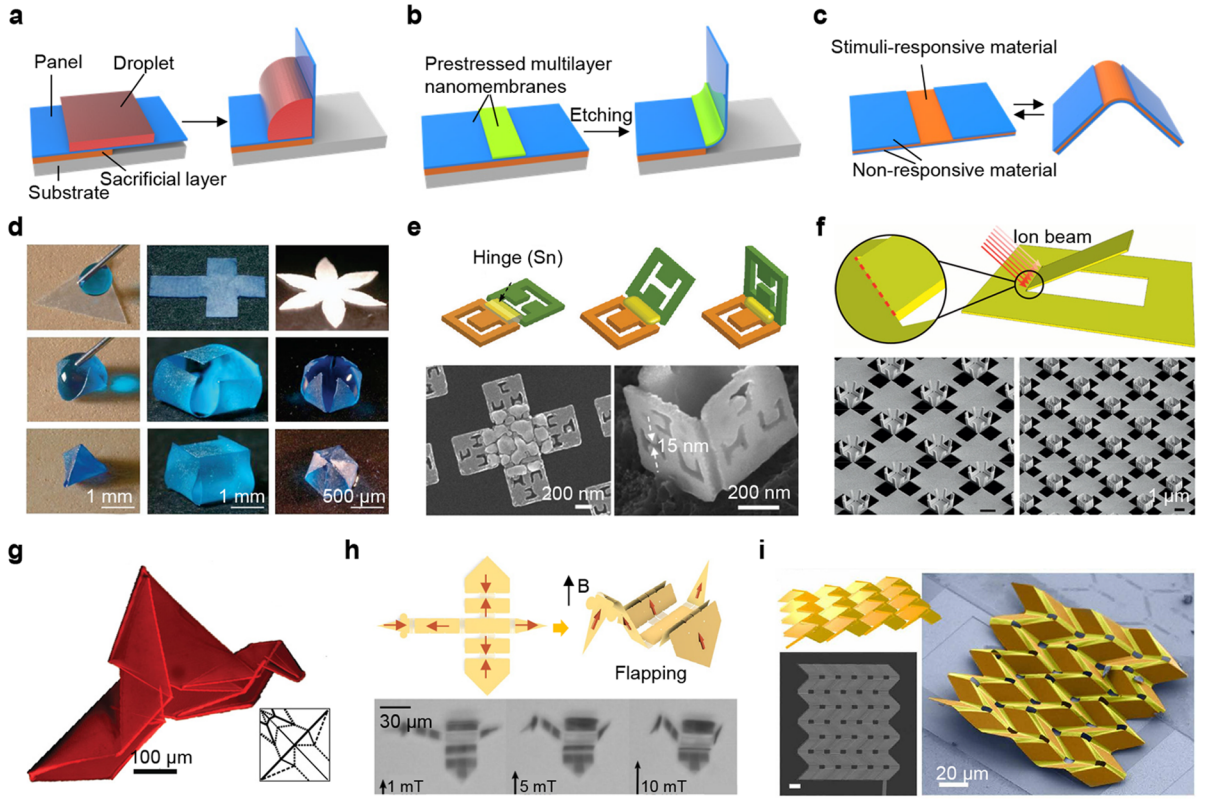

Figure 3. Assembly based on folding deformations. (a–c) Representative folding strategies using capillary forces, residual stresses, and stimuli-responsive materials. (d) Optical images of folded PDMS pyramids, cubes, and quasispheres formed using capillary forces. Reproduced with permission from ref 111. Copyright 2007 Springer AIP Publishing. (e) Folded 3D polyhedral nanostructures by the reflow of Sn within hinges. Reproduced with permission from ref 113. Copyright 2009 American Chemical Society. (f) Folding based on residual stresses introduced during focused ion beam (FIB) irradiation. Reproduced with permission from ref 177. Copyright 2015 Springer Nature. (g) Reversible folding of a multilayered origami structure in hydrogels. Reproduced with permission from ref 178. Copyright 2014 Wiley. (h) Magnetically controlled folding of a flapping "bird". Reproduced with permission from ref 183. Copyright 2019 Springer Nature. (i) Miura-origami microstructure formed through electrochemical actuation. Reproduced with permission from ref 122. Copyright 2021 The American Association for the Advancement of Science.

The residual-stress-induced rolling assembly is typically accomplished through releases of heteroepitaxial crystalline bilayers[91,92,136,137] (Figure 2a), prestressed nonepitaxial nanomembranes[108,162,163] (Figure 2b), and other layered heterogeneous structures.[94] Figure 2a illustrates the rolling of a typical heteroepitaxial bilayer crystalline film (consisting of **materials 1** and **2** with different sets of lattice constants $\mathbf{a}_1$ and $\mathbf{a}_2$) by the use of photoresist as the sacrificial layer. In this case, the residual stress that rolls up the bilayer crystalline film roots in the different stress states (i.e., tension and compression in the different layers) caused by lattice mismatch (i.e., $\mathbf{a}_1 > \mathbf{a}_2$). Figure 2b shows the rolling assembly of a prestressed nonepitaxial nanomembrane through the use of sacrificial layer. Removal of the sacrificial layer releases the prestress and rolls up the nanomembrane. Responsive-material-induced rolling assembly approaches are achieved by rationally creating stress gradients in heterogeneous films composed of stimuli-responsive and nonresponsive materials (Figure 2c).

2.1.1. Residual-Stress-Induced Rolling Assembly. Using lattice mismatch-induced residual stresses, epitaxially grown heterogeneous membrane structures consisting of various crystalline materials can be rolled-up to form 3D tubular or helical structures in high precision.[91,92,137,142] The geometrical parameters of the prepared tubular or helical microstructures (e.g., tube diameter, bending angle, helical pitch, helicity angle and etc.) can be controlled by changing processing parameters (e.g., etching time),[91,92] tuning material properties (e.g., elastic modulus, lattice constants)[136,137] and selecting different geometries of precursors.[137] For example, through controlled release of a SiGe-based (Si/Ge bilayer) heterogeneous thin film (by adjusting the etching time of the sacrificial layer), a nanotube with diameter of 530 nm was formed along the [010] direction (Figure 2d).[91] Harnessing the anisotropic stiffness of a InGaAs/GaAs bilayer, 3D helical structures with engineered pitches were prepared by controlling the angles between the stripes and their crystal orientation (i.e., [100] direction).[144] Parameters (e.g., the orientation angles of planar precursors) that control the helicity angle, chirality, diameter, and pitch of resulting nanohelices were investigated.[142] Figure 2e showcases SiGe/Si/Cr helical nanoribbons with well-defined widths (from 1.30 μm to 0.70 nm) and orientation angles (i.e., between stripes and crystal orientation), which were fabricated using the residual-stress-induced rolling.[137] Through controlled release of sacrificial layers, the rolling assembly can also be accomplished on nonepitaxially grown nanomembranes (e.g., with single or multiple layers).[108,162] For instance, based on rolling assembly approaches, nanotubes with controlled diameters and lengths were prepared using nanomembranes consisting of a variety of functional materials, including Pt, Pd/Fe/Pd, TiO_2, ZnO, Al_2O_3, Si_xN_y, Si_xN_y/Ag, diamond-like carbon, and SiO/SiO_2 (Figure 2f).

https://doi.org/10.1021/acs.chemrev.3c00335
Chem. Rev. 2023, 123, 11137−11189

Additionally, other strategies have also been reported to introduce residual stresses for the rolling assembly. For example, taking advantages of grain coalescence-induced capillary forces,[93] the rolling assembly of tubular and arc-shaped microstructures was realized by melting patterned Sn films on top of the planar precursors. The release of mismatched tensile stresses in layered elastomeric composites was exploited to form arc or helical shapes through rolling.[94] Recently, the engineered plastic strains during peeling processes were harnessed to allow controlled rolling of planar films into various 3D architectures.[164]

2.1.2. Responsive-Material-Induced Rolling Assembly. The second class of rolling assembly approaches mainly leverage engineered stress gradients created by the utility of specific characteristics of various stimuli-responsive materials, such as actuation of smart materials (e.g., hydrogels, liquid crystal elastomers, shape memory polymers/alloys),[109,115−118] varied thermal expansion coefficients,[245] material phase transitions,[119,162,163] among others.[123] Hydrogel-based composites are capable of forming complex 3D configurations (Figure 2g) by swelling-driven rolling assembly.[115] By programming the actuation of thin liquid crystal elastomer (LCE) sheets through ordered alignments of mesogens, complex 3D shapes were demonstrated by rolling assembly.[116] In addition to the above single-step rolling, a two-stage rolling assembly can also be achieved to allow developments of actuators capable of reversible 3D-to-3D deformations. For instance, utilizing U-shaped shape memory alloy (SMA) wires embedded in a bilayer elastomer with an engineered strain mismatch (i.e., one layer is with prestretch, the other is unstretched), 3D structures were fabricated, featuring a fast 3D-to-3D actuation capability.[109,161] Particularly, the predetermined strain mismatch of the two elastomeric layers led to the first rolling assembly stage that formed an arc-shaped initial configuration of the actuator. Harnessing the shape memory effect of the embedded SMA wires, secondary reversible rolling was achieved to generate driving forces. A similar two-stage rolling assembly was also realized, taking advantage of the photothermally induced phase transition of VO_2 nanomembranes.[163] In detail, tubular VO_2 nanomembranes with predefined geometries were first assembled using residual-stress-induced rolling. Then, the photothermally induced phase transition led to the second order of reversible rolling assembly, featuring precisely controlled curvature regulation. An active metasurface composed of artificial cilia (i.e., arc-shaped Pt/Ti bilayer ribbons, Figure 2h)[123] was fabricated following the same sequence of two-stage rolling assembly but enabled by electrochemical redox reactions of Pt/PtO_x.

2.2. Folding Assembly

Folding assembly approaches exploit localized bending deformations to fold planar precursors with predefined creases into various 3D geometries, such as polyhedral or origami structures. The forces that lead to folding can be classified as external forces[111−114,176] (e.g., capillary forces) and internal forces[110,122,167,174,178] (e.g., forces induced by engineered strain mismatch). The external-capillary-force-induced folding relies on the surface tension of liquid materials such as melted metals and droplets to drive the assembly process (Figure 3a). Meanwhile, internal forces can be introduced by using prestressed nanomembranes or responsive materials, as demonstrated in Figure 3b,c. This section reviews folding assembly methods through capillary-force-induced, residual-stress-induced, and responsive-material-induced routes.

2.2.1. Capillary-Force-Induced Folding Assembly. The most straightforward way to leverage capillary forces is by using droplets. For example, pyramids, cubes, and quasi-spheres were formed using PDMS precursors with predesigned triangular, crossing, or flower-like shapes (Figure 3d).[111,112] Particularly, the area reduction of the liquid−air interface via evaporation indicates the consumption of total surface energy of the original droplet. Apart from the dissipated energy (e.g., in forms of heat), the rest of the consumed surface energy transfers to the elastic strain energy of the patterned precursors, allowing the controlled folding of these structures into 3D configurations. Analytical models that capture mechanisms of folding assembly approaches through capillary forces were established.[112,168] Reversible folding assembly routes were later developed to form deformable 3D structures.[176]

In addition to droplets, building meltable hinges using materials with relatively low melting points (e.g., metallic materials such as In and Sn) can also accomplish folding in a well-controlled manner.[113,114] Because of the compatibility with mature planar microfabrication methods, the folding of 3D structures can be implemented at nanoscale. For instance, 3D folding microcontainers capable of chemical encapsulation, guided delivery, and spatially controlled chemical reactions were demonstrated by using melting of the patterned Sn solder hinges.[114] Similarly, Figure 3e demonstrates the folding assembly of stable 3D polyhedral nanostructures driven by the reflow of Sn within the hinges.[113]

2.2.2. Residual-Stress-Induced Folding Assembly. Advanced processing techniques of thin films can accurately confine residual stresses at hinged regions to enable controlled folding deformations. Commonly used approaches for this purpose include ion-beam irradiation,[177,246] as well as heteroepitaxial and nonepitaxial deposition processes.[95,97,98,167]

Focused ion beams (FIBs) can create voids at hinges, and, then, fill them with energized ions to simultaneously release compressive stresses and fold planar structures into many desired 3D configurations (Figure 3f).[177] Through heteroepitaxial thin-film deposition, complex 3D micro-origami structures were demonstrated.[95] In addition, harnessing residual stress during nonepitaxial growth of Cr layer, 3D microgrippers that could be thermally or chemically actuated were fabricated using the folding assembly.[167]

2.2.3. Responsive-Material-Induced Folding Assembly. Folding assembly using responsive materials can form 3D architectures with high levels of geometric complexity. For example, an origami "bird" structure was assembled using trilayer polymer films with different degrees of photo-cross-linking, capable of swelling-induced reversible folding (Figure 3g).[178] Heterogenous layered structures composed of shape memory polymers (SMPs), paper, and resistive circuits, were exploited to form thin film-shaped flexible actuators (TFFAs).[174] Harnessing the folding assembly of these TFFAs, a facile fabrication route to shape-shifting crawling robots with complex 3D configurations was established.[175] By introducing magnetically controlled single-domain nanomagnet arrays in the folding assembly process, an origami "bird" that could flap its wings under an out-of-plane magnetic field was fabricated (Figure 3h).[183] Through the use of residual-stress-induced folding and the introduction of electrochemically responsive Pt/Ti hinges, 3D micro-origami structures capable of reversible

https://doi.org/10.1021/acs.chemrev.3c00335
Chem. Rev. 2023, 123, 11137−11189

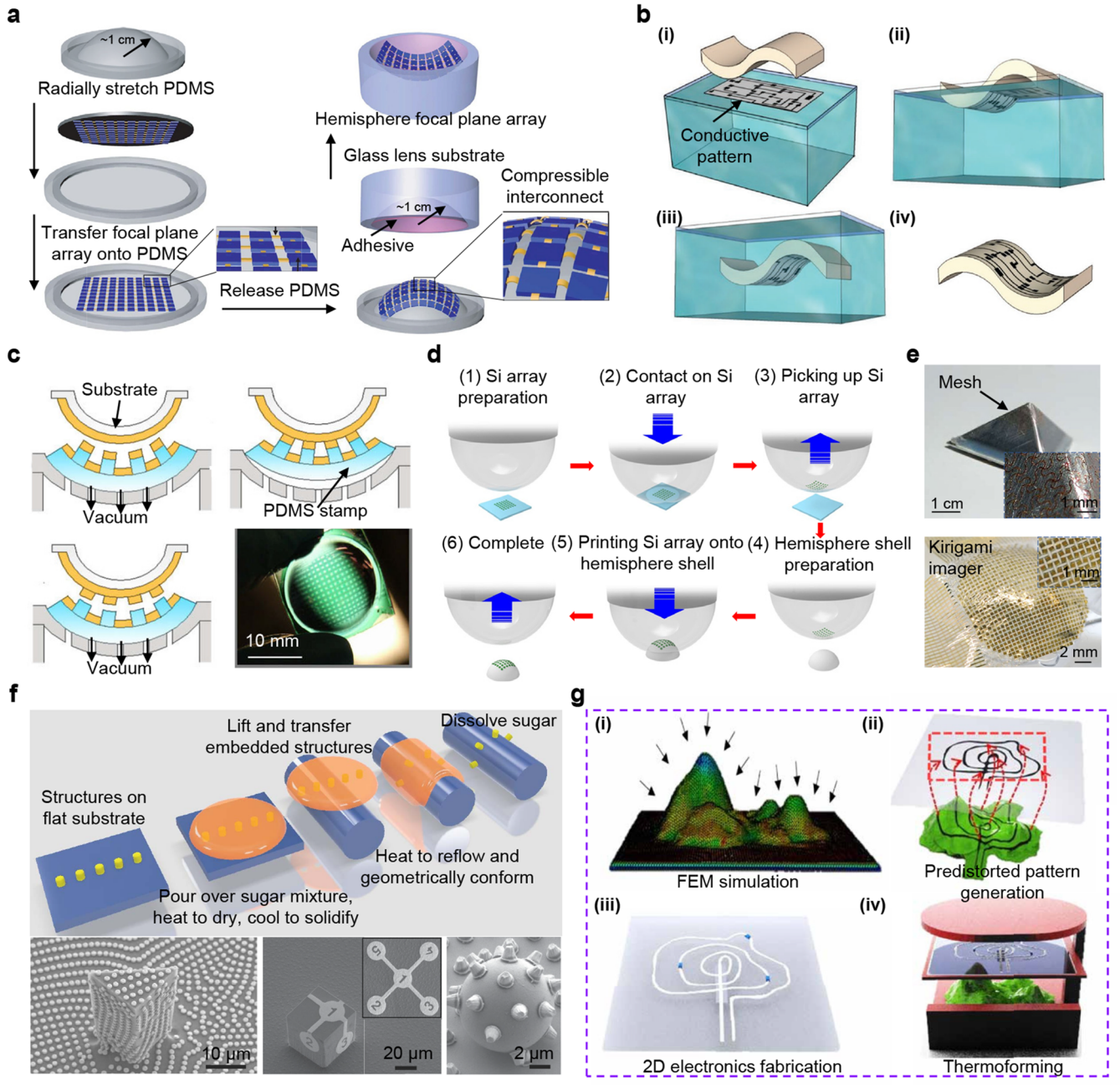

Figure 4. Curving-induced assembly using transfer printing techniques. (a) Assembly of a hemispherical silicon focal array through the use of a biaxial prestretch that flattens the substrate to facilitate the transfer printing. Reproduced with permission from ref 39. Copyright 2008 Springer Nature. (b) Assembly of electrical circuits on wavy substrates via hydro-printing. Reproduced with permission from ref 196. Copyright 2017 Wiley. (c) Vacuum-assisted transfer printing strategy. Reproduced with permission from ref 186. Copyright 2008 Elsevier. (d) Transfer printing using pneumatically inflated elastomeric balloons as conformal stamps. Reproduced with permission from ref 201. Copyright 2019 Springer Nature. (e) Optical images of the serpentine metal mesh on the pyramid surface and the convex-shaped kirigami imager. Reproduced with permission from ref 201. Copyright 2019 Springer Nature. Reproduced with permission from ref 130. Copyright 2021 Springer Nature. (f) Assembly of conformal 3D electronics through thermoforming of a patterned 2D precursor structure. Reproduced with permission from ref 207 under CC BY. Copyright 2021 The American Association for the Advancement of Science. (g) Microscale transfer printing on curved substrates using reflowable stamps. Reproduced with permission from ref 203 under CC BY. Copyright 2022 The American Association for the Advancement of Science.

deformation were prepared and demonstrated as actuators (Figure 3i).[122]

2.3. Curving-Induced Assembly

Curving-induced assembly approaches can allow formation of 3D flexible electronics that conform to arbitrary curvilinear surfaces.[102] Curving-induced assembly relies on various transfer printing techniques to integrate planar electronic devices with complex 3D curved surfaces.[106] This section reviews two typical transfer printing strategies for curving-induced assembly, including planar[39,99] and nonplanar strategies.[195,196,201,205,207,247,248]

2.3.1. Curving-Induced Assembly Based on Planar Transfer Printing. The curving-induced assembly[39] based on planar transfer printing (Figure 4a) involves multiple steps that

https://doi.org/10.1021/acs.chemrev.3c00335
Chem. Rev. 2023, 123, 11137−11189

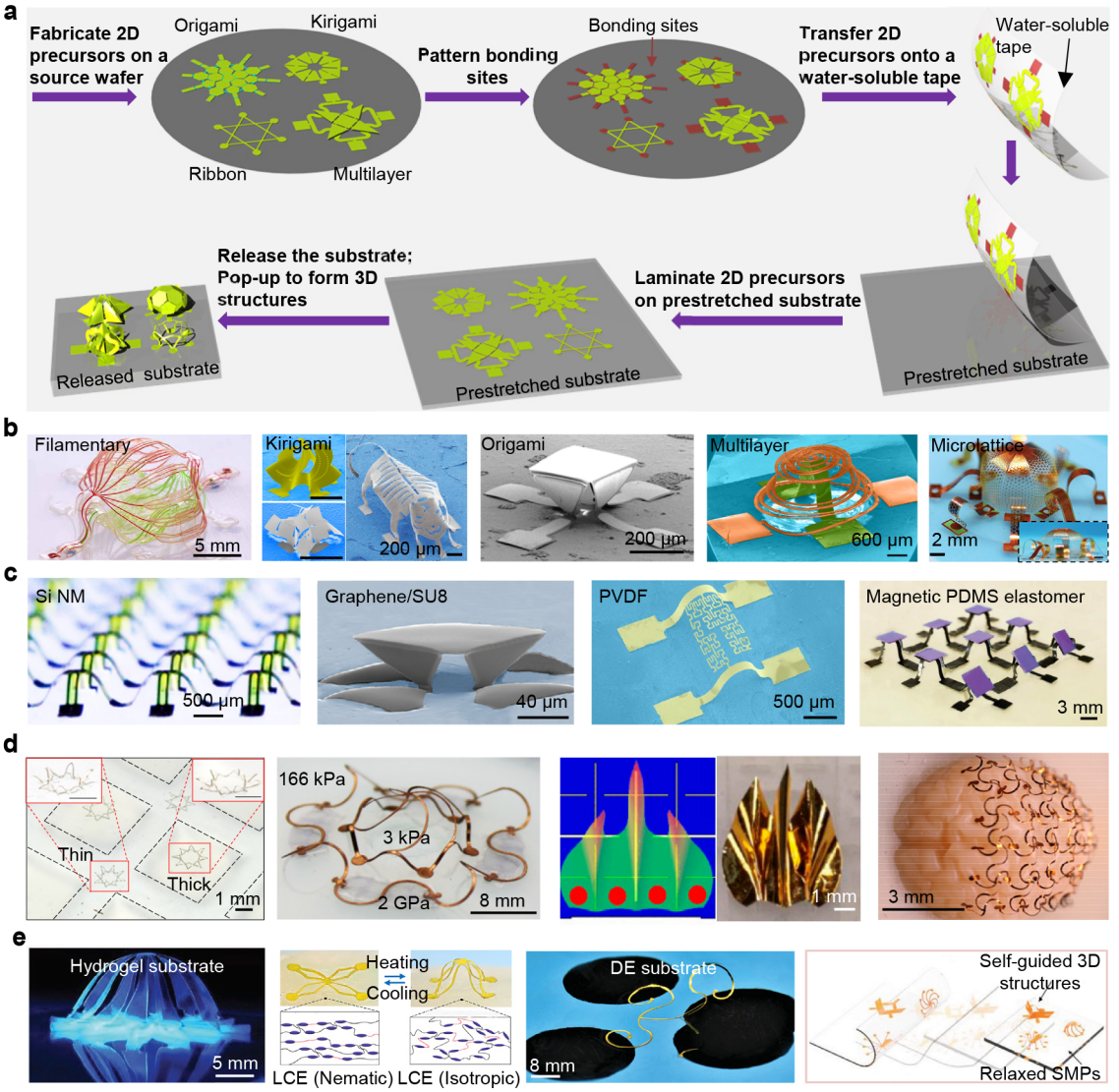

Figure 5. Buckling-guided assembly: schematic illustrations, 2D precursor designs, and substrate designs. (a) Schematic illustrations of the process of buckling-guided assembly. (b) Typical 3D mesostructures formed using various 2D precursor designs (filamentary, kirigami, origami, multilayer, and microlattice designs). Reproduced with permission from ref 236. Copyright 2021 The American Association for the Advancement of Science. Reproduced with permission from ref 120. Copyright 2015 National Academy of Sciences. Reproduced with permission from ref 210. Copyright 2016 Wiley. Reproduced with permission from ref 121 under CC BY. Copyright 2016 The American Association for the Advancement of Science. Reproduced with permission from ref 138. Copyright 2023 The American Association for the Advancement of Science. (c) 3D mesostructures with a diversity of composing materials (e.g., doped silicon, graphene, PVDF and magnetic PDMS elastomer). Reproduced with permission from ref 249. Copyright 2018 American Chemical Society. Reproduced with permission from ref 233. Copyright 2020 Wiley. Reproduced with permission from ref 132. Copyright 2019 Springer Nature. Reproduced with permission from ref 237. Copyright 2021 Wiley. (d) Typical substrate designs used in the buckling-guided assembly, including substrates with engineered thickness/modulus, kirigami substrates, and curved substrates. Reproduced with permission from ref 212. Copyright 2017 Wiley. Reproduced with permission from ref 224. Copyright 2019 American Chemical Society. Reproduced with permission from ref 232. Copyright 2019 National Academy of Sciences. Reproduced with permission from ref 240 under CC BY. Copyright 2022 The American Association for the Advancement of Science. (e) Assembly based on substrates composed of different active materials (e.g., hydrogel, LCE, DE, and SMP). Reproduced with permission from ref 230. Copyright 2019 Wiley. Reproduced with permission from ref 234. Copyright 2021 American Chemical Society. Reproduced with permission from ref 225. Copyright 2019 Oxford University Press. Reproduced with permission from ref 226. Copyright 2019 Wiley.

include: (i) fabrication of a 3D intermediate elastomer substrate (i.e., hemispherical PDMS substrate) and the planar device (i.e., focal array); (ii) flattening the as-prepared 3D intermediate substrate followed by the transfer printing of the as-fabricated device onto the flattened substrate; and (iii) relaxation of the substrate followed by the transfer printing of the curved device from substrate to the target curved surface. Electronic devices that conform to complex curved surfaces, such as golf balls, pyramidal substrates, convex paraboloid substrates, and even human heart models were prepared through this type of curving-induced assembly.[99]

2.3.2. Curving-Induced Assembly Based on Nonplanar Transfer Printing. Various nonplanar transfer printing techniques, such as hydroprinting,[195,196] vacuum-assisted transfer printing,[186] transfer printing using specifically architected 3D flexible stamps[190,201] (e.g., hierarchical stamps and pneumati-

https://doi.org/10.1021/acs.chemrev.3c00335
Chem. Rev. 2023, 123, 11137−11189

cally inflatable balloon stamps) have been developed to enable curving-induced assembly. These techniques feature the direct formation of conformable electronics on complex curved 3D substrates.

Hydroprinting (Figure 4b (i–iv)) contains four steps: (i) printing patterned electrical circuits on a water-soluble substrate, dissolving the substrate to release the circuits, and floating them on the air–water interface; (ii) letting the curved target substrate approach the floating circuits on the interface; (iii) immersing the target substrate to form strong conformal contact with flexible electronic circuits; and (iv) flipping and drying the substrate with integrated circuits.[196] Vacuum-assisted transfer printing (Figure 4c) leverages low rigidities of PDMS stamps to form conformal contact with the target substrate.[186] Hierarchical perfluoropolyether stamps capable of adaptive deformations were adopted to allow curving-induced assembly of 3D conformal electronic devices on curved substrate with micropatterns.[190] By the use of a pneumatically inflated elastomeric balloon as a conformal stamp for both pickup and delivery (Figure 4d), nonplanar transfer printing of flexible electrical circuits can also be accomplished.[201] The high level of deformability of the above balloon stamp allows the assembly of flexible electronics on many complex 3D surfaces, such as the pyramid surface shown in the top panel of Figure 4e.[201] The concept of kirigami was also introduced to improve the conformability of planar electronic circuits to nondevelopable curvy surfaces.[130,206,208] For example, an array of ultrathin silicon optoelectronic pixels with kirigami design was formed on a spherical cap by curving-induced assembly (Figure 4e, bottom panel).[130] Recently, a microscale transfer printing approach (Figure 4f) was developed using reflowable materials (e.g., sugar mixture) that can stretch to conform to surfaces with complex topographies and small curvature radii.[207] Apart from the above, nonplanar direct printing method harnessing thermosplasticity was employed to assemble liquid metal circuits on irregular 3D surfaces (Figure 4g).[203]

In summary, the curving assembly methods based on nonplanar transfer printing are more straightforward and effective, when compared to those via planar transfer printing techniques. However, the accurate positioning and alignment of electronic components with respect to the target substrates often stand as technical issues hindering their widespread practical applications, especially on small scales. In particular, the hydroprinting technique features fast and low-cost manufacturing, but the process can be completed only under aqueous environments. The nonplanar transfer printing through the use of elastomeric stamps (e.g., PDMS) stands as the most common and facile method. However, the limited deformability of bulky stamps hinders their application in the fabrication of electronic devices on surfaces with large curvatures as well as the preparation of devices consisting of fragile elements. When comparing with bulky stamps, the flexible balloon stamps present better deformability, which can be utilized to prepare electronic devices on surfaces with complex curvatures. Transfer printing techniques taking advantages of reflowable materials are capable of fabrication of micro- to nanoscale devices on curved complex surfaces. However, the underlying mechanisms of the associated interface mechanics (e.g., adhesion and delamination) need to be better understood. The nonplanar transfer printing based on thermoplasticity features low-cost, rapid fabrication. However, due to the requirement of the heating process, it might not be ideal for the manufacturing of electronic devices consisting of temperature sensitive elements.

2.4. Buckling-Guided Assembly

Buckling-guided assembly approaches[103,106] are usually accomplished by sequential processes that include (i) design and preparation of 2D precursors with predefined geometries, (ii) selective bonding (e.g., typically covalent bonding) of 2D precursors onto a prestrained elastomer substrate with controlled loading magnitudes, and (iii) release the prestrain of the substrate to finish the assembly. The detailed schematic illustrations of an exemplary buckling-guided assembly procedure are shown in Figure 5a. Buckling-guided assembly methods allow access to a wide range of complex 3D geometries with dimensions from tens of centimeters down to a few hundreds of nanometers. The excellent compatibility with well-established planar manufacturing techniques endows the applicability to a broad family of functional materials, spanning both organic and inorganic materials, such as polymers (e.g., polyimide (PI), PDMS, SU-8, polyvinylidene fluoride (PVDF), SMP and etc.), metals (e.g., Cu, Au, Ag, SMA and etc.), semiconductors (e.g., Si, Ge, GaAs), ceramics (e.g., lead zirconium titanate (PZT)) and other electronic materials (e.g., graphene, carbon nanotube (CN) and etc.). This section reviews buckling-guided assembly approaches from perspectives that control such a process, including 2D precursor designs, substrate designs, loading-path-based strategies, schemes for interface control, and strategies for freestanding 3D mesostructures.

2.4.1. 2D Precursor Designs. Various 2D precursor designs, involving filamentary,[103,209,223,236] kirigami,[120] origami,[210,213] multilayer,[121] and microlattice designs,[138] were developed to enable formation of 3D architectures with high degrees of complexities and diversities (Figure 5b). Filamentary designs (Figure 5b, filamentary)[236] typically consist of slender thin ribbons to ensure that large out-of-plane bending and twisting deformations can be induced to realize their transformation into desired 3D configurations such as helices[209] and frameworks.[223] Kirigami designs (Figure 5b, kirigami) feature the reduction of stress concentration during buckling-guided assembly by introducing strategic cuts, thereby enabling access to diverse 3D membrane mesostructures (e.g., bionic "tiger").[120] Origami designs (Figure 5b, origami) usually harness engineered folding creases in 2D precursors to form various 3D mesostructures by buckling-guided assembly.[210] Multilayer designs are realized by the use of patterned 2D precursors with predefined multilayer layouts, rendering densely distributed complex 3D multilayer configurations (Figure 5b, multilayer).[121] Recently, inspired by cellular biological surfaces, a rational microlattice design strategy was developed as a powerful route to achieve desired stiffness distribution of 2D microfilms, thereby allowing their transformation into programmable 3D curved mesosurfaces through the buckling-guided assembly.[138] A wide range of materials were incorporated with the above divergent 2D precursor designs, enabling the manufacturing of many different architected multifunctional flexible electronic devices (Figure 5c).[132,233,237,249]

2.4.2. Substrate Designs. Various substrate design strategies, including substrates with engineered thickness[212]/modulus,[224] kirigami designs,[232] substrates with curved 3D configurations (i.e., for ordered buckling-guided assembly)[240] and hierarchical designs,[241] are devised to enable different forms of forces applied to the 2D precursor, thereby enriching the family of accessible 3D architectures through the buckling-guided assembly. Using substrates with engineered distributions of stiffness (e.g., Figure 5d, first and second column, by changing

https://doi.org/10.1021/acs.chemrev.3c00335
Chem. Rev. 2023, 123, 11137–11189

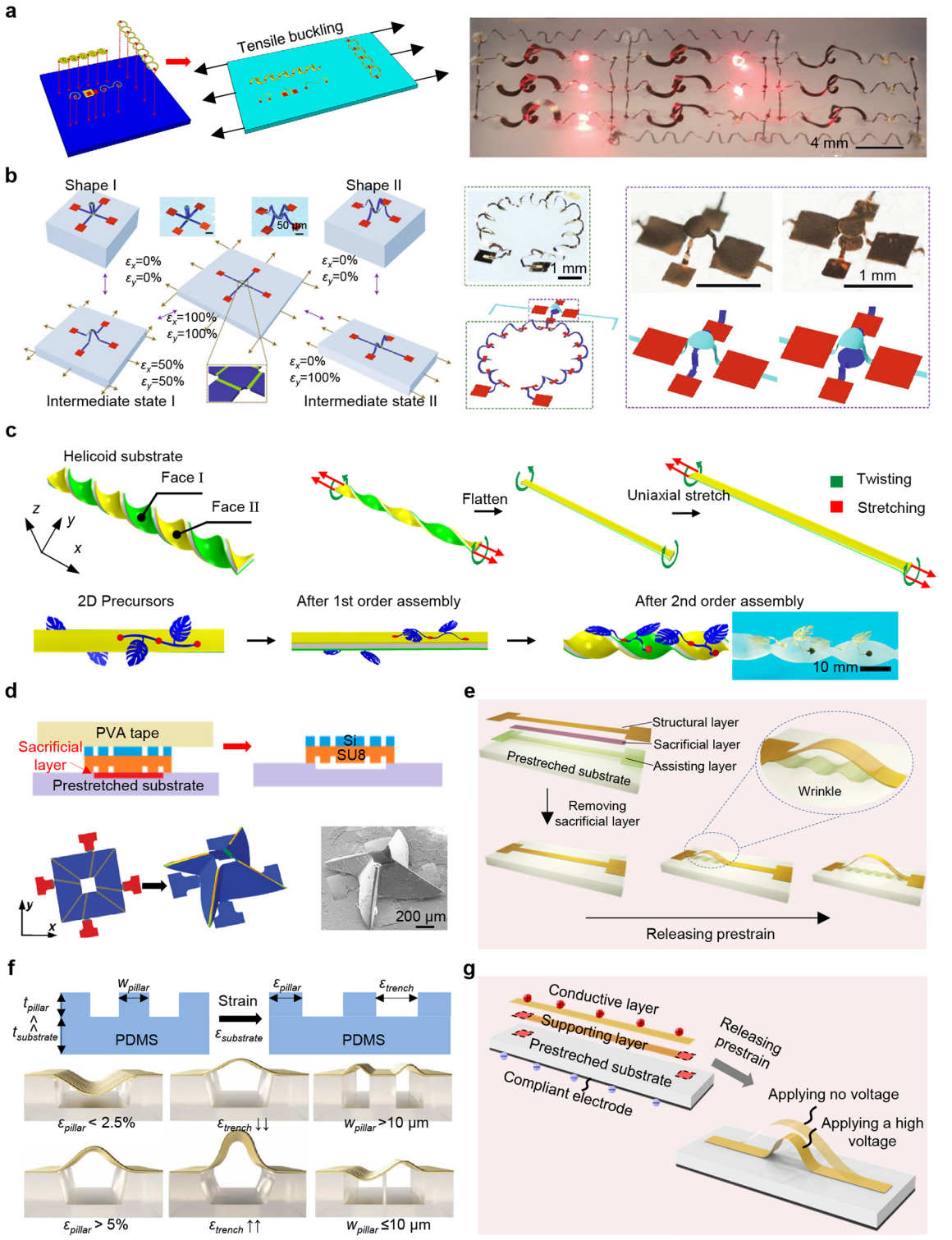

Figure 6. Buckling-guided assembly: loading-path-based strategies and schemes for interface control. (a) Tensile buckling strategy for the assembly of stretchable LED arrays. Reproduced with permission from ref 216. Copyright 2018 Springer Nature. (b) Loading-path controlled strategy for the assembly of bistable 3D mesostructures and radiofrequency (RF) circuits. Reproduced with permission from ref 124. Copyright 2018 Springer Nature. (c) Ordered assembly process of 3D leaf-like structures on a helicoidal substrate with FEA predictions and an optical image. Reproduced with permission from ref 240 under CC BY. Copyright 2022 The American Association for the Advancement of Science. (d) Interface weakening through use of sacrificial layers. Reproduced with permission from ref 210. Copyright 2016 Wiley. (e) Wrinkling-assisted strategy for controlled interface delamination. Reproduced with permission from ref 244. Copyright 2023 Elsevier. (f) Interface control through use of elastomer substrates with microstructured surfaces. Reproduced with permission from ref 242 under CC BY. Copyright 2023 Springer Nature. (g) Electroadhesion-mediated strategy for controlled interface adhesion. Reproduced with permission from ref 243. Copyright 2023 ASME INTERNATIONAL.

https://doi.org/10.1021/acs.chemrev.3c00335
Chem. Rev. 2023, 123, 11137−11189

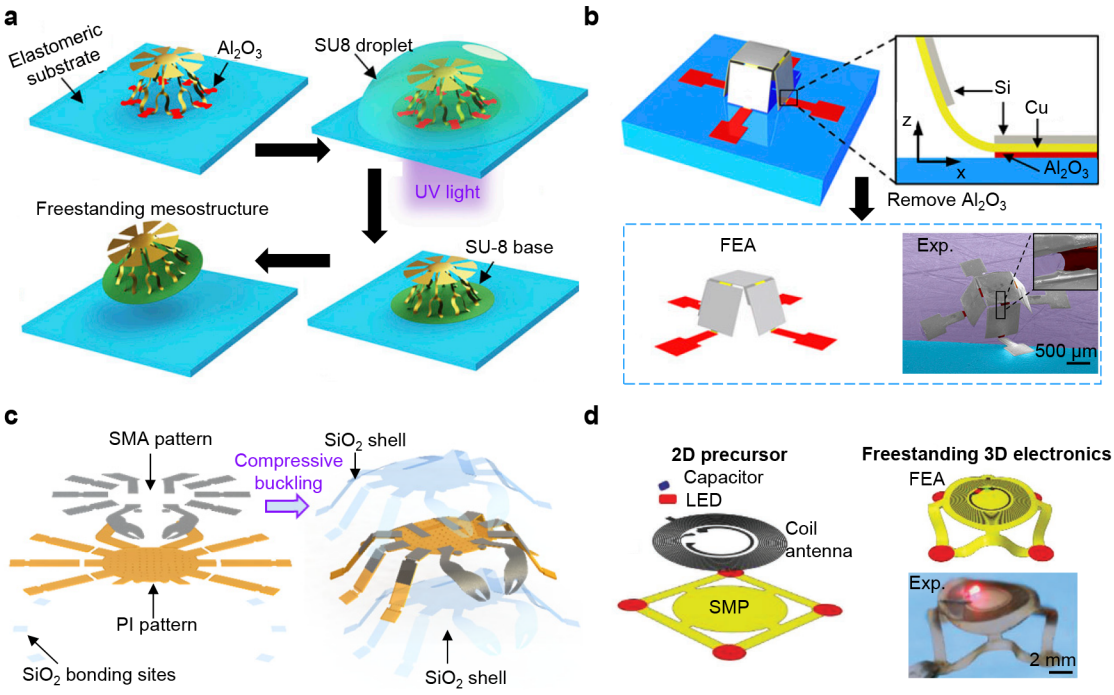

Figure 7. Buckling-guided assembly: strategies for freestanding 3D mesostructures. (a) Process of forming freestanding 3D mesostructures by the use of the SU-8 base. Reproduced with permission from ref 214 under CC BY. Copyright 2017 National Academy of Sciences. (b) 3D shape fixation enabled by controlled plasticity of the metal layer. Reproduced with permission from ref 214 under CC BY. Copyright 2017 National Academy of Sciences. (c) Peekytoe crab-like freestanding 3D mesostructure formed by introducing a conformal SiO_2 shell after the assembly. Reproduced with permission from ref 17. Copyright 2022 The American Association for the Advancement of Science. (d) SMP-based freestanding 3D electronic devices. Reproduced with permission from ref 228. Copyright 2018 Wiley.

thickness[212] and modulus,[224] respectively), varied compressive strains are applied to different local regions of the 2D precursor. As such, the spatially varying 2D-to-3D transformation can be realized, leading to the formation of 3D mesostructures with a desired gradient of the height (i.e., the dimension along the out-of-plane direction). Substrates with kirigami designs allow large rotational motions, thus, enabling additional local twisting deformations of 2D precursor structures (Figure 5d, third column).[232] By the use of substrates with curved 3D configurations, an ordered buckling-guided assembly can be accomplished, allowing transformation of 2D precursors into sophisticated 3D structures on diverse curved surfaces, such as the microscale helical networks assembled on a brain-like surface (Figure 5d, rightmost).[240] The hierarchical design strategy of the substrate renders the buckling-guided assembly of not only the 2D precursors but also the secondary layer of the substrate during the same process, allowing the creation of 3D mesostructures mounted at multiple-level 3D frameworks with complex configurations.[241]

Additionally, the use of responsive materials in the substrate allows more flexible loading forms for the buckling-guided assembly, when comparing to substrates consisting of conventional elastomeric materials (Figure 5e).[234] For example, the use of thermally responsive hydrogels[230] or LCEs[234,235] can enable thermal-mechanically controlled buckling-guided assembly in a reversible manner. Dielectric elastomers were also used as substrates for electro-mechanically controlled buckling-guided assembly, achieving sequential and local loading with desired strain distributions.[225] Furthermore, by the use of SMP substrates, the buckling-guided assembly can be exploited to form 3D structures with certain level of reconfigurability.[226]

2.4.3. Loading-Path-Based Strategies. By controlling loading paths and forms, the deformation modes of patterned 2D precursors can be enriched during the buckling-guided assembly to enhance the geometric diversity of the resulting 3D architectures. As an example, the tensile loading simplifies the process of buckling-guided assembly, and extends the accessible range of 3D topologies by avoiding the prestretch of elastomeric substrates (Figure 6a, flexible LED array assembled by tensile buckling).[216] By selecting the time sequences or release path of biaxial prestrain in the substrate, specially engineered 2D precursors can be assembled into different stable 3D configurations, thereby allowing the formation of reconfigurable 3D mesostructures.[124,139,250] For instance, as shown in Figure 6b (left), the simultaneous release of equal 100% biaxial strain results in a "pop-up" structure of Shape I, while the sequential release of biaxial strain (i.e., first release the prestrain in *x*-axis, followed by the *y*-axis) reshapes the 2D cross-ribbon structure into a "pop-down" structure of Shape II.[124] Based on this concept, many reconfigurable flexible devices, such as 3D radiofrequency (RF) circuits, can be formed by the buckling-guided assembly (Figure 6b (right)). Taking advantages of such sequential and directional control of loading paths, a bottom-up design route to geometrically reconfigurable 3D mesostructures was established using ribbon-formed components as building blocks.[139] Furthermore, by buckling-guided assembly with ordered loading paths, various 3D mesostructures are formed on complex curved surfaces. Taking the ordered loading[240] using helicoid substrates as an example (Figure 6c), the substrate was first flattened by applying torsional loadings (720°), followed by an additional uniaxial prestretch (20%). After selective bonding of the 2D precursor, release of the prestretch (20% uniaxial prestrech) enabled the first-order assembly of leaf-

https://doi.org/10.1021/acs.chemrev.3c00335
Chem. Rev. 2023, 123, 11137−11189

Table 1. Comparison of Four Main Types of Mechanically-Guided 3D Assembly Methods

Assembly methods	Typical geometries	Achievable minimum scales	Reversibility	Reference
Rolling assembly	Tubes, helices, etc.	Sub-10 nm	Irreversible/reversible	91, 136, 156, 162, 163
Folding assembly	Polyhedron, origami forms, etc.	Hundreds of nanometers	Irreversible/reversible	112, 114, 122, 171
Curving-induced assembly	Curvilinear forms	Tens of micrometers	Irreversible	39, 99, 102, 130, 207
Buckling-guided assembly	A wide range of complex 3D geometries	A few micrometers	Reversible	103, 104, 106, 221, 242

like 3D structures on both sides of the flattened substrate, and further release of the torsion allowed transformation of the substrate into the helicoid surface, resulting in the spatial rearrangement of two leaf-like 3D structures during the second-order assembly.

2.4.4. Schemes for Interface Control. The buckling-guided assembly approach requires simultaneous and selective formations of weak interfaces that ensure full delamination of desired parts of precursors and strong interfaces that firmly bond the selective sites of precursor on the substrate (i.e., bonding sites).[222] At the macroscale, the structural stiffnesses of 2D precursors are usually sufficient to drive the delamination during buckling-guided assembly, and therefore, the interface control strategies are focused on building strong interfaces that bond the precursor with the substrate. Differently, at the micro- to nanoscale, the unavoidable influences by van der Waals forces and drastically reduced structural stiffnesses make the delamination very difficult. In this case, engineered weak interfaces are necessary to ensure a successful assembly process.

Strategies relying on the use of sacrificial layers to create gaps between 2D precursors and substrates are promising to build weak interfaces, rendering the successful assembly of an origami structure (i.e., with relatively large surface contact) by the buckling-guided approach (Figure 6d).[210] In addition, the use of assisting layers to introduce initial disturbance to the buckling-guided assembly can also effectively facilitate the delamination of precursors.[132,244] For instance, a patterned PI ribbon was adopted as an underlying supporting layer for the assembly of thin PVDF structures with ultralow stiffnesses (e.g., serpentines).[132] Recently, a wrinkling-assisted interface control strategy was developed to evidently facilitate the delamination at desired regions of the film/substrate system.[244] In particular, an additional assisting layer was exploited such that the original film−substrate interface was replaced by a weaker film-assisting-layer interface, and the formed wrinkles in the assisting layer induce additional driving forces to separate the film-assisting-layer interface (Figure 6e). Besides, the microtexturing of substrate surfaces is found effective to control the interface during the buckling-guided assembly.[231,242] As shown in Figure 6f, by the use of substrates with patterned voids, the direction (i.e., pop-up and pop-down), magnitude, and mode of buckling deformations can be accurately controlled by varying the pillar strain (ε_{pillar}), trench strain (ε_{trench}), and boundary constraints (W_{pillar}).[242]

Apart from creating weak interfaces to facilitate delamination, building strong interfaces in a controlled manner was also explored to enrich the obtainable 3D architectures through buckling-guided assembly. For example, the electroadhesion-mediated strategy was developed to achieve controlled adhesion by varying the applied voltages during the buckling-guided assembly, giving rise to various reconfigurable 3D mesostructures (Figure 6g).[243]

2.4.5. Strategies for Freestanding 3D Mesostructures. Based on the buckling-guided assembly, several approaches have been proposed to achieve freestanding 3D mesostructures after separation from the substrate, including the use of photo-cross-linkable bases,[214] introducing plastic deformations,[213,239] creating portable mechanical constraints,[17,138,227] and exploiting materials with shape memory effects.[228,235] For example, by drop casting of SU-8 and photo-cross-linking from the backside, a freestanding 3D mesostructure with a very thin SU-8 base of a similar size can be prepared (Figure 7a).[214] Plastic deformations of metallic[213,214] and thermoplastic materials[239] were also employed to maintain the assembled 3D configurations. For example, the plastic deformations of the copper layer were utilized to maintain the 3D configuration of a cubic structure after the release from the substrate, as shown in Figure 7b.[214] In addition, mechanical constraints were also utilized to fix the assembled 3D configurations after removing the substrate, such as building mechanical interlocks[227] (e.g., elements composed of lugs and hooks) or creating stiffer conformal encapsulating shells[17] (e.g., SiO_2 in Figure 7c). Furthermore, materials with shape memory effects, such as SMPs[228] and LCEs,[234,235] can also be exploited to fix the as-assembled configurations and form freestanding 3D mesostructures, as demonstrated in Figure 7d.

By means of rolling assembly, folding assembly, curving-induced assembly, and buckling-guided assembly, 3D architectures with numerous geometric configurations, such as tubular, helical, polyhedral, origami, hemispherical, irregularly curved, and complex forms, can be manufactured using various functional materials ranging from polymers, metals, high-performance single-crystal semiconductors, to 2D materials and other electronic materials. A detailed comparison table (Table 1) is presented, summarizing typical geometries, achievable scales and reversibility of the four main mechanically-guided assembly methods. In particular, rolling assembly methods are usually exploited to prepare tubular or helical 3D configurations, with the accessible curvature radius down to sub-10 nm.[136] The rolling process can be either reversible or irreversible, depending on the applied mechanisms/materials (e.g., the use of hydrogels, LCEs, and other stimuli-responsive materials could result in reversible rolling). The typical geometries achievable by the use of folding assembly methods include polyhedron and other origami forms, and the minimum structural dimension of such folded configurations (i.e., in the range of hundreds of nanometers[114]) is slightly higher than the rolled ones, due to their higher levels of structural complexities. Curving-induced assembly usually requires the use of predesigned substrates to provide a base for the deformable device precursor to form desired 3D configurations through various transfer printing techniques, and its minimum achievable structural dimension could be tens of micrometers.[207] The buckling-guided assembly methods require the use of elastomer substrates to transform planar device precursors with well-designed geometries into a broad family of complex 3D configurations. Such methods are highly scalable, and can be exploited to fabricate 3D architected devices ranging from submicrometers to tens of centimeters.[221,242] To summarize, these mechanically-guided assembly methods have clearly outlined the routes to the constructions of architected flexible

https://doi.org/10.1021/acs.chemrev.3c00335
Chem. Rev. 2023, 123, 11137−11189

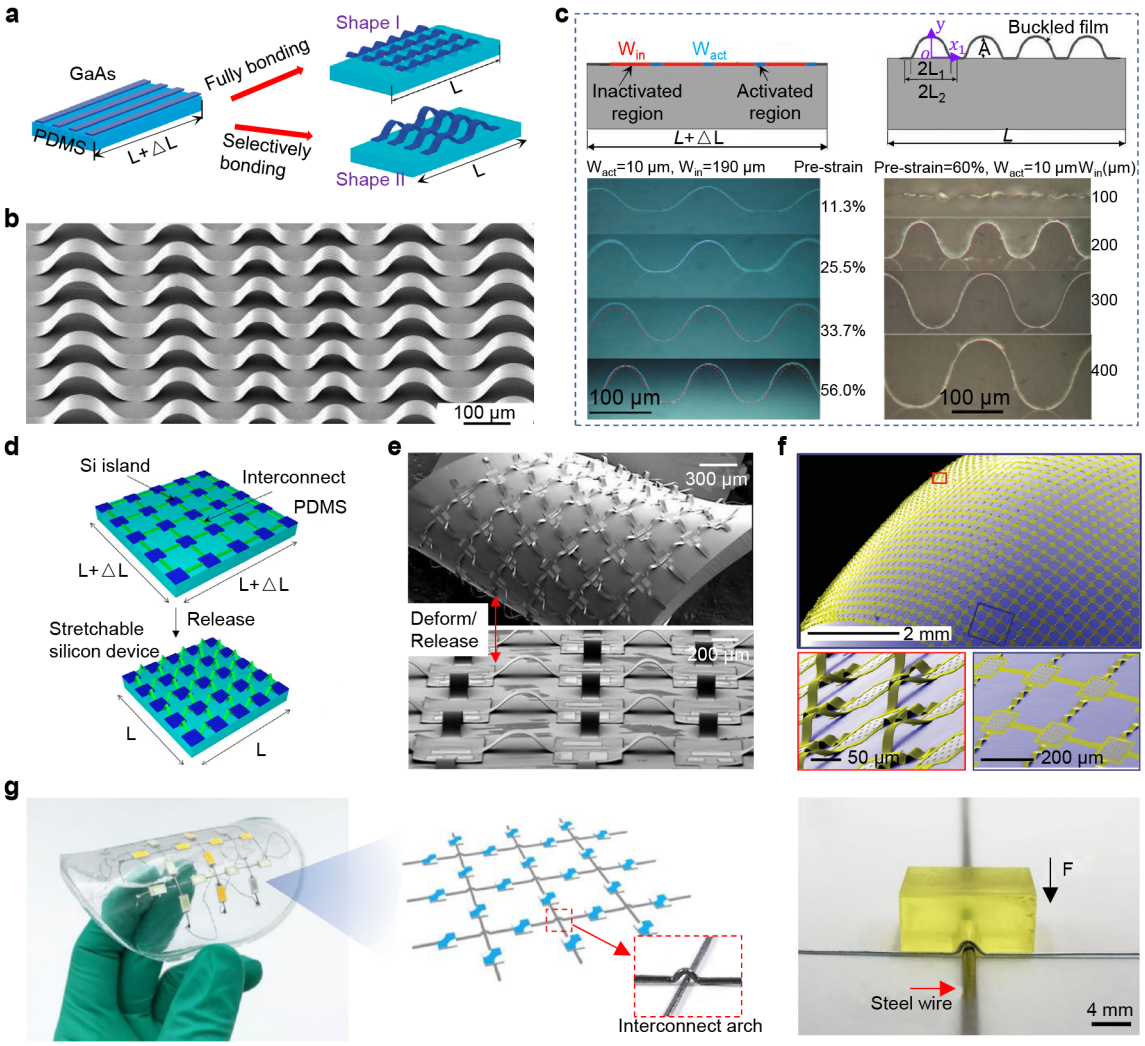

Figure 8. 3D arc-shaped interconnects. (a) Schematic illustration of the fabrication strategy of wavy structures based on the buckling-guided assembly. Reproduced with permission from ref 38. Copyright 2006 Wiley. (b) SEM image of a wavy structure array. Reproduced with permission from ref 37. Copyright 2006 Springer Nature. (c) Schematic illustration of the process for fabricating wavy structures on PDMS substrates (Top) and GaAs ribbons formed on PDMS substrates with different prestrains and different widths (W_{in}) of the inactivated region (Bottom). Reproduced with permission from ref 37. Copyright 2006 Springer Nature. (d) Schematic illustrations of the representative fabrication process for island-bridge structures on an elastomeric substrate via buckling-guided assembly. Reproduced with permission from ref 263. Copyright 2009 AIP Publishing. (e) Deformed configuration of the island-bridge structure under bending. Reproduced with permission from ref 40. Copyright 2008 National Academy of Sciences. (f) Island-bridge structures on a curved surface. Reproduced with permission from ref 99. Copyright 2009 Wiley. (g) Flexible electronics consisting of arc-shaped liquid metal interconnects. The left panel shows a flexible LED array with arc-shaped interconnects, and the right panel illustrates the preparation process. Reproduced with permission from ref 270. Copyright 2023 Springer Nature.

electronic devices, by first building the structures of devices (i.e., interconnects and main bodies) and second incorporating structural functionalities.

3. 3D INTERCONNECTS

Conventional interconnects mainly use inorganic electronic materials, such as metals (e.g., Au, Ag, and Cu) and semiconductors (e.g., Si), that do not stretch much (i.e., the fracture strain of silicon is only ca. 1%).[2] In order to build architected flexible electronic devices, the conductivity and stretchability of the exploited interconnects are required simultaneously. Therefore, constructing interconnects with flexible structures using high performance inorganic electronic materials is complementary. Thinning membranes to extreme makes brittle inorganic materials bendable.[251] For example, the Si nanomembrane with a thickness down to ca. 2 nm exhibits flexural rigidities far smaller (e.g., by 15 orders of magnitude) than those of bulk wafers (with thickness of ca. 200 μm). Based on this principle, 3D interconnects in the forms of arc-shaped,[31,37−40,99,251−276] serpentine,[40,277,278] and helical[103,209,279−282] are designed and fabricated to provide high levels of stretchability, flexibility, and conformability that fulfill the requirements of 3D architected flexible electronic devices.

3.1. 3D Arc-Shaped Interconnects

This section reviews 3D arc-shaped interconnects based on their different structural designs, including wavy designs, island-bridge designs, and other designs.

3.1.1. Wavy Designs. Given that there are plenty of reviews[252,264,265,268] addressing wavy designs in forms surface wrinkles (Figure 8a, shape I), here, we review only the wavy

https://doi.org/10.1021/acs.chemrev.3c00335
Chem. Rev. 2023, 123, 11137−11189

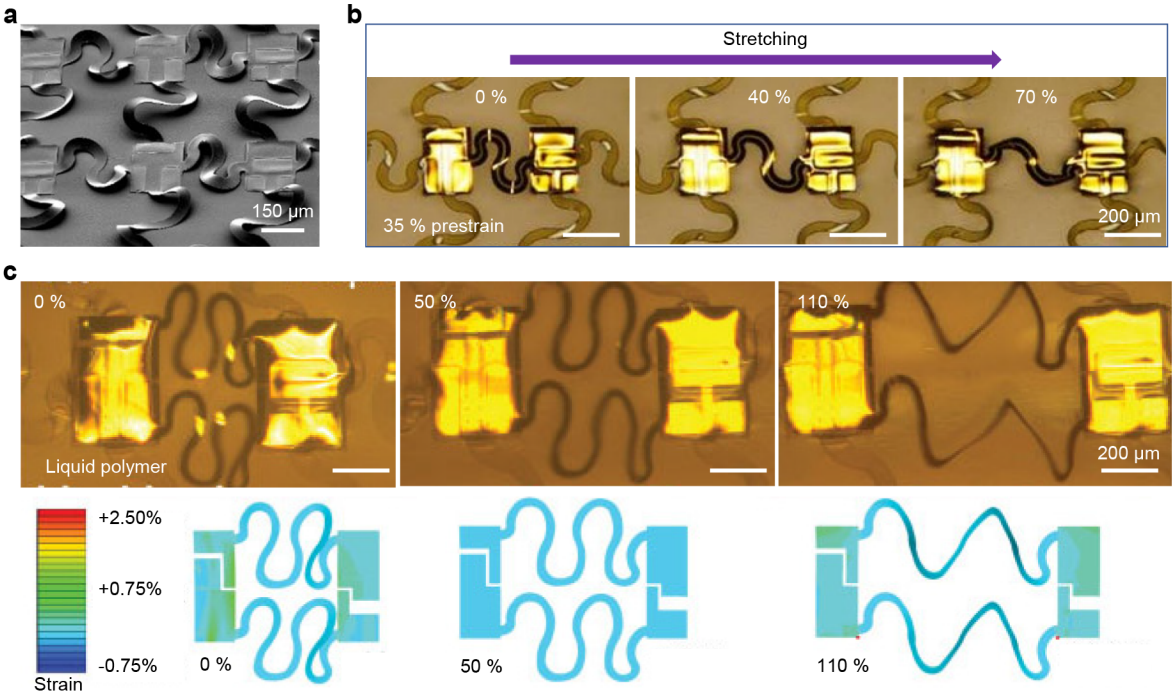

Figure 9. 3D serpentine interconnects. (a) SEM image of a stretchable CMOS inverter array using 3D serpentine interconnects. Reproduced with permission from ref 40. Copyright 2008 National Academy of Sciences. (b) Optical images of 3D serpentine interconnects under stretch. Reproduced with permission from ref 40. Copyright 2008 National Academy of Sciences. (c) Optical images and FEA results of deformed configurations of 3D serpentine interconnects under uniaxial stretching. The color in the FEA results denotes the magnitude of the maximum principal strain. Reproduced with permission from ref 278. Copyright 2009 Wiley.

designs in forms of out-of-plane 3D configurations (Figure 8a, shape II).[38] Such wavy designs formed by the buckling-guided assembly (Figure 8b,c) represent early forms of stretchable electronics consisting of rigid functional components.[37] Analytical models of such wavy structures have been developed to predict the buckling configuration and peak strain during the assembly.[37]

The buckling profile can be expressed by a sinusoidal function as

$$w = \begin{cases} w_1 = \frac{1}{2}A\left(1 + \cos\frac{\pi x_1}{L_1}\right), & -L_1 < x_1 < L_1 \\ w_2 = 0, & L_1 < |x_1| < L_2 \end{cases} \quad (1)$$

where w is the deflection along the y axis, A is the buckling amplitude to be determined, x_1 is the ribbon direction, $2L_1 = W_{in}/(1 + \varepsilon_{pre})$ is the buckling wavelength, $2L_2 = W_{in}/(1 + \varepsilon_{pre}) + W_{act}$ is the sum of activated (with strong chemical bonds) and inactivated (with unmodified surface chemistry) regions after relaxation, and ε_{pre} is the prestrain of the elastomeric substrate (Figure 8c).

Minimization of the total energy (U_{tot}) consisting of bending energy and membrane energy with respect to the buckling amplitude A gives

$$A = \frac{4}{\pi}\sqrt{L_1 L_2(\varepsilon_{pre} - \varepsilon_c)}, \ \varepsilon_{pre} > \varepsilon_c \quad (2)$$

where $\varepsilon_c = \frac{h^2\pi^2}{12L_1^2}$ is the critical strain for buckling, in which h denotes the film thickness. The experimental and theoretical profiles of buckled GaAs thin films formed on the PDMS substrate with different ε_{pre} and W_{in} values agree well (Figure 8c). The peak strain in the buckled thin film is $\varepsilon_{peak} \approx \pi\frac{h}{L_1}\sqrt{\frac{L_2}{L_1}\varepsilon_{pre}}$, which is typically much smaller than the prestrain.

3.1.2. Island-Bridge Designs. Evolving from wavy structures, island-bridge designs were later developed and widely used for flexible electronics.[39,40,256,263,274,275] Similar to arc-shaped wavy designs, arc-shaped island-bridge designs are also formed through the buckling-guided assembly. Figure 8d illustrates the fabrication process of a typical island-bridge structure, where discrete islands (e.g., containing rigid functional components) adhered to an elastomer substrate are connected by stretchable bridges (e.g., electrically conductive interconnects).[263] Notably, owing to low levels of strain in islands (i.e., mechanical strain isolation), such designs can simultaneously provide high stretchability and excellent protection of functional electronic components. Therefore, flexible electronic devices using island-bridge designs can withstand high-degrees of bending and twisting deformations (Figure 8e),[40] and conform to curved 3D surfaces such as hemispheres (Figure 8f).[99]

Many theoretical models were developed to guide the designs of arc-shaped island-bridge interconnects in 3D forms.[256,263,274,275] For example, a mechanical model to predict the buckling configurations was developed by assuming the ribbon as a clamped beam of sinusoidal form.[263] However, this model is not accurate enough in the regime of large compressions (e.g., compressive strain >40%). To improve the accuracy, a finite deformation model was later established, enabling precise predictions of deflections and peak strains in island-bridge designs.[274] Additionally, the mechanics of island-bridge interconnects in curvilinear electronic devices were also investigated to allow a rational design.[256,275]

https://doi.org/10.1021/acs.chemrev.3c00335
Chem. Rev. 2023, 123, 11137−11189

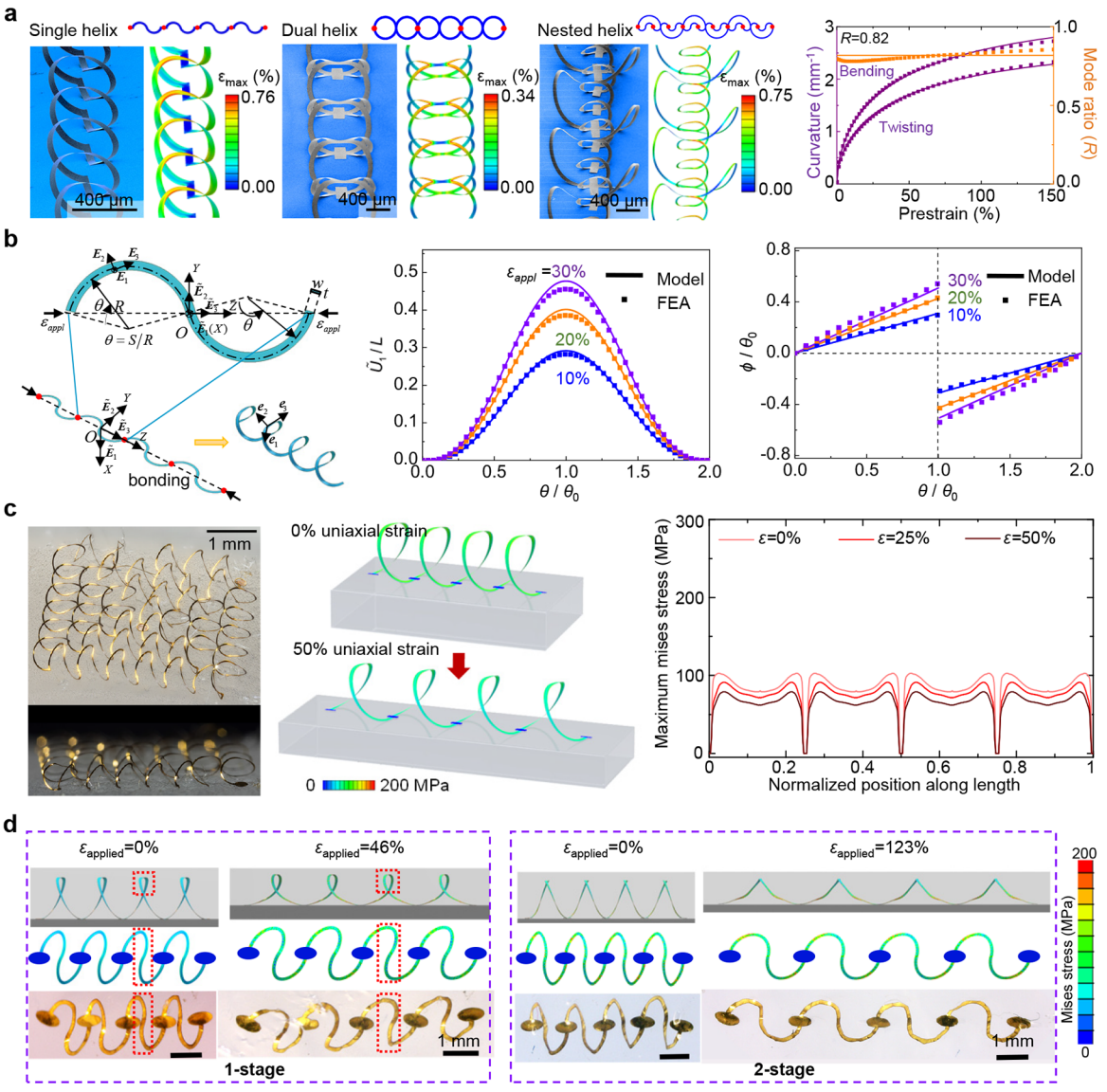

Figure 10. 3D helical interconnects. (a) Helical interconnects with three typical precursor designs. The left panel shows SEM images of single-helix, dual helix, and nested helix designs with their corresponding FEA predictions. The right panel demonstrates the dependences of average curvature components and the mode ratio of a 3D helical interconnect on the prestrain. Reproduced with permission from ref 103. Copyright 2015 The American Association for the Advancement of Science. (b) Illustration of the mechanics model for the buckling-guided assembly of helical interconnects, along with the predictions and FEA results on the distribution of dimensionless pop-up displacement and twist angle for a typical helical mesostructure (with an arc angle of $\theta_0 = 150°$ for the 2D precursor). Reproduced with permission from ref 209. Copyright 2016 Wiley. (c) Assembled 3D helical coils: optical images (left), deformations and Mises-stress distributions of a 3D coil based on FEA (middle), and distribution of maximum Mises stress for each cross section along the natural coordinate normalized by the arc length (right). Reproduced with permission from ref 280 under CC BY. Copyright 2017 Springer Nature. (d) Optical images and FEA results of both undeformed and deformed 3D helical interconnects with Mises-stress distributions in the conditions of one-stage (left) and two-stage encapsulating processes (right). Reproduced with permission from ref 279. Copyright 2019 Wiley.

Arc-shaped interconnects based on the curving-induced assembly were also proposed.[270] In particular, by harnessing the fluidity and high conductivity of liquid metal alloys, stretchable 3D interconnects were prepared for uses in electronic devices. As shown in Figure 8g, exploiting the solid−liquid phase transition and plastic deformations of the liquid metal alloy (i.e., Ga-based liquid metal alloys), 3D arc-shaped interconnects were fabricated through the curving-induced assembly.[270]

3.2. 3D Serpentine Interconnects. Compared to arc-shaped 3D interconnects, serpentine interconnects in 3D forms exhibit higher levels of stretchability.[40,278] As shown in Figure 9a, a stretchability of 70% was achieved in flexible electronic devices by using 3D serpentine interconnects formed by the buckling-guided assembly. In particular, as shown in Figure 9b, for a system assembled with 35% prestrain, when the uniaxial stretching gradually increased to 40%, the 3D serpentine interconnects almost returned to their planar configurations. Through in-plane rotation and out-of-plane buckling of 3D serpentine interconnects, the whole system can accommodate up to 70% tensile strain without failure. By tuning the assembly parameters (e.g., prestrains) and geometric layouts (e.g., the

https://doi.org/10.1021/acs.chemrev.3c00335
Chem. Rev. 2023, 123, 11137−11189

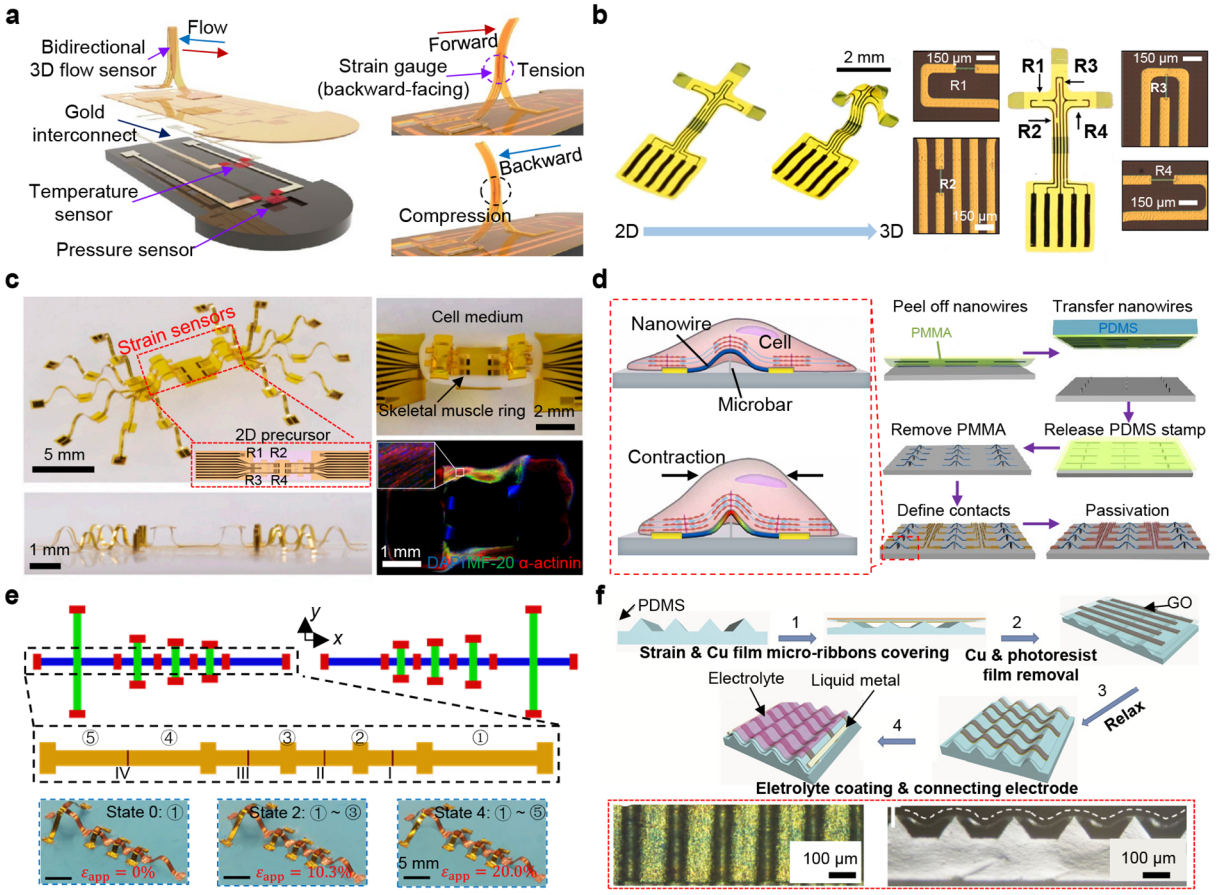

Figure 11. Devices in 3D arc-shaped forms. (a) Schematic and exploded-view illustrations of a 3D flow sensor. Reproduced with permission from ref 286. Copyright 2023 Springer Nature. (b) Assembly of a 3D piezoresistive sensor capable of normal/shear force measurements: deformed configurations using the compressive buckling (left) and optical images of the circuit design (right). Reproduced with permission from ref 133. Copyright 2019 American Chemical Society. (c) Design of compliant 3D frameworks instrumented with arc-shaped strain sensors for monitoring millimeter-scale muscle tissues. Reproduced with permission from ref 287. Copyright 2021 National Academy of Sciences. (d) Fabrication process of a 3D nanotransistor for simultaneous measurements of electrical and mechanical cellular responses. Reproduced with permission from ref 126 under CC BY. Copyright 2022 The American Association for the Advancement of Science. (e) Design and fabrication of a ribbon-like dipole antenna with tunable frequency. Reproduced with permission from ref 284. Copyright 2019 Wiley. (f) Fabrication of a stretchable microsupercapacitor composed of wavy-structured electrode arrays. Reproduced with permission from ref 285. Copyright 2015 Wiley.

number of arcs, Figure 9c), the stretchability of 3D serpentine interconnects can be further improved.[278]

3.3. 3D Helical Interconnects

Interconnects with 3D helical designs, commonly generated through the buckling-guided assembly of 2D filamentary serpentine precursors,[103,209,279,280,282] present higher elastic stretchability, when comparing to arc-shaped 3D interconnects and 3D serpentine interconnects. This section highlights the design principles and encapsulation strategies of the 3D helical interconnects.

As shown in Figure 10a, by varying the geometries of 2D precursors and distributions of bonding sites, divergent helical interconnects can be fabricated, including single helices, dual helices, nested coaxial structures, among others.[103] The average curvature components and mode ratio ($\kappa_{twist}/\kappa_{bend}$) can be calculated using finite element analyses (FEA), as shown in Figure 10a (right) for a typical 3D single helix. To understand the influences of the prestrain and geometric designs of 2D precursors on the resulting 3D helical configurations, an analytical model of compressive buckling based on the energy method was established. This model gives accurate predictions of deformed configurations and maximum strains of a single 3D helix (Figure 10b, left), which agreed well with FEA and experimental results.[209] In particular, when a helical interconnect is uniaxially stretched ($\varepsilon_{stretch} \leq \varepsilon_{pre}$), the out-of-plane displacement (U_1), the curvature components ($\hat{\kappa}_2$ and $\hat{\kappa}_3$), as well as the maximum principal strain (ε_M) follow a similar square root scaling

$$U_1, \hat{\kappa}_2, \hat{\kappa}_3, \varepsilon_M \propto \sqrt{\frac{\varepsilon_{pre}}{1+\varepsilon_{pre}} - \frac{\varepsilon_{stretch}}{1+\varepsilon_{stretch}}}, \text{ for } \varepsilon_{stretch} \leq \varepsilon_{pre} \quad (3)$$

Uniformly distributed maximum principal strains along the whole structure, ensure the exceptionally large stretchability and mechanical robustness of 3D helical interconnects (Figure 10c).[280]

In practical applications, the solid encapsulation usually results in an obvious reduction of the interconnect stretchability due to the mechanical constraints. Specifically, when compared to 3D arc-shaped and serpentine designs, the helical designs show more uniform distributions of strains at lower magnitudes,

https://doi.org/10.1021/acs.chemrev.3c00335
Chem. Rev. 2023, 123, 11137−11189

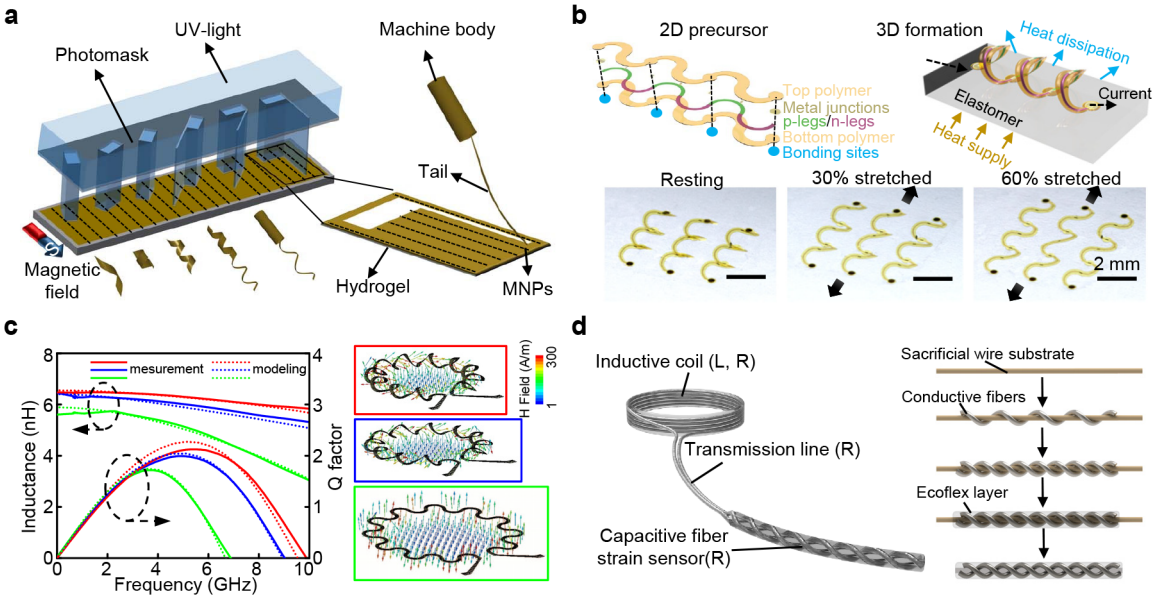

Figure 12. Devices in 3D helical forms. (a) Mass production procedure of soft 3D helical microswimmers through swelling-induced rolling. Reproduced with permission from ref 160 under CC BY. Copyright 2019 The American Association for the Advancement of Science. (b) Fabrication of 3D thermoelectric coils through the buckling-guided assembly. Reproduced with permission from ref 289 under CC BY. Copyright 2018 The American Association for the Advancement of Science. (c) A stretchable 3D toroidal helical inductor with tunable electrical properties. Reproduced with permission from ref 103. Copyright 2015 The American Association for the Advancement of Science. (d) Schematic illustrations of a wireless strain-sensing system and the fabrication process of capacitive fiber strain sensors. Reproduced with permission from ref 281 under CC BY. Copyright 2021 Spring Nature.

thereby rendering higher elastic stretchability. In this case, the mechanical constraints induced by solid encapsulation are more significant for interconnects with helical designs. To offer a stretchability higher than that of the conventional strategy of direct encapsulation (or one-stage encapsulation), a two-stage encapsulation strategy that involved prestretching the helical interconnects and then adding in encapsulation materials under the prestretched state was developed. Theoretical and experimental results showed that this two-stage encapsulation strategy can delay the occurrence of stress concentration by preunwinding the knot structural features. As such, a significantly enhanced elastic stretchability after encapsulation was achieved, when comparing with conventional one-stage encapsulation methods (Figure 10d).[279]

To summarize, in order to fabricate architected electronic devices with high levels of stretchability, the development of 3D interconnects with predesigned deployable geometries are essential. When compared with planar interconnects, the arc-shaped interconnects could provide moderate levels of extra stretchability owing to their out-of-plane structural configurations. The helical interconnects feature a relatively uniform curvature distribution, thereby allowing uniformly distributed strains along the whole structure under stretching, which could achieve higher levels of stretchability than arc-shaped interconnects.

4. 3D DEVICE FORMS

Flexible electronics with architected 3D configurations can better mimic and conform to the structural forms of natural species with complex spatial geometries, when compared to those in planar device structures. This section reviews diverse 3D forms of flexible electronics manufactured using mechanically-guided assembly methods, including 3D arc-shaped forms,[126,132,133,240,242,283−287] 3D helical forms,[103,145,160,236,281,288,289] tubular forms,[91,147,162,290−293] polyhedral forms,[172,181,294−298] hemispherical forms,[39,101,102,129,130,194,197,198,217,240,299−301] conformally wrapping forms[97,125,127,128,167,184,287,302−310] and other complex 3D forms,[17,99,122,138,191,203,240,311] through summarizing and discussing the representative functional devices that benefit from their unique structural characteristics.

4.1. 3D Arc-Shaped Forms

Flexible electronic devices in 3D arc-shaped forms are usually fabricated through buckling-guided assembly and curving-induced assembly approaches. Harnessing the discrete design concept, the geometric configuration and deformation of each consisting segment of a device in 3D arc-shaped form can be individually engineered, exhibiting many structural characteristics that induce various functionalities, such as decoupled sensing of physical signals (e.g., mechanics and electromagnetic fields).[133,284]

For example, a device in the form of 3D herringbone pattern consisting of two concave arcs (Figure 11a) was fabricated for bidirectional measurements of flow rates.[286] In particular, a strain sensor was integrated on one of the two arcs (Figure 11a, left one in the top right panel). Upon the reception of incoming flows in the forward direction (as shown in Figure 11a, top right), the strain sensor underwent tensile deformations. Under a reversed flow direction, the strain sensor experienced compressive deformations. Thereby, harnessing such a specifically designed arc-shaped form, the device was capable of bidirectional quantitative measurements of flow velocity. As shown in Figure 11b, an arc-shaped 3D structure, assembled using buckling-guided approaches from a planar crossing ribbon, was adopted as the device configuration.[133] Due to the four deformable arcs that can provide multiple channels for the collection of mechanically driven resistance changes, decoupled quantitative sensing of both in-plane and out-of-plane applied

https://doi.org/10.1021/acs.chemrev.3c00335
Chem. Rev. 2023, 123, 11137−11189

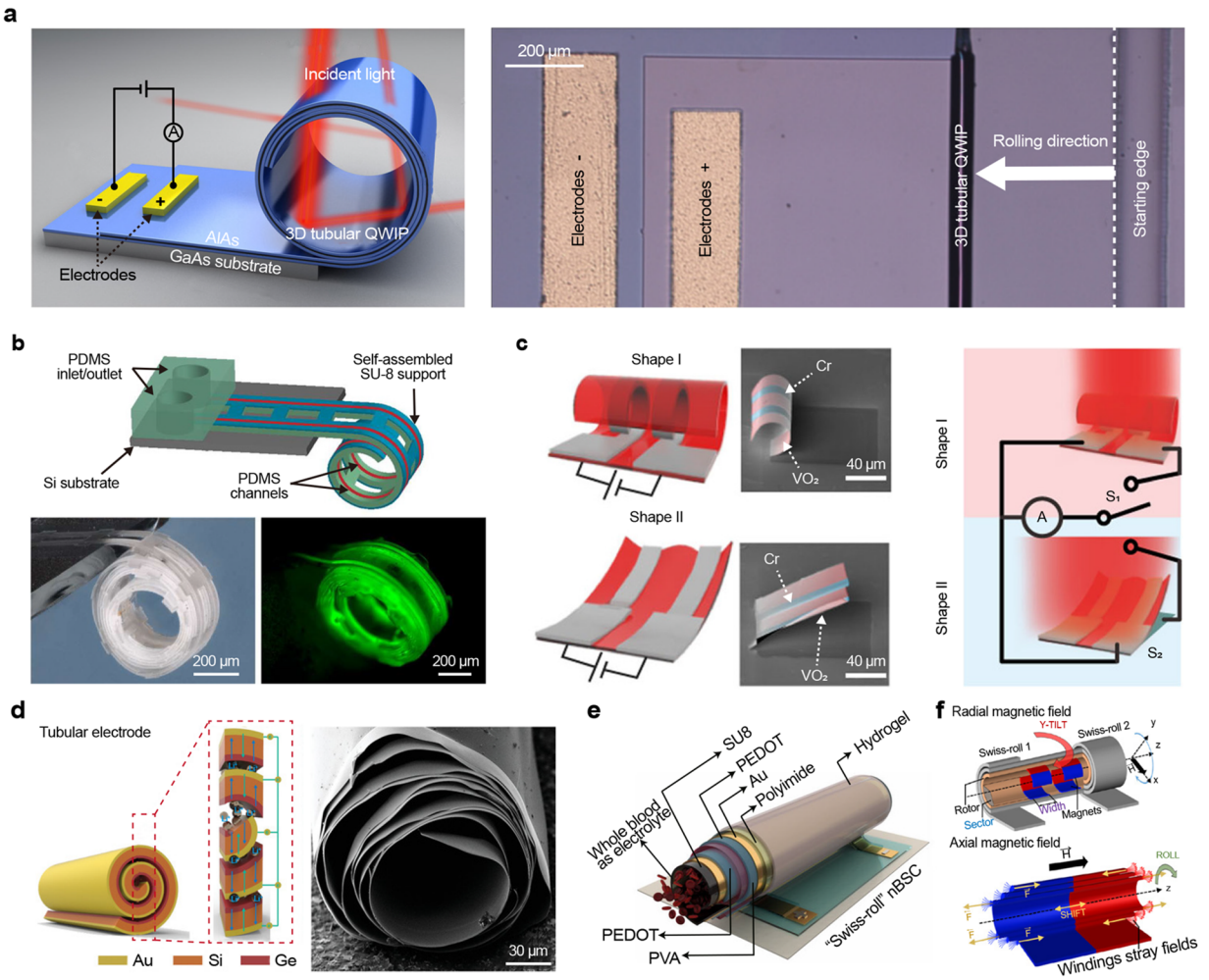

Figure 13. Devices in 3D tubular forms. (a) Schematic diagram and optical image of a 3D tubular quantum well infrared photodetector (QWIP). Reproduced with permission from ref 293 under CC BY. Copyright 2016 The American Association for the Advancement of Science. (b) A self-assembled microfluidic device for flow control and visualization. Reproduced with permission from ref 147. Copyright 2011 Springer Nature. (c) Tubular MEMS actuators and switches using VO_2 nanomembranes. Reproduced with permission from ref 162 under CC BY. Copyright 2021 Springer Nature. (d) Schematic illustrations of the ion diffusion and charge transport path of a tubular micro-lithium-ion battery manufactured by residual-stress-induced rolling (right) and the corresponding titled cross-sectional SEM image of an as-prepared spiral electrode (left). Reproduced with permission from ref 313. Copyright 2020 Wiley. (e) A "Swiss-roll" nano-biosupercapacitor (nBSC) used in biological electrolytes. Reproduced with permission from ref 292 under CC BY. Copyright 2021 Springer Nature. (f) Self-assembly of a "Swiss-roll" structure assisted by external magnetic fields. Reproduced with permission from ref 291 under CC BY. Copyright 2019 Springer Nature.

forces (e.g., pressure and shear force) was achieved. Furthermore, a flexible electronic device with complex 3D arc-shaped form that incorporates spatially distributed strain sensors, was fabricated to monitor the contractile forces of engineered optogenetic muscle tissue rings in high precision (Figure 11c).[287] In this particular case, the two arc-shaped ribbons in the center of the device (Figure 11c, top right), with flat tops and tiny prominent cantilevers (i.e., as hooks), served as a compressible support for the incorporated strain sensors on the outer surfaces of the arc-shaped ribbons to accomplish the measurements of vertically distributed contractile deformations. Figure 11d shows a flexible device in a very simple 3D arc-shaped configuration formed using curving-induced assembly.[126] Particularly, the microbars designed to curve the nanowires were also utilized to support the on-top arc-shaped structures with low bending stiffness, rendering a conformally contacted interface between nanowires and cell walls at the initial state. Meanwhile, upon cell contractions, such arc-shaped 3D nanowires allowed postdeformations that can be leveraged for simultaneous measurements of both electrical and mechanical cellular responses. In another case, mechanically triggered switches were devised for 3D RF antennas using a complex arc-shaped 3D configuration formed by buckling-guided assembly (Figure 11e).[284] In detail, the "on/off" states were realized by the shape morphing controlled through loading strains. As shown in Figure 11f, by the use of arc-shaped 3D ribbons, flexible graphene microsupercapacitors were fabricated, featuring an high stretchability of 100% (i.e., uniaxial).[285]

4.2. 3D Helical Forms

Flexible electronic devices in 3D helical forms can be assembled through approaches harnessing rolling, curving, and buckling. Similar to helical interconnects, devices in 3D helical forms render excellent stretchability and bendability. The structural configuration of 3D helices can be utilized to manufacture devices with novel structure-induced functionalities such as actuations in liquids[145,160] and spiral growth.[310]

https://doi.org/10.1021/acs.chemrev.3c00335
Chem. Rev. 2023, 123, 11137−11189

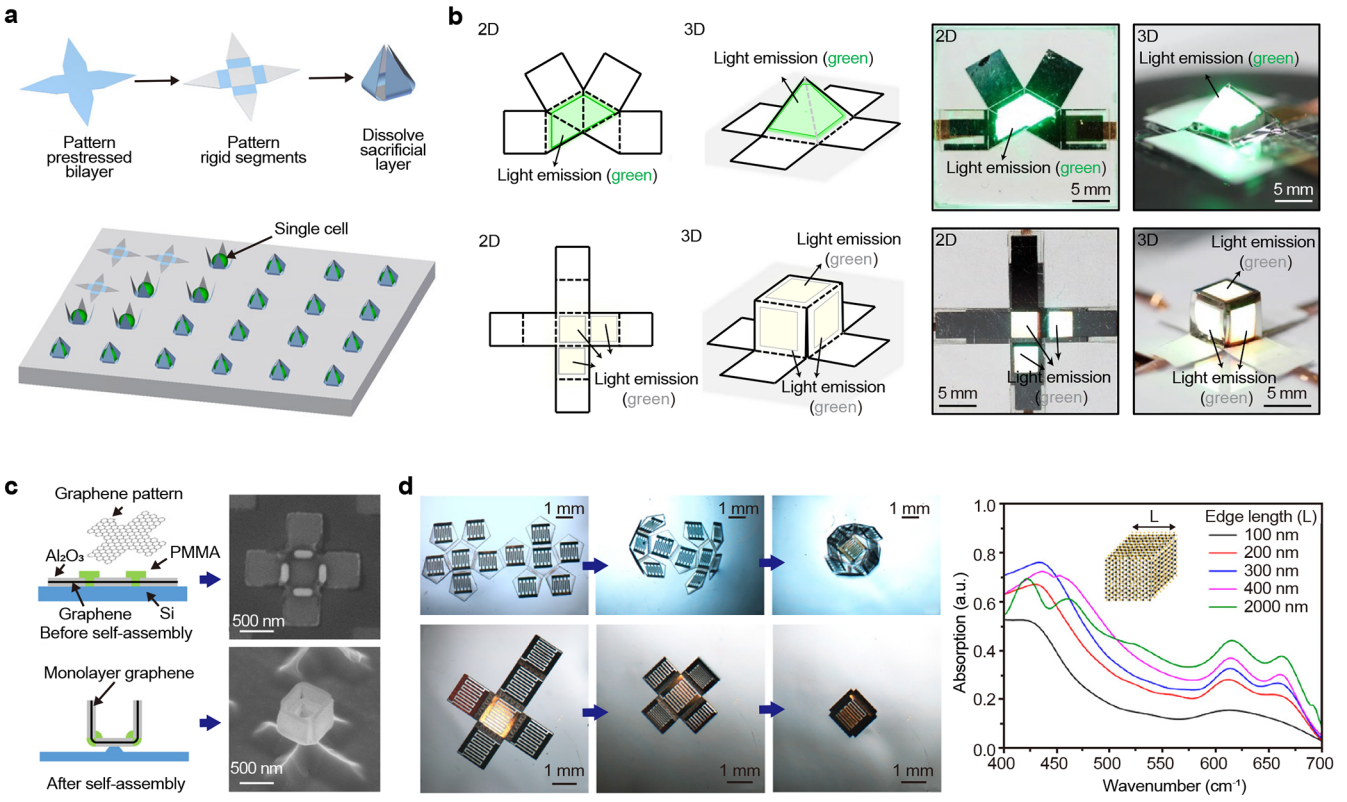

Figure 14. Devices in 3D polyhedral forms. (a) Fabrication and operation of single-cell grippers made of the SiO/SiO_2 bilayer. Reproduced with permission from ref 295. Copyright 2014 American Chemical Society. (b) Design and fabrication of various 3D architectures by folding preprogrammed ultrathin quantum-dot light-emitting diodes (QLEDs). Reproduced with permission from ref 297. Copyright 2021 Springer Nature. (c) Assembly of a monolayer graphene-based cubic structure. Reproduced with permission from ref 294. Copyright 2017 American Chemical Society. (d) Folding of hinged 3D MoS_2-Au-SU-8 photodetectors with enhanced optical absorption. Reproduced with permission from ref 296. Copyright 2019 American Chemical Society.

For example, as shown in Figure 12a, bioinspired 3D helical structures prepared through swelling-induced rolling assembly were exploited to achieve controlled motions for swimming robots.[160] The large out-of-plane deformations (i.e., vertical displacements) of 3D helical architectures were harnessed to create high temperature gradients for efficient thermoelectrical energy harvesting (Figure 12b).[289] In particular, the use of 3D helical structures significantly increased the altitude intercept between the heat receiving surface (i.e., the device surface that was in contact with the heat supplier) and the heat dissipation surface (i.e., the suspended top surface of the device) of the device (Figure 12b, top right), thereby generating an enlarged temperature gradient within the 3D device when compared with those in planar forms. As shown in Figure 12c,[103] the spatial characteristics of 3D helical structures were exploited to reduce the substrate parasitic capacitance of an inductor, resulting in improved electrical performances (e.g., the maximum Q factors and resonant frequencies increased from 1.7 to 2.2 and from 6.8 to 9.5 GHz, respectively). Harnessing the tunable structural gaps between two interwoven helices upon stretching (Figure 12d) (i.e., consisting of conductive polyurethane-based stretchable fibers embedded with Ag nanoparticles), capacitive strain sensors were fabricated through curving-induced assembly.[281]

4.3. Tubular Forms

Flexible electronic devices in tubular forms are primarily fabricated by rolling assembly approaches.[91] Owing to their structural characteristics (e.g., hollow tubular configurations, micro- to nanoscale diameters, multilayered shells and etc.), tubular flexible electronic devices exhibit unique physical properties, such as controlled light interactions (e.g., scattering and absorption[293,312]), fluidic controls,[147] high density material integrations,[291,292,313] and so on.

For instance, tubular 3D quantum well infrared photodetectors (QWIPs) could render enhanced responsivity and detectivity (Figure 13a).[293] In particular, the tubular form of the photodetector provided efficient pathways for light coupling and enabled the elimination of the requirement for external light coupling structures, featuring a wide detection angle (i.e., $\pm 70°$) for infrared lights. Additionally, by variation of the structural configurations of such photodetectors, tunable photocurrents and responsivities were also achieved.

The tubular form can also be utilized to facilitate microfluidic controls.[147] For example, through rolling assembly, a tubular SU-8 structure was exploited to reshape planar microfluidic networks into a 3D configuration with controlled curvatures (Figure 13b). In addition, through the use of a tubular configuration (Figure 13c),[162] a bifunctional device was manufactured and utilized for the actuation of a microelectromechanical system (MEMS) as well as electrically/optically controlled switching.

The layered shell structures of tubular configurations were also exploited to integrate more functional materials for flexible energy devices to achieve energy densities/capacities comparable to rigid ones.[291,292,313−315] For example, a tubular microbattery fabricated by rolling assembly of Au/Ge/Si trilayer

https://doi.org/10.1021/acs.chemrev.3c00335
Chem. Rev. 2023, 123, 11137−11189

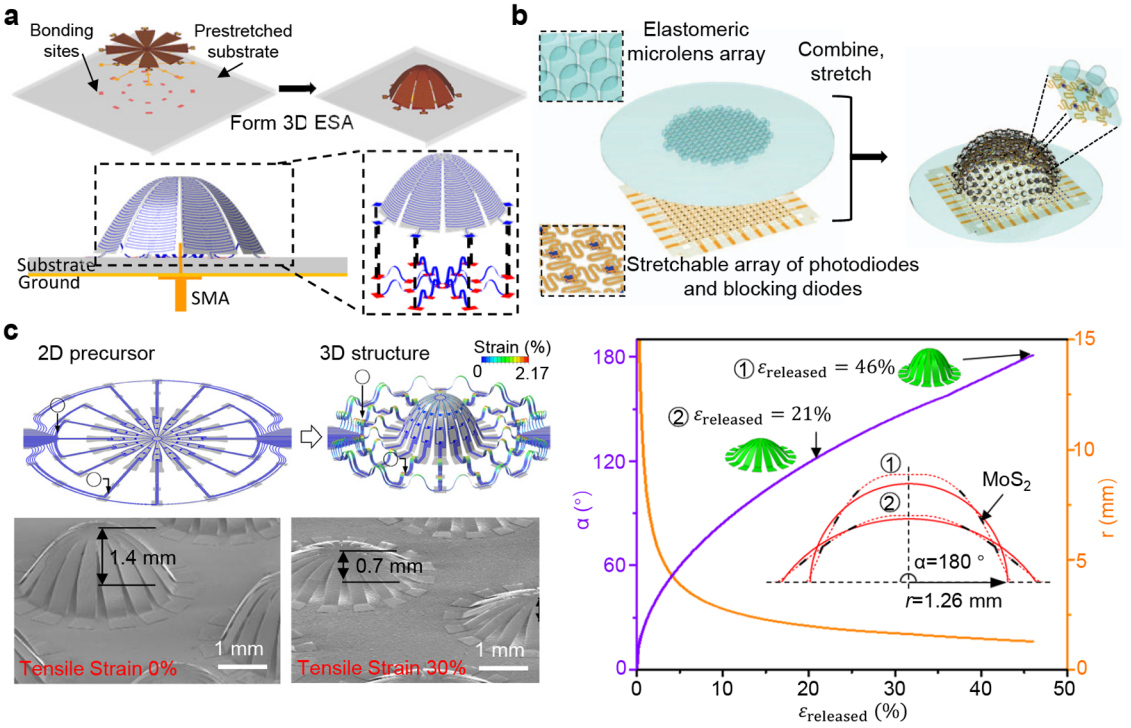

Figure 15. Devices in hemispherical forms. (a) Fabrication of electrically small antennas (ESAs) by buckling-guided assembly. Reproduced with permission from ref 301. Copyright 2018 Wiley. (b) Schematic illustrations of components and integration schemes for a digital camera in the form of a hemispherical, apposition compound eye. Reproduced with permission from ref 129. Copyright 2013 Springer Nature. (c) Design and fabrication of hemispherical devices for photodetection and imaging. Reproduced with permission from ref 217 under CC BY. Copyright 2018 Springer Nature.

nanomembranes was demonstrated to obtain high capacity and excellent cycling performance (Figure 13d).[313] Using "Swiss-roll" structures, robust nano-biosupercapacitors (nBSCs) consisting of multilayered shells (as shown in Figure 13e) were prepared and functioned as *in vivo* smart dusts as well as the microrobotic systems for healthcare.[292] Additionally, by incorporating thin magnetic films in a similar "Swiss-roll" configuration, the rolling assembly process could be precisely controlled using magnetic fields, resulting in various sophisticated 3D geometries (Figure 13f).[291]

4.4. Polyhedral Forms

Flexible electronic devices in polyhedral forms are usually manufactured using folding assembly methods.[172,181] Polyhedral forms, such as pyramids and cubes, stand as a typical type of spatial configuration that can facilitate structural functionalities involving capturing,[125,134,184,295,316−318] sensing,[294,296,298,319] light emitting,[297,320] and the rest.

Through the folding of patterned bilayer thin films, microgrippers were manufactured enabling controlled captures (e.g., folding angles) of single cells (Figure 14a).[295] Foldable polyhedral displays consisting of ultrathin quantum dot light-emitting diodes (QLEDs) were fabricated (Figure 14b), featuring stable operations during transformations among various structural configurations (e.g., the airplane, butterfly, pyramid, and cube).[297] In addition, a cubic monolayer graphene device (Figure 14c) was manufactured, achieving enhanced volumetric light confinements on both the surfaces and the designed hinges/edges.[294] Similarly, by folding MoS_2-Au-SU-8 photodetectors into cubes and dodecahedrons, an enhanced optical absorption within visible range (400−700 nm) was also achieved through the structure-induced light interactions (e.g., scattering and trapping) at the boundaries and corners (Figure 14d).[296]

4.5. Hemispherical Forms

Flexible electronic devices in hemispherical forms are usually fabricated through curving-induced and buckling-guided assembly methods. Hemispherical forms with structural expansions in vertical directions can enhance the performances of electromagnetic devices, such as antennas, by offering more surfaces to integrate electronic circuits with longer paths while maintaining a small overall projection dimension of the device.[299,301] For example, as shown in Figure 15a, through the buckling-guided assembly, an electrically small antenna (ESA) was manufactured in a hemispherical form with significantly enhanced electrical paths, featuring a high Q factor and tunable resonant frequencies.[301]

In addition, hemispherical forms can also serve as an isotropic spatial integration platform, thereby enabling flexible optoelectronic devices with omnidirectional sensing/imaging capabilities and reduced geometric distortions.[39,101,129,130,194,197,198,217] For instance, as shown in Figure 15b, through the curving-induced assembly, an arthropod-inspired digital camera was developed, featuring a wider field of view and a more homogeneous intensity when comparing to nonhemispherical cameras. Notably, origami and kirigami designs were also exploited to enhance the conformability of the planar structures to the hemispherical surfaces.[130,197] In another case, a hemispherical photodetector was manufactured (Figure 15c),[217] where the omnidirectional 3D integration enabled by the isotropic configuration of a hemispherical form allowed the simultaneous measurements of both light intensities and incident angles.

https://doi.org/10.1021/acs.chemrev.3c00335
Chem. Rev. 2023, 123, 11137−11189

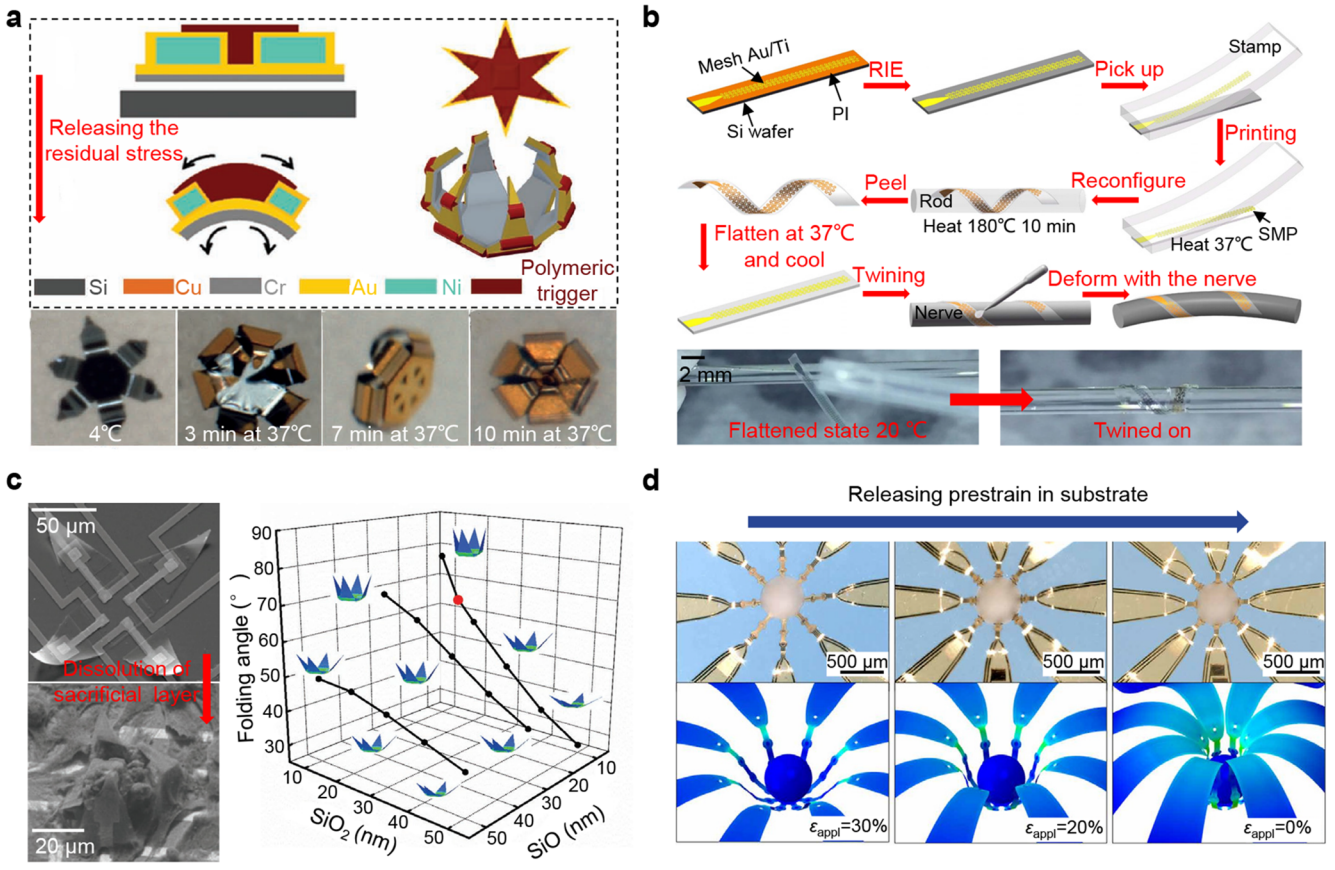

Figure 16. Conformally wrapping devices. (a) Fabrication and actuation of microgrippers driven by thermally induced residual stresses. Reproduced with permission from ref 303. Copyright 2012 Wiley. (b) Fabrication of a twining electrode with optical image showing its climbing process on a glass tube. Reproduced with permission from ref 310 under CC BY. Copyright 2019 The American Association for the Advancement of Science. (c) SEM images of a wrapping shell with multiple electrodes and FEA results showing the dependence of folding angle on the SiO/SiO_2 thicknesses. Reproduced with permission from ref 125. Copyright 2018 Wiley. (d) Buckling-guided assembly of a 3D multifunctional neural interface wrapping a neural spheroid. Reproduced with permission from ref 127 under CC BY. Copyright 2021 The American Association for the Advancement of Science.

4.6. Conformally Wrapping Forms

The formations of conformally wrapping devices usually involve complex deformation modes (refs 97, 125, 127, 128, 167, 184, 287, 302−310). Similar to polyhedral forms, devices in conformally wrapping forms can also facilitate capturing, owing to their semiclosed/closed structural configurations. An obvious difference between conformally wrapped configurations and polyhedral forms lies in the conformability of constructed interfaces between the captured object and a device. To be noted, in this review, conformally wrapping forms denote the assembled structures of architected flexible electronic devices that feature wrapping capabilities to form conformal contacts with their captured objects at the micro- to nanoscale (e.g., cells, organoids, and the rests), which should be distinguished from those macroscale 3D flexible electronic devices.

Microgrippers capable of controlled capture and release were demonstrated in conformally wrapping forms for various *in vivo* applications (e.g., surgery).[97,167,303] For instance, thermally actuated wrapping grippers with different dimensions ranging from 300 μm to 1.5 mm (Figure 16a) were fabricated using rolling assembly, enabling *in vivo* tissue extractions from living organisms.[303] Harnessing the shape memory effect of SMPs, twining neural interfaces were generated in forms of conformally wrapping helices, featuring body-temperature-driven postassembly climbing motions (Figure 16b).[310] The devices in conformally wrapping forms can also facilitate the *in situ* monitoring of living organisms. As shown in Figure 16c, through the residual-stress-induced rolling assembly, conformally wrapping electronic interfaces were manufactured, capable of single-cell monitoring (i.e., cardiomyocytes).[125] In particular, taking advantage of the engineered strain mismatches between SiO_2 and SiO layers (i.e., by varying the widths and thicknesses), the deformation angles of the structure can be tuned to achieve a conformal contact with cellular surfaces. Devices in conformally wrapping forms can also enable the spatial integration of biosensors, thereby allowing 3D electrical mapping and monitoring for neurons.[127,305,309] For example, through the buckling-guided assembly, a 3D device consisting of a high-density electrode array that gently wrapped around the surface of a spheroid was fabricated, capable of *in situ* monitoring of cellular growth and intercellular communications (Figure 16d).[127]

4.7. Other Complex Forms

Apart from the above, many other 3D configurations are also exploited for architected flexible electronics, such as compliant configurations,[191,203,240] complex origami/kirigami configurations,[17,120,122] and architectures with rationally designed microlattices[138,321] that are capable of replicating curved biological surfaces.

https://doi.org/10.1021/acs.chemrev.3c00335
Chem. Rev. 2023, 123, 11137−11189

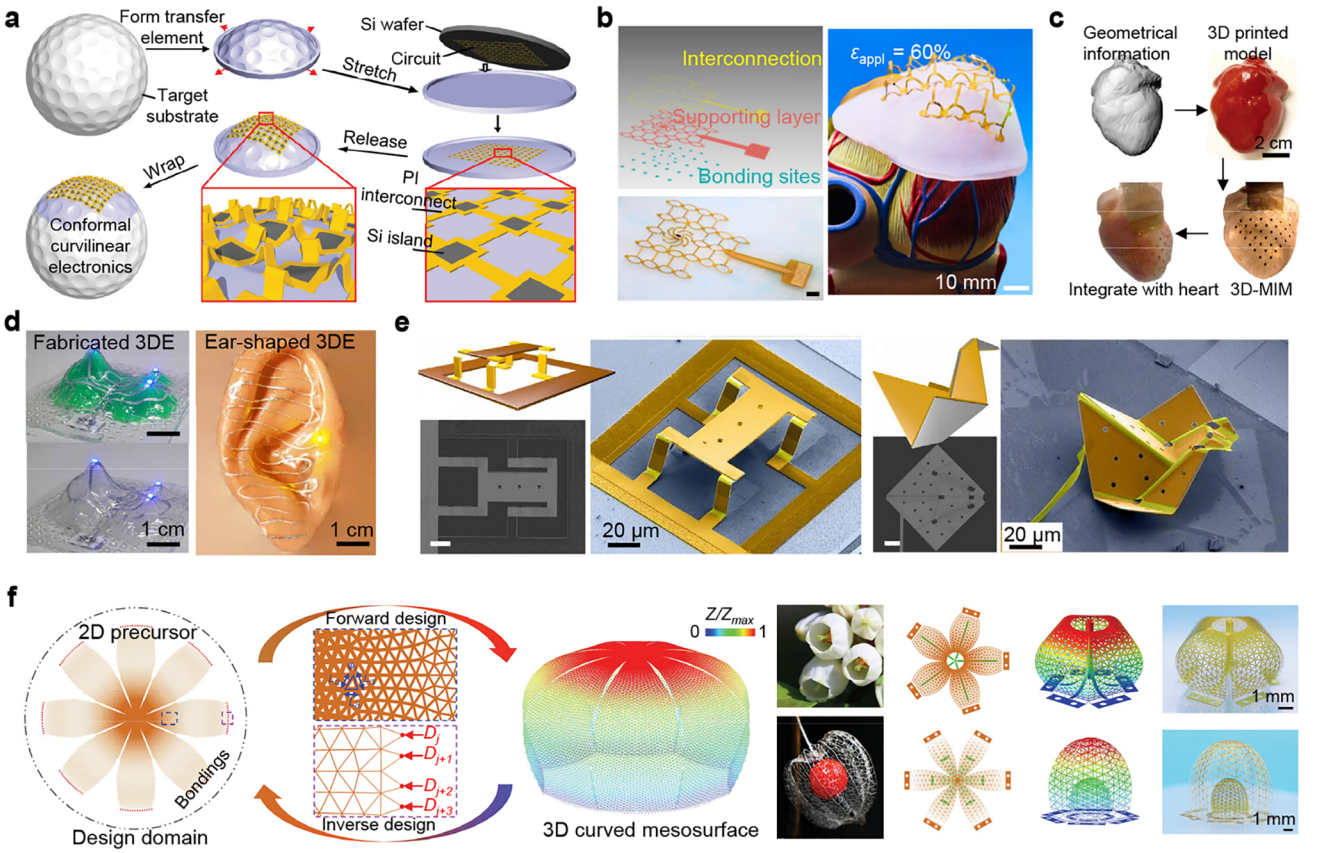

Figure 17. Devices in other complex 3D forms. (a) Schematic illustration of curvilinear silicon mesh circuits that wrap around a golf ball. Reproduced with permission from ref 99. Copyright 2009 Wiley. (b) A 3D electronic device capable of conformal attachment on a heart model. Reproduced with permission from ref 240 under CC BY. Copyright 2022 The American Association for the Advancement of Science. (c) Design and fabrication of 3D multifunctional integumentary membranes (MIMs) for spatiotemporal cardiac measurements. Reproduced with permission from ref 191 under CC BY. Copyright 2014 Springer Nature. (d) 3D electronics capable of conformal contact with complexly curved surfaces. Reproduced with permission from ref 203 under CC BY. Copyright 2021 The American Association for the Advancement of Science. (e) Origami microactuators with various folding configurations. Reproduced with permission from ref 122. Copyright 2021 The American Association for the Advancement of Science. (f) 3D mesotructures with complexly curved surfaces using microlattice designs: schematic illustrations (left) and inverse designs of blueberry flower and *P. philadelphica* berry (right). Reproduced with permission from ref 138. Copyright 2023 The American Association for the Advancement of Science.

Figure 17a shows an electronic interface in a curvilinear form, manufactured by the use of curving-induced assembly (associated with local buckling), which was able to conform to many curved surfaces, such as a golf ball.[99] An ordered two-stage buckling-guided assembly strategy was developed to transform planar electronic devices into sophisticated 3D forms that can conform to a variety of curved surfaces, such as the apex of a heart model (Figure 17b).[240] Figure 17c demonstrates a flexible electronic device in the form of a 3D integumentary thin membrane manufactured by the curving-induced assembly.[191] In particular, the heart-shaped 3D thin-film configuration allowed the device to form conformal contact with the beating heart and function as an artificial pericardium. Furthermore, using the curving-induced assembly based on the thermoforming,[203] mountain-shaped and ear-shaped 3D electronics were also fabricated (Figure 17d).

Origami designs were also utilized to further enhance the shape-morphing capabilities of devices in forms of complex 3D geometries. As shown in Figure 17e, a series of origami-inspired 3D structures were fabricated using the folding assembly (i.e., induced by electrochemically driven redox reactions), enabling the development of microscale 3D shape-memory actuators.[122]

Recently, a microlattice design strategy that featured programmable control of structural stiffnesses (i.e., by tuning the porosity distribution of microlattices) was developed, enabling the fabrication of devices in almost arbitrarily curved 3D architectures that can replicate complex biological surfaces (Figure 17f), such as the blueberry flower and *Philadelphica* berry (Figure 17f, right panel).[138]

In summary, there are numerous 3D forms in which each demonstrates unique structural functionalities throughout the broad family of architected flexible electronics. The core functionalities of a conventional rigid device are mainly achieved by circuit designs, while for architected flexible electronics, their functionalities are achieved by designs of both electrical circuits and structural configurations. Among different 3D device forms, due to their elementary structural configurations, the overall 3D geometries of arc-shaped devices could be easily shaped to fit the requirements of mechanical sensing, which have found essential applications in strain sensors. Owing to their unique biomimetic hydrodynamic characteristics, the helical forms are ideal for swimming microrobots, which can be applied for drug delivery. Thanks to their unique micro- to nanoscale hollow configurations, the tubular forms hold great potential in photodetectors and microfluidic devices. Notably, through the use of

https://doi.org/10.1021/acs.chemrev.3c00335
Chem. Rev. 2023, 123, 11137−11189

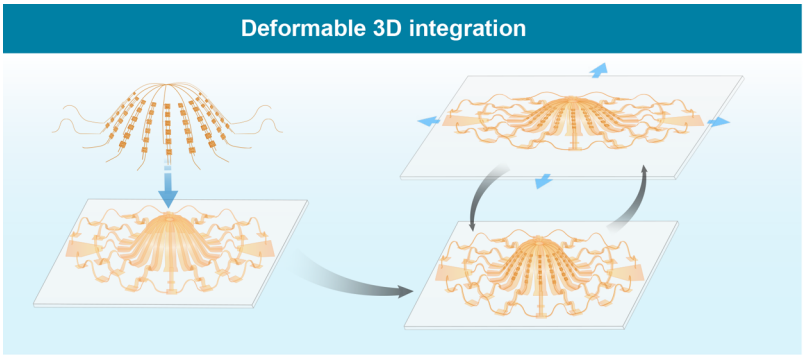

Figure 18. Schematic illustrations of typical cases for 3D integrations. By the use of a complex arc-shaped design (as a representative form), functional electronic components are spatially integrated, while providing significantly enhanced biaxial stretchability and flexibility.

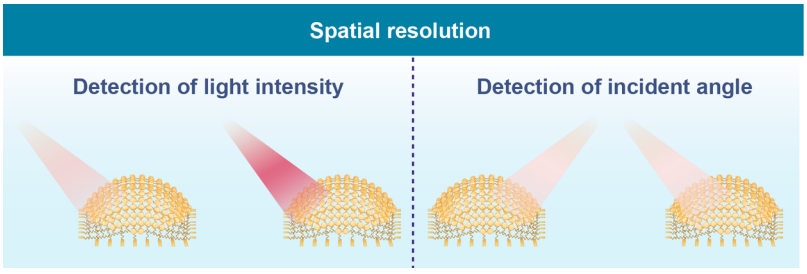

Figure 19. Schematic illustrations of a typical case of spatial resolution. Harnessing the hemispherical configuration integrated with arrays of photodetectors, both the intensities and incident angles can be simultaneously measured. Notably, photodetection is only shown as a representative case. Sensing of other directional dependent signals with spatial resolution, such as sound, thermal radiations, vibration, and the rest, can also be achieved through specific 3D structural designs in other forms.

multilayered shells, tubular structures were also exploited to fabricate devices (e.g., microbatteries) with high energy densities. The polyhedral forms are suitable for object capturing at the micro- to nanoscale (e.g., microgrippers) and light interaction (e.g., photodetectors and solar cells), owing to their open 3D cavities and nanoscale structural features at hinges. The hemispherical forms, featuring omnidirectional structural expansions in vertical directions, represent an ideal class of 3D configurations for electromagnetic devices (e.g., antennas) and optoelectronic devices (e.g., photodetectors). The conformally wrapping devices with semiclosed/closed structural configurations are suitable for applications in biological/biomedical devices for cell/tissue/organ monitoring.

5. STRUCTURE-INDUCED FUNCTIONALITIES

Conventionally, the functionalities of electronic devices usually indicate the electrical roles that integrated circuits play. Since the 20th century, rapid developments of human society have emerged technological revolutions in many aspects, such as Internet of Things (IoT), personalized medicine, human-machine interactions and others. As a consequence, the accessible functionalities of electronic devices have been drastically expanded. Different 3D configurations have been developed to induce unique structural functionalities, thereby adding more dimensions to the design of flexible electronics. Such structural revolutions have transformed the roles of electronic devices from solely electrical to mechanoelectrical,[22,132,280] optoelectrical,[130,217] magnetoelectrical,[322] thermoelectrical,[61,289] chemoelectrical,[236,242,323,324] bioelectrical,[127,138,325−327] and physically intelligent.[18,22,328,329]

In many of the reviewed cases in previous sections, structures do play vital roles in the achievement of their functionalities. However, when it comes to function-driven structural designs of devices, the routes become blurry. Therefore, it is essential to draw clear guidelines to navigate the function-driven structural designs of architected flexible electronic devices. In this section, various structure-induced functionalities, including high areal density 3D integration with spatial resolution, high-efficiency energy harvesting, 3D compliant electronic interfaces, reconfiguration, growth, and structural evolution, are reviewed and discussed, each with exemplary sketches illustrating their structural configurations and functionalities.

5.1. High Areal Density 3D Integration with Programmable Spatial Resolution

Electronic devices in planar forms utilize only in-plane spaces to integrate functional circuits, usually with a limited areal density in the cases of stretchable designs.[68,330−335] Various 3D configurations enabled by mechanically-guided assembly methods stand as promising platforms to achieve higher areal densities in flexible electronics, owing to their capabilities of expanding the distributions of functional circuits/elements into out-of-plane spaces with programmable spatial resolutions. In terms of achieving higher areal densities, both the multilayer flexible PCB (FPCB) and mechanically-guided assembly methods can be exploited.[121,333,336] In comparison to mechanically-guided assembly methods, the fabrication of multilayer FPCB is more simple and low cost. However, in order to fabricate architected 3D flexible electronics with specific structure-induced functionalities, mechanically-guided assembly methods are more suitable. Notably, the construction of 3D architectures would result in unavoidable spatial density loss of the device due to the spatial voids generated by the mechanically-guided assembly.

As illustrated in Figure 18, the idea can be simply analogized as building flexible/stretchable "flyovers" consisting of high-

https://doi.org/10.1021/acs.chemrev.3c00335
Chem. Rev. 2023, 123, 11137−11189

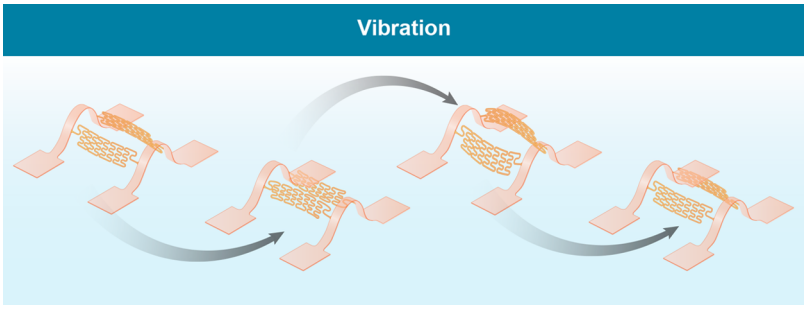

Figure 20. Schematic illustrations of a typical case of energy harvesting. The ultralow stiffness of a serpentine design can be utilized to fabricate an energy harvesting device (through vibrations) only by the formation of 3D architectures that allow fully suspended serpentines under operation modes.

density electrical circuits. Harnessing 3D structural characteristics, more surface area could be utilized for device integration when compared with planar configurations of the same projection area. In particular, the original in-plane surfaces for integrations (i.e., the projection area) are retained, while extra surfaces are created through the structural pop-up.[127,181,217,249,337] Furthermore, the use of multilayer designs could also increase the areal density of the resulting flexible electronic devices, by simply adding more layers for integration while keeping the in-plane projection area unchanged.[121]

Apart from high areal densities, the 3D integration also enabled a variety of architected flexible electronic devices with programmable spatial resolutions for sensing of various physical/chemical signals. For instance, a comprehensive photodetection should involve not only the intrinsic physics of incident light, such as wavelength, light intensity, and polarization, but also the external information on light sources, for instance, the incident angles and source locations. As shown in Figure 19, the sensing with desired spatial resolutions can be realized by creating a 3D dome structure (or other 3D structures that can provide spatial distributions of functional materials/electronic elements) through the use of the buckling-guided assembly. Furthermore, through the integrations of various functional semiconductors (e.g., MoS_2,[194,217,296,338] MoO_2,[339] ZnO,[340−344] TiO_2,[345,346] perovskites,[347,348] etc.) at the preset spatial locations, mechanically-guided methods can also facilitate the manufacturing of diverse sensors with spatial resolutions, enabling detections of different physical/chemical signals in 3D spaces, such as sound fields, thermal fields, magnetic fields, volumetric distributions of volatile organic compounds (VOCs), dispersions of toxic nanoparticles, among others.

5.2. High-Efficiency Energy Harvesting

Vibrational energies are abundant in nature. To harvest such form of energies, well-defined 3D architectures with engineered low stiffness regions that can vibrate without mechanical constraints are often required.[349] In planar devices, to achieve such functionality, cantilevers made of advanced electronic materials (e.g., graphene, PZT or III-V semiconductors) are usually manufactured with delicate multistep processing procedures. Such complicated manufacturing routes have set a series of grand challenges for their mass productions. In stark contrast, harnessing mechanically-guided structural design and 3D assembly methods (e.g., buckling-guided assembly), devices that sense and harvest vibrational energies can be facilely fabricated.[132,219] For instance, 3D architected flexible electronic devices with specifically designed local stiffness (i.e., the use of suspended serpentines with ultralow stiffness at the vibrational regions of the device) can vibrate and resonate upon receiving external stimuli so as to convert and generate energies in forms of electrical currents or voltages (Figure 20). Additionally, the use of mesostructures with ultralow stiffnesses would significantly reduce the resonant frequencies at small scales, thereby enabling efficient energy harvesting of low-frequency vibrations using miniaturized devices. Since the motions of human body and organs are usually in the range of several to tens of Hz, these 3D architected energy harvesters can be used to power biointegrated electronics. Furthermore, by incorporating multistable components in the 3D architecture, the bandwidth can be widened to improve the efficiency of vibration energy harvesting.

Aside from the vibrational energies, photogenerated energies (often in form of solar energies) are also ubiquitous in nature. The existing devices for photoenergy harvesting or conversion are mostly in planar configurations, such as solar cells,[76,350,351] photoelectrochemical water splitting (PEC) cells,[352−354] devices for artificial photosynthesis,[355] photocatalytic CO_2 reductions cells,[348,356] and so on. Due to the angle-dependent optical properties of 2D structures (e.g., absorption, reflection, transmittance, scattering, and other forms of optical interactions), planar devices are not able to take full use of solar energies (e.g., shadowing caused by low incident angles of lights). The existing forms of domes or hemispherical configurations in architected flexible electronics manufactured through mechanically-guided assembly methods can be leveraged to resolve the above issue. For example, a 3D electronic device capable of 360° light harvesting and light tracking can be fabricated, representing a promising form of photoenergy-conversion devices.[357]

5.3. 3D Compliant Electronic Interfaces

Complex 3D surfaces with sophisticated curvature distributions are found in both natural creatures and artificial objects, spanning cells, organoids, human bodies, machines, vehicles, and robots. Flexible electronic devices that can conform to such curved surfaces can serve as compliant electronic interfaces that induce minimal mismatch stresses, thereby allowing long-term monitoring of either biological or artificial objects (e.g., a single cell, organoids, tissues, organs, auto instruments, and so on). By the use of mechanically-guided assembly methods, many 3D compliant electronic interfaces are enabled for such purposes (e.g., twining neural electrode,[310] multifunctional electronic interface wrapping a spheroid,[127] complex interfaces between heart and thin electronic membrane,[191] and so on[128,302,309]). For instance, through the buckling-guided assembly, flexible electronic devices with 3D concave structures can be manufactured, holding promising potential to achieve controlled

https://doi.org/10.1021/acs.chemrev.3c00335
Chem. Rev. 2023, 123, 11137−11189

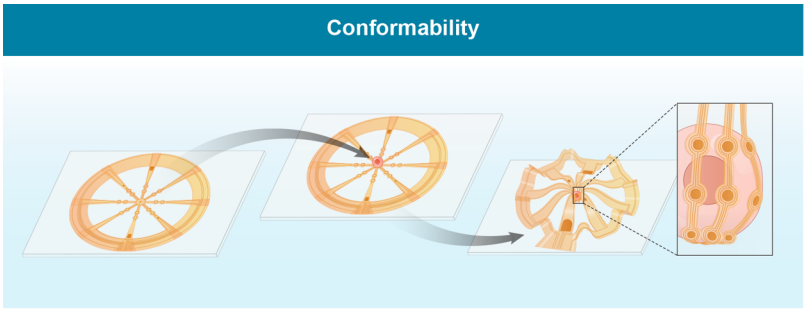

Figure 21. Schematic illustrations of a typical case for 3D compliant electronic interfaces. A flexible cell device showcases the formation of a compliant conformal interface between the surfaces of an electronic device and a cellular membrane assisted by mechanically-guided assembly.

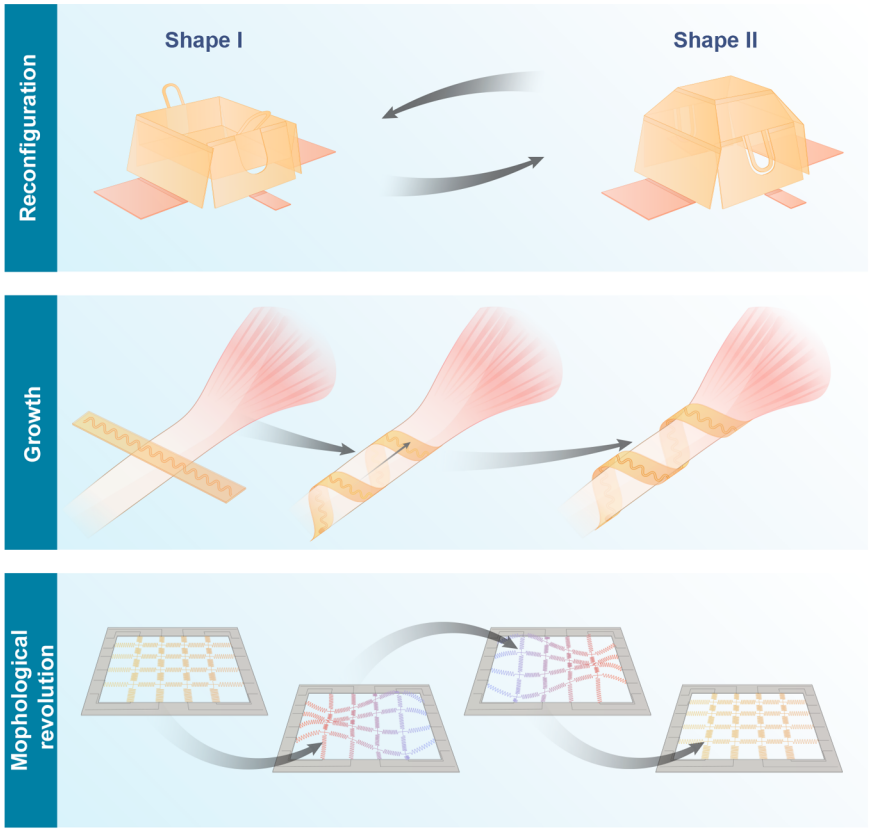

Figure 22. Schematic illustrations of a typical case for reconfiguration, growth, and morphological evolution. A representative reconfigurable device is shown in the top row, enabling reversible shape transformation between two stable shapes (shape I and shape II, respectively). The second row shows a flexible device that can first form conformal contact with a muscle tendon by body temperature actuated shape morphing. Then, taking advantage of the 3D helical structure, such device can climb along the tendon. Last but not least, harnessing the flexibility and stretchability, such device can grow with the tendon, showing no oblivious mechanical constrains to the tendon during growth. The third row shows a morphable electronic device (assisted by machine leaning) that can sense the structure and self-evolve to the target 3D configurations by electromagnetically controlled actuation.

capture of a single cell or organoid and conformal interfaces between the electronic surface and cellular membrane surface (Figure 21).

5.4. Growth, Reconfiguration, and Structural Evolution

Structural evolutions (not limited by the concepts of morphogenesis, organogenesis, or others), such as growth, shape changing, and complex structural transformations, are of pivotal importance for biology. By an artless biomimetic thinking, morphable devices that can reconfigure, grow, reshape, or even structurally evolve represent a more advanced form than those with fixed 3D geometries.

For instance, 3D architectures with multistable steady states can be reshaped by adopting different strategic loading paths (Figure 22, first row) during the buckling-guided assembly. Such reconfigurable flexible electronics have emerged with various new applications in the fields of electromagnetic devices and soft robotics.[16,139,358]

As illustrated in Figure 22 (second row), electronic devices with highly flexible designs, such as helical structures[310,359] are able to (i) spontaneously conform to the curved surface of a certain biological tissue (e.g., muscle tendon); (ii) climb along the 3D geometries of their attached tissue; and (iii) grow together with the tissue. Such growable designs could facilitate fundamental biological studies of living organisms (e.g., organs,

https://doi.org/10.1021/acs.chemrev.3c00335
Chem. Rev. 2023, 123, 11137−11189

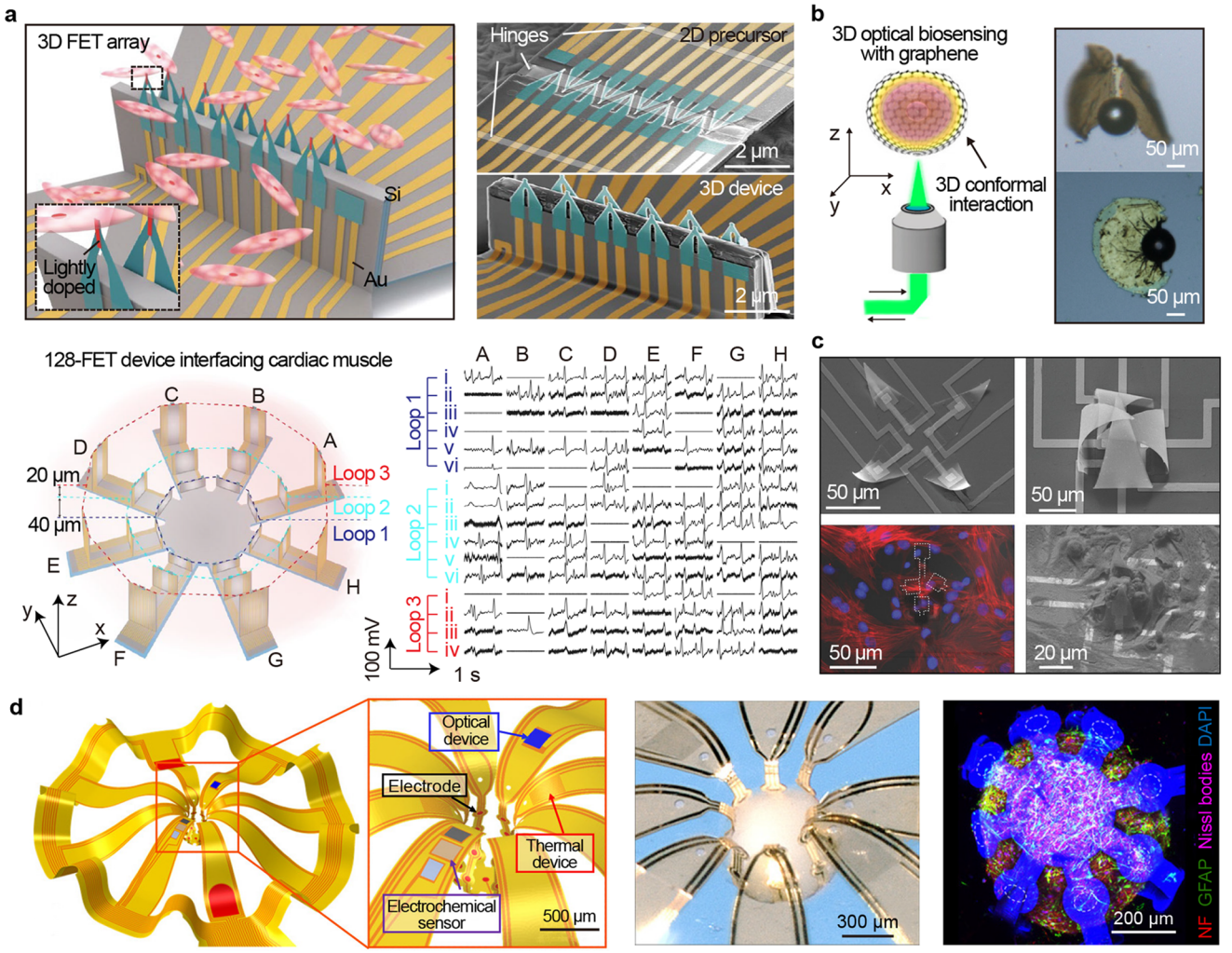

Figure 23. 3D biological electronics for fundamental studies of cells and organoids. (a) Design and construction of 3D FET arrays using compressive buckling and the intracellular recording of electrophysiological signals from neonatal rat cardiomyocytes. Reproduced with permission from ref 325. Copyright 2022 Springer Nature. (b) An ultrathin and flexible biosensing platform that wraps around a micro-object, allowing for 3D molecular spectroscopy via SERS. Reproduced with permission from ref 316. Copyright 2019 American Chemical Society. (c) Curved shell with spatially distributed electrodes, which wrap around the cardiomyocyte cell for electrophysiological monitoring. Reproduced with permission from ref 125 under CC BY. Copyright 2018 Wiley. (d) 3D neural interface with a microelectrode array, which can wrap a neural spheroid for spatiotemporal mapping. Reproduced with permission from ref 127 under CC BY. Copyright 2021 The American Association for the Advancement of Science.

muscles, tendons, neurons, among others) by providing morphable electronic platforms for long-term *in situ* monitoring of their biological behaviors during growths.

Very recently, a new type of electromagnetically controlled metasurfaces capable of dynamic morphological evolutions has been demonstrated.[360] Using discrete morphable serpentine units consisting of polymeric materials and patterned electronic circuits, centimeter-scale morphable surfaces (Figure 22, third row) that can rapidly self-evolve to the target 3D configuration are developed through mechanically-guided methods. Particularly, their structural evolutions are achieved by programming the spatially distributed Lorenz forces applied to the various units. Such self-evolving electronics have already fuzzed up the boundaries of 2D and 3D devices.

In conclusion, structure-induced functionalities (i.e., enabled by mechanically-guided assembly) are diverse and sometimes case-by-case, which opens up a new perspective for the design of architected flexible electronics. Devices that can vibrate and harvest mechanical energies, omnidirectionally absorb and convert incident photoenergies, spatially receive and sense physical/chemical signals, deform and conform to curved natural/artificial surfaces, and grow and evolve spontaneously were just scientific fictions decades ago. Despite this exciting progress, enriched device functionalities induced by structural designs that mostly originated from intuitive inspirations, due to the lack of rational function-driven structural designs. Open opportunities lie in the developments of interdisciplinary function-driven design paradigms that could rationally link diverse functionalities to the corresponding class of 3D architectures.

6. APPLICATIONS

The intriguing structure-induced functionalities enabled by the mechanically-guided 3D assembly have significantly pushed the research frontiers of flexible electronics, and led to the developments of many new devices,[5,361−363] enabling a broad spectrum of applications.[104,105,364−366] This section reviews applications of architected flexible electronics spanning various

https://doi.org/10.1021/acs.chemrev.3c00335
Chem. Rev. 2023, 123, 11137−11189

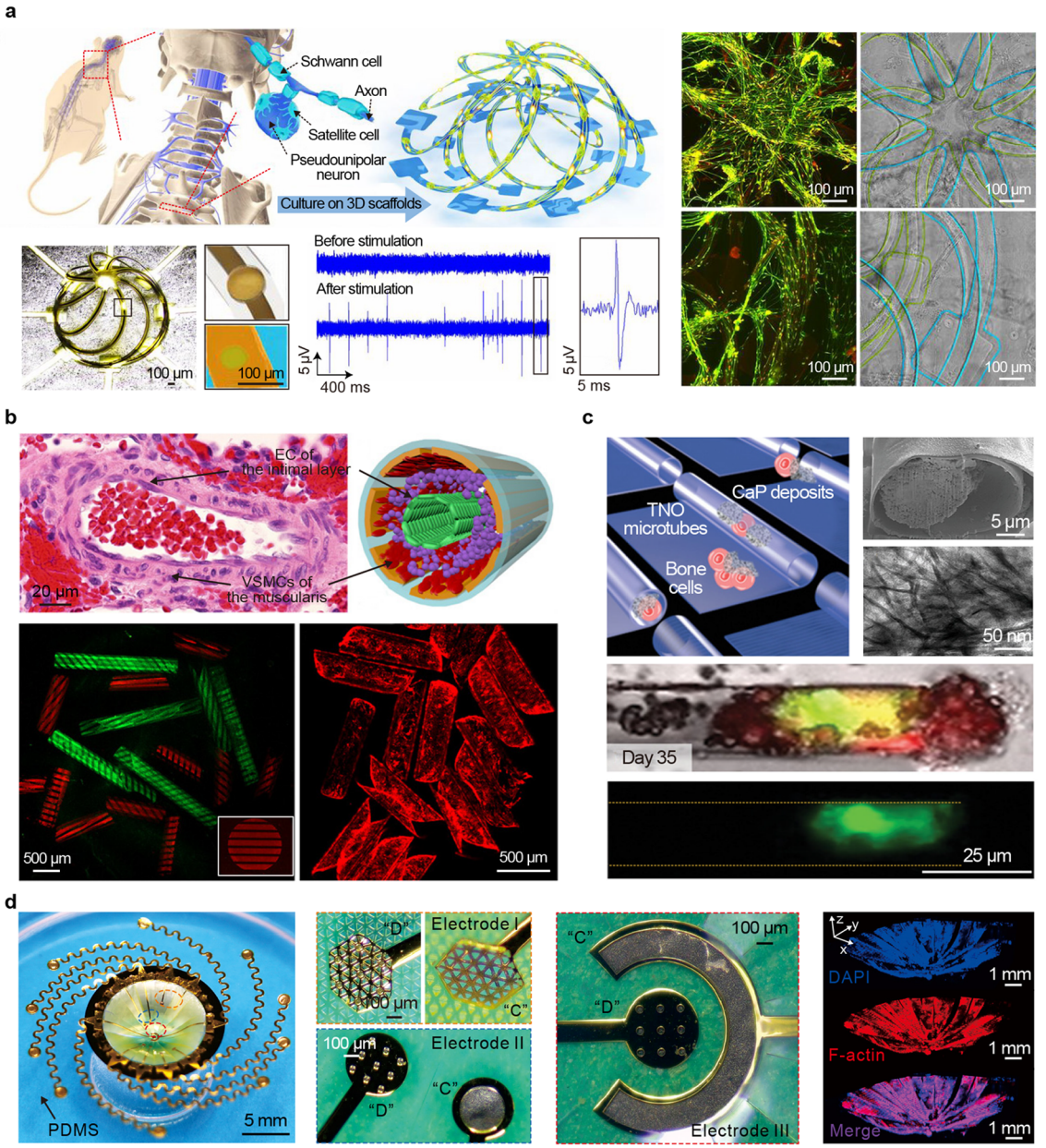

Figure 24. 3D biological electronics for tissue engineering. (a) 3D electronic scaffolds for DRG neural networks with uniform dispersions of cells allowing study of the electrophysiological behaviors of the growing. Reproduced with permission from ref 214 under CC BY. Copyright 2017 National Academy of Sciences. (b) Biomimetic tubular architectures that are similar to human small muscular distal acinar pulmonary arteries enables higher activation of cells. Reproduced with permission from ref 374 under CC BY. Copyright 2020 The American Association for the Advancement of Science. (c) *In vitro* 3D electronic platforms for studying bone cell−material interactions during osteogenic cell differentiation. Reproduced with permission from ref 375 under CC BY. Copyright 2021 Wiley. (d) Spherical cap-shaped electronic cell scaffold with integrated sensing capabilities. Reproduced with permission from ref 138. Copyright 2023 The American Association for the Advancement of Science.

emerging fields including biology, biomedicine, electromagnetics, optoelectronics, energy, and robotics.

6.1. Biological Devices

6.1.1. Cell Devices. Architected flexible electronic devices stand as powerful tools to capture and read dynamic electrophysiological signals of cellular processing (e.g., growth, differentiation, replication, and apoptosis) and intercellular communications from the perspective of a single cell.[125,182,295,367−371] As shown in Figure 23a, a flexible electronic platform consisting of a 3D field-effect transistor (FET) array (i.e., with up to 128 FETs as demonstrated) was developed by the use of buckling-guided approaches, with capabilities of recording transmembrane potentials in cardiomyocytes. In particular, the measurements based on this platform indicated an intracellular signal conduction velocity of 0.182 m s^{-1}, which was around five times higher than that of intercellular signal conduction.[325]

Using the mechanically-guided assembly, various microgrippers were also fabricated for single-cell capturing and manipulations (such as extraction, delivery, and controlled release). For instance, arrayed biocompatible grippers, harnessing engineered actuation through SiO/SiO_2 bilayers, were fabricated for precise extraction and delivery of single

https://doi.org/10.1021/acs.chemrev.3c00335
Chem. Rev. 2023, 123, 11137−11189

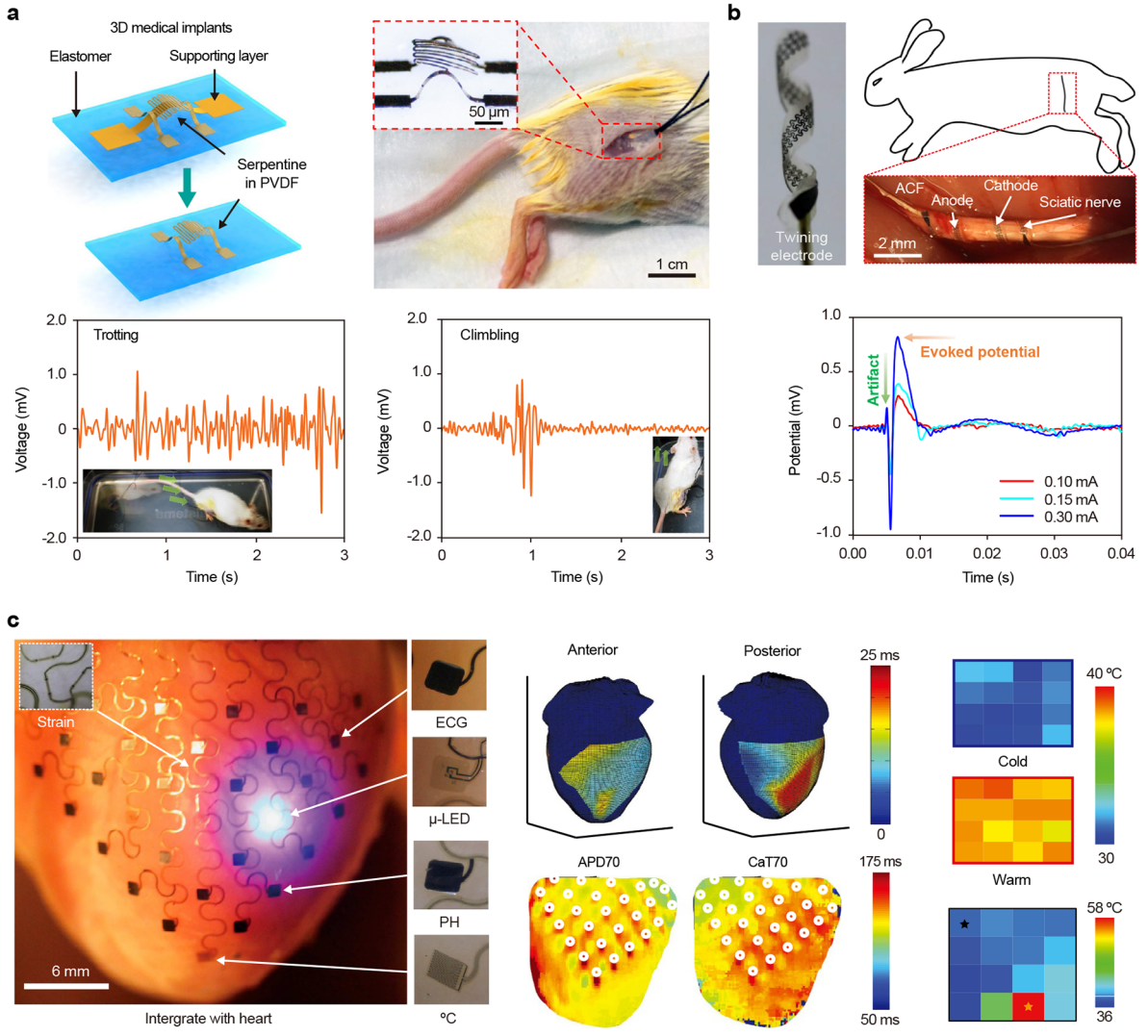

Figure 25. 3D biomedical electronics for *in vivo* monitoring of physiological signals. (a) 3D piezoelectric implants capable of voltage measurements during different actions. Reproduced with permission from ref 132. Copyright 2019 Springer Nature. (b) 3D deformable twining electrode for *in vivo* vagus nerve stimulation (VNS). Reproduced with permission from ref 310 under CC BY. Copyright 2019 The American Association for the Advancement of Science. (c) 3D multifunctional integumentary membranes (3D-MIMs) integrated with a rabbit heart for spatiotemporal measurements of electrical signaling of both pH and temperature. Reproduced with permission from ref 191 under CC BY. Copyright 2014 Springer Nature.

cells.[184,295] Later, by further introduction of responsive materials, such as magnetic materials or thermally responsive materials,[184] remote controls of such grippers were enabled. Such microgrippers show great promise for high-throughput biopsies. For example, a flexible electronic device, capable of mechanical trapping and surface-enhanced Raman spectroscopy (MT-SERS),[372] was developed as a new tool for simultaneous capturing, profiling, and 3D microscopic mapping of intrinsic molecular signatures of a single living cell (Figure 23b).[316] By further integration of microelectrodes on top of the microgrippers, electronic platforms that allowed spatiotemporally recordings of living cells were also developed.[125] In particular, utilizing residual-stress-induced rolling, such grippers were able to conformally wrap around a single cell to record the propagation of action potentials (Figure 23c). Flexible arrays of tubular electronics consisting of rolled-up transparent oxides (i.e., SiO/SiO_2) were also exploited as platforms for cultures[369] and encapsulations of living mammalian cells (i.e., HeLa cells),[370] resulting in different cellular assemblies and chromosomal instability during cell divisions. Later on, by further incorporating impedimetric microfluidic sensors into the above platform, simultaneous analyses of single human monocytes and their mediated activations were achieved.[373]

6.1.2. Organoid Devices. Zooming out from the single-cell perspective, architected flexible electronics have also significantly enriched the methodologies for organoid studies.[127,128,147,184,236,305] The development of multifunctional compliant 3D electronic frameworks stood as a representative achievement in this field.[236] Equipped with sensors that respond to various physical/chemical signals (Figure 23d),[127] such frameworks enabled both *in vitro* and *in vivo* biological investigations, such as the recording of coordinated bursting events, regrowth of bridging tissues in cortical spheroids and mechanical characteristics of organoids.[305] In addition, shell microelectrode arrays (MEAs) were developed to study brain organoids,[128] featuring high signal-to-noise ratio sensing and 3D

https://doi.org/10.1021/acs.chemrev.3c00335
Chem. Rev. 2023, 123, 11137−11189

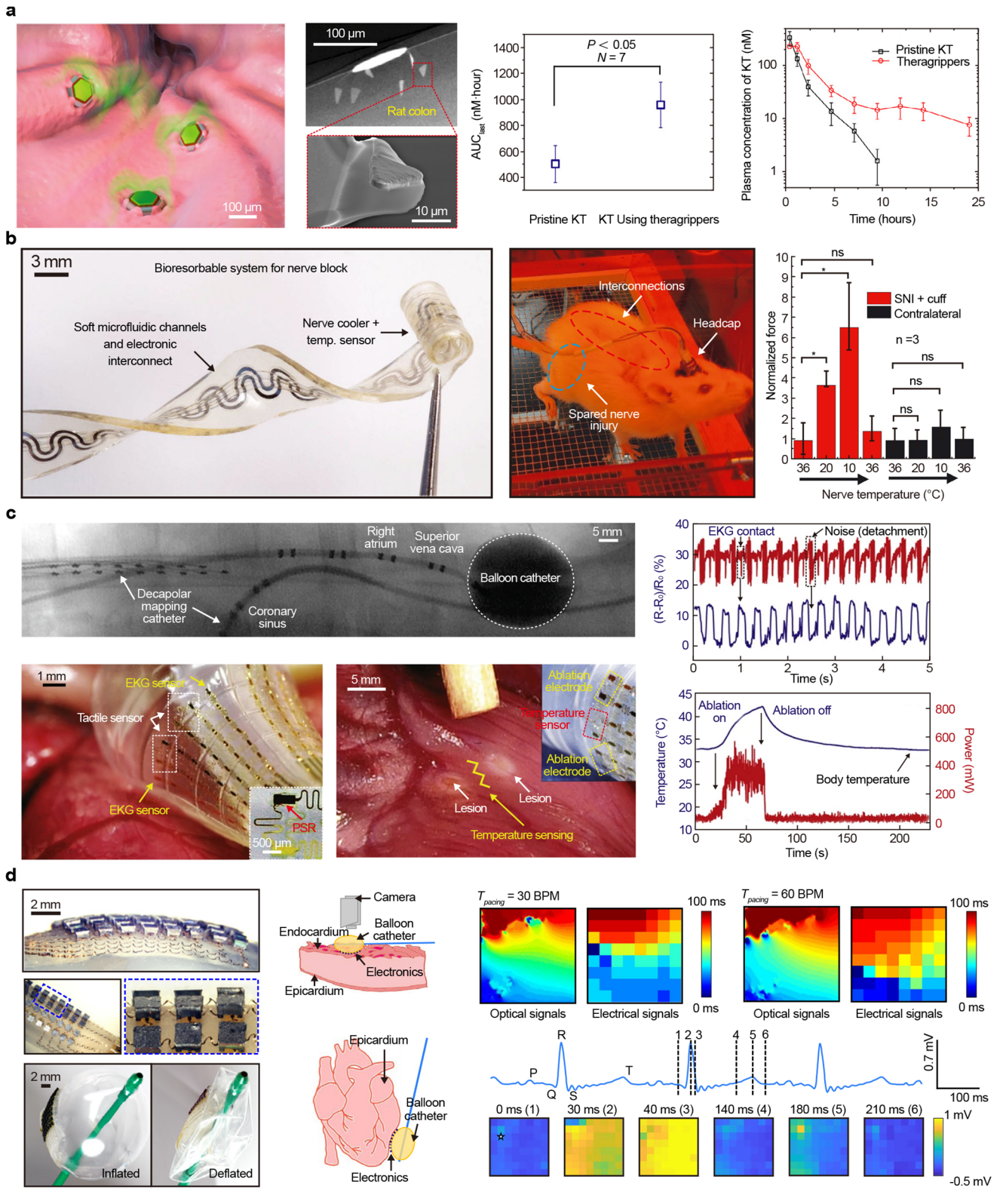

Figure 26. 3D biomedical electronics for therapeutics and surgeries. (a) Submillimeter-scale bioinspired latching tools for enhanced drug release and retention. The right two panels show extended and higher exposures of ketorolac compared to pristine drug. Reproduced with permission from ref 134 under CC BY. Copyright 2020 The American Association for the Advancement of Science. (b) 3D bioresorbable peripheral nerve-cooling and temperature-sensing device for pain blocking. Reproduced with permission from ref 388. Copyright 2022 The American Association for the Advancement of Science. (c) Multifunctional 3D electronic balloon catheter for *in vivo* electrophysiological/temperature mapping and RF ablation. Reproduced with permission from ref 188. Copyright 2011 Springer Nature. (d) 3D electronic catheters for diagnosis and treatments, including endocardial electrophysiological studies, electrogram measurements, and RF ablation. Reproduced with permission from ref 135. Copyright 2020 Springer Nature.

https://doi.org/10.1021/acs.chemrev.3c00335
Chem. Rev. 2023, 123, 11137−11189

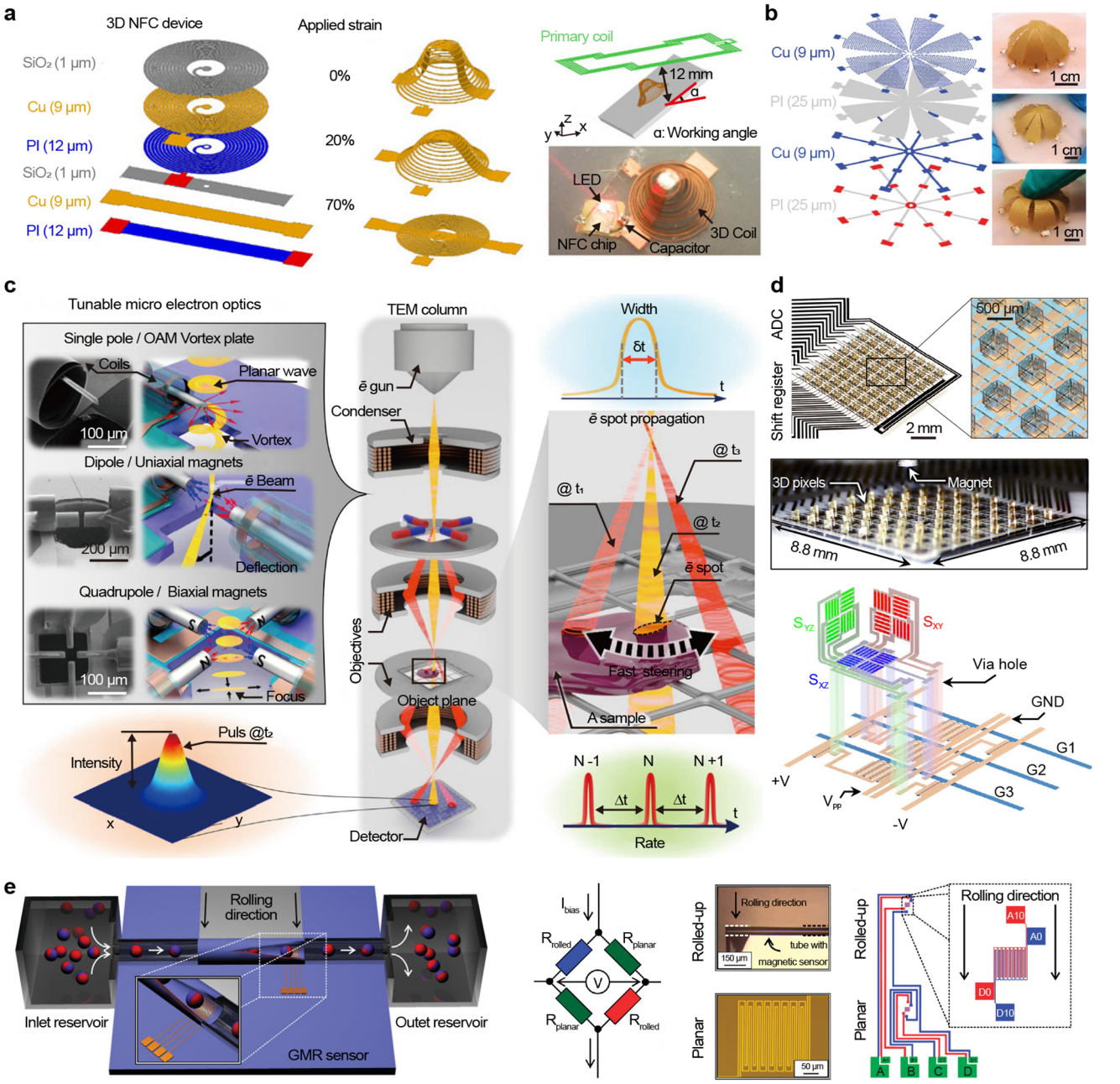

Figure 27. 3D electromagnetic devices. (a) 3D near-field communication (NFC) device. Reproduced with permission from ref 121 under CC BY. Copyright 2016 National Academy of Sciences. (b) Hemispherical electrically small antenna (ESA) with an outstanding quality factor. Reproduced with permission from ref 301. Copyright 2018Wiley. (c) Rolling assembly of tunable 3D magnetic micro-optics for the manipulation of high-energy electron beam. Reproduced with permission from ref 405 under CC BY. Copyright 2022 Springer Nature. (d) 3D micro-origami sensors capable of static mapping of the magnetic flux and dynamic tracking of magnetic objects in 3D space. Reproduced with permission from ref 98 under CC BY. Copyright 2022 Springer Nature. (e) Fully integrated tubular giant magnetoresistance (GMR) sensor that acts as a fluidic channel for in-flow detection of magnetic particles with high signal-to-noise ratio and sensitivity. Reproduced with permission from ref 148. Copyright 2011 American Chemical Society.

spatiotemporal recording. Furthermore, compliant 3D arc-shaped structures integrated with strain sensors were exploited to characterize engineered muscle tissues at the millimeter-scale,[287] offering high-sensitivity measurements of contractile forces and motions with temporal resolutions. Complex 3D microfluidic architectures were also manufactured for artificial vascular networks, indicating potential applications in 3D cell cultures, engineered tissues, and artificial organs.[147,236] Self-powered micro-oscillating systems with low power consumptions were also developed to mimic and replace nature's propulsion and pumping units at low Reynolds numbers,[328] offering open opportunities for the constructions of artificial lives.

6.1.3. Electronic Tissue Scaffolds. Mechanically-guided assembly methods have also driven the development of tissue engineering,[214,287,374,375] by creating electronic tissue scaffolds that are capable of *in situ* monitoring and stimulations. For example, through the buckling-guided assembly, a 3D flexible

https://doi.org/10.1021/acs.chemrev.3c00335
Chem. Rev. 2023, 123, 11137−11189

electronic device with a double-layer-cage configuration was fabricated and utilized as electronic cellular scaffolds for the engineering of dorsal root ganglion (DRG) neural networks (Figure 24a).[214] Particularly, such electronic scaffolds facilitated the growth of organized lamellae by providing electrical simulations in terms of capacitive charge injections. Photopatterned tubular biomimetic microvessels were prepared,[374] featuring enhanced endothelial longevity and nitric oxide production, making them promising platforms for investigations of microvascular pathobiology in human diseases like pulmonary hypertension (Figure 24b). Transparent tubular scaffolds, namely bioartificial endocrine pancreas (BAEP), were also developed to enable an efficient mass transport.[376] In addition, examinations of human mesenchymal stem cell migration, adhesion, and osteogenic differentiation were achieved through the use of flexible electronic tissue scaffolds (Figure 24c).[375] Furthermore, *in situ* studies of retinal pigment epithelium (RPE) cells were enabled by the development of spherical cap-shaped electronic cell scaffolds, featuring noninvasive monitoring of spatially distributed physiological activities, such as growth and apoptosis (Figure 24d).[138]

6.2. Biomedical Devices

6.2.1. *In Situ* Monitoring Devices. 3D flexible electronics manufactured through mechanically-guided methods have emerged as promising tools for *in vivo* monitoring of physiological signals for living organisms, such as tissues and organs.[132,191,280,286,302,310,377−384] For example, 3D piezoelectric microsystems (Figure 25a) were fabricated for implantable monitoring of muscle activities (e.g., trotting and climbing), providing platforms for *in vivo* biological interactions without obvious irritations or mechanical constraints.[132] Other 3D forms with high stretchabilities were exploited in wireless skin-compatible electronic sensors, enabling the tracking of spatial motions and the monitoring of electrophysiological signals.[280] Climbing-inspired twining electrodes based on shape memory effect of helical SMP structures,[310] were fabricated for peripheral neuromodulation (Figure 25b), which can reduce substantially mechanical and geometrical mismatches at the electrode-nerve interfaces. 3D multifunctional membranes[191] were designed for spatiotemporal cardiac measurements and stimulations across the entire epicardium. Such membranes could maintain a stable biotic/abiotic interface during cardiac cycles, standing as promising platforms for cardiac studies (Figure 25c). Additionally, other flexible electronics assembled through the use of mechanically-guided methods, such as biosupercapacitors[292] and physical sensors,[135,378] were also exploited for *in situ* monitoring.

6.2.2. *In Situ* Therapeutic Devices. Architected flexible electronic devices have also found immense potential in therapeutic applications, such as drug delivery[134,317,385−387] and pain management.[304,388−392] Many morphable microdevices with specific structural designs were utilized to fabricate microgrippers for *in situ* therapeutics, which can efficiently deliver drugs within biological lumens (e.g., the gastrointestinal (GI) tract).[134] For example, inspired by hookworms, microgrippers that can autonomously latch onto the mucosal tissue were manufactured (Figure 26a, left panel), rendering *in vivo* drug delivery performances of an almost 2-fold exposure (i.e., oral ketorolac tromethamine without the use of microgrippers, Figure 26a, middle panel) as well as a significantly enhanced retention (i.e., a 6-fold increase in the elimination half-life of a model analgesic, ketorolac tromethamine) (Figure 26a, right panel). Flexible electronic devices with rationally designed 3D shapes were also developed for pain management by blocking peripheral nerve activities.[304,388,393] For instance, bioresorbable curling flexible microfluidic devices, featuring precisely controlled delivery of cooling power at arbitrary depths in living tissues, stood as promising tools for pain blocking (Figure 26b).[388] Architected flexible electronic devices in 3D helical forms were also manufactured, featuring spontaneous constructions of conformal neural interfaces around small living nerves during the insertion.[304]

6.2.3. Surgical Instruments. Owing to the excellent conformability with the biological surfaces of organs, instrumented flexible devices for surgery were developed.[135,188,219,394−397] For instance, the pressing demand of functional integration for catheters in clinics pushed the development of miniaturized flexible electronic devices with various 3D architectures.[398−402] A multifunctional flexible surgical instrument in the form of a balloon catheter was developed,[188] capable of temperature sensing, mapping of cardiac electrophysiological signals with a high signal-to-noise (SNR) ratio of 60 dB, as well as *in situ* treatments using RF electrodes (maximum power 600 mW) for controlled, localized tissue ablations (temperature rise ∼10 °C) (Figure 26c). In particular, the use of such instruments in live animal models of rabbits was demonstrated. Harnessing a similar device configuration, integrated catheters for cardiac surgeries were further developed by researchers,[135] enabling high-density spatiotemporal mappings of temperature, pressure, and electrophysiological signals by three layers of 8 × 8 electrodes. Such an instrumented catheter is capable of performing programmable electrical stimulation, RF ablation, as well as electroporation (Figure 26d).

6.3. Electromagnetic Devices

6.3.1. 3D Antennas. Flexible 3D antennas with various structural configurations were developed through mechanically-guided methods.[121,139,301,322,403,404] For example, a 3D spiral inductor for near-field communication (NFC) was fabricated, exhibiting significantly enhanced Q factors and almost doubled voltages over a wide range of working angles (i.e., from 0° to 50°) when compared to devices in planar forms (Figure 27a).[121] Flexible hemispherical ESAs were also manufactured to offer ideal communication performances (Figure 27b).[301] In particular, the assembled ESA offered a high radiation efficiency of 83% and a tunable center frequencies upon stretching (i.e., 1.08−0.935 GHz). A morphable device in the form of folded 3D serpentines was also manufactured by the buckling-guided assembly, which can serve as robust antennas for telecommunications (i.e., very slight frequency change from 5.2 to 5.32 GHz during the 2D-to-3D transformation).[403] In addition, a bottom-up design strategy based on elementary reconfigurable structures of simple ribbon geometries was also developed, enabling demonstration of multimodal antennas with reconfigurable radiation patterns.[139] Furthermore, 3D RF/microwave transformers, consisting of tubular membrane arrays, were fabricated by rolling assembly, featuring an ultracompact device footprint and a performance-scalability that is in stark contrast with conventional 2D devices (i.e., the performance of 3D transformer increases with scaling, while 2D devices do not).[322]

6.3.2. Other Electromagnetic Devices. Other applications of mechanically assembled electromagnetic devices include micro/nano-magnets,[405−407] spectroscopies,[408] and electromagnetic sensors.[98,148,319,409] For instance, 3D magneti-

https://doi.org/10.1021/acs.chemrev.3c00335
Chem. Rev. 2023, 123, 11137−11189

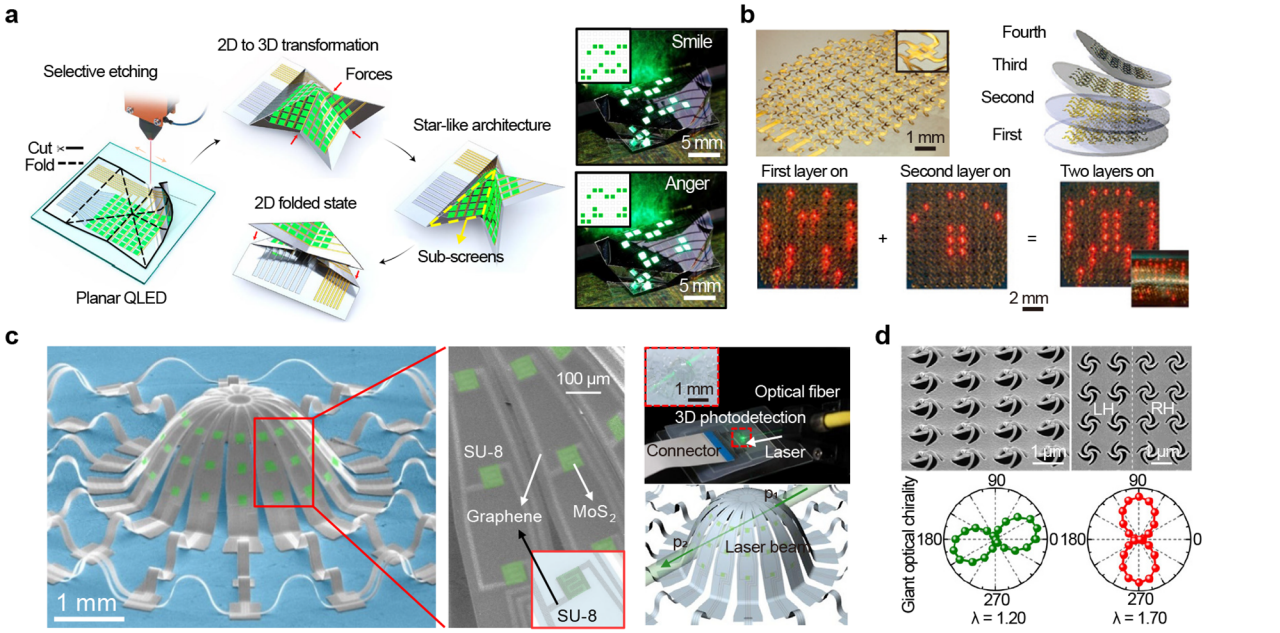

Figure 28. 3D optoelectronic devices. (a) Schematic illustration of the 3D foldable QLED display and experimental demonstrations. Reproduced with permission from ref 297. Copyright 2021 Springer Nature. (b) 3D flexible waterproof display composed of a stacked array of inorganic LEDs. Reproduced with permission from ref 45. Copyright 2010 Springer Nature. (c) 3D photodetection and imaging system that can simultaneously measure the light direction, intensity, and the incident angle. Reproduced with permission from ref 217 under CC BY. Copyright 2018 Springer Nature. (d) Residual-stress-induced assembly of 3D pinwheel-like nanostructures for the manipulation of the optical chirality. Reproduced with permission from ref 246 under CC BY. Copyright 2018 The American Association for the Advancement of Science.

cally charged particle optics in tubular forms were developed. Particularly, such particle optics can generate alternating magnetic fields of about ±100 mT with frequencies up to a hundred MHz, thereby providing adequate optical powers required for applications like electron beam deflection, focusing, and wavefront shaping (Figure 27c).[405] Furthermore, microcoils formed by rolling assembly were also integrated into microfluidic circuits for miniaturized nuclear magnetic resonance (NMR). Specifically, such tubular devices resulted in a reduction of background noise (by effective encapsulation) and a high filling factor of samples in the measurement domain, thereby rendering high-resolution chemical analysis of samples with tiny quantities.[408] In another case, folding assembly was utilized to fabricate high-density arrays of cubic magnetic sensors for the measurements of 3D magnetic vector fields.[98] Such arrays were also integrated into e-skins with embedded magnetic "hairs", enabling real-time multidirectional tactile perceptions (Figure 27d). Tubular giant magnetoresistance (GMR) devices were integrated with electronic fluidic systems,[319] enabling counting of magnetic objects by sensing their weak magnetic fields (Figure 27e)[148] and measurements of viscosity/velocity of fluids.[409]

6.4. Optoelectronic Devices

6.4.1. 3D Displays. Various flexible 3D displays were manufactured through mechanically-guided assembly.[45,297,410−416] Figure 28a presents a 3D foldable quantum dot light-emitting diodes (QLEDs) display that showed negligible illumination degradation under cycled folding deformations with extreme small bending radii.[297] Ultrathin displays of inorganic light-emitting diodes (LEDs) (i.e., AlInGaP) were manufactured, capable of integration with various unusual substrates, such as papers, Al foils, catheter balloons, and glass/plastic tubes and fibers (Figure 28b).[45] Furthermore, a 3D display consisting of a 7 × 7 micro-LED pixel array was manufactured, showing unaffected performance upon biaxial stretching up to 100%.[412]

Origami and kirigami designs were also exploited to enhance the conformability of 3D flexible displays.[410] For example, a kirigami-based wrapping method was developed for the fabrication of conformal electroluminescent (EL) devices on various curved surfaces.[320]

Morphable 3D displays were also achieved by the use of responsive substrates.[411,413] For example, a morphable display was manufactured by integrating electrically actuated substrates with LED arrays/EL materials, exhibiting unvaried illuminations during complex deformations.[411] Additionally, by the use of low melting point alloy (LMPA)-graphene nanoplatelets (GNPs)-elastomer composites, 3D morphable displays were also fabricated, featuring rapid electrothermal actuation capabilities and stable illuminations under various 3D configurations.[413]

6.4.2. 3D Devices for Photodetection and Light Manipulation. Various 3D flexible photodetectors were fabricated by the use of mechanically-guided assembly methods.[331,417,418] For example, as shown in Figure 28c, photodetectors in the forms of 3D domes exhibited unique structural superiorities, featuring the simultaneous measurement of both light intensity and incident angles.[217] Specifically, given the spatially distributed photoresponsive MoS_2 films, an incident light could illuminate different MoS_2 films from both the entry and exit sites, thereby resulting in increased photocurrents in the corresponding regions. Through imaging of these photoresponsive regions, the directions of incoming lights can be determined. Additionally, the spatial integration of various optoelectronic elements (e.g., n-channel Si NM MOSFETs, Si NM diodes, and p-channel silicon MOSFETs) with a variety of

https://doi.org/10.1021/acs.chemrev.3c00335
Chem. Rev. 2023, 123, 11137−11189

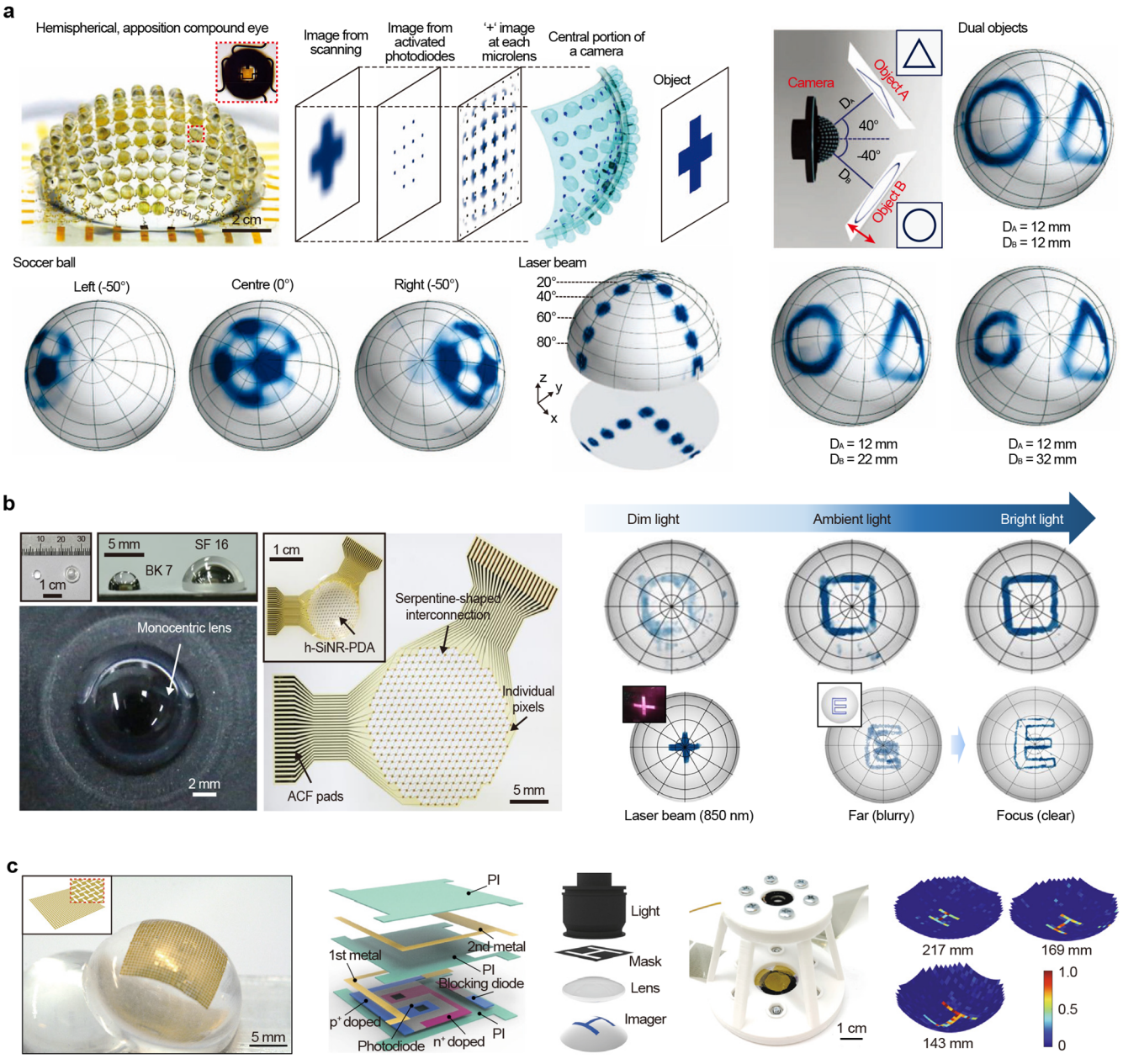

Figure 29. 3D electronic eye cameras. (a) Bioinspired designs of a hemispherical, apposition compound eye camera with wide field of view similar to typical insect. Reproduced with permission from ref 129. Copyright 2013 Springer Nature. (b) A bioinspired camera mimicking aquatic vision with improved sensitivity to incident light. Reproduced with permission from ref 426. Copyright 2020 Springer Nature. (c) Curvy shape-adaptive imagers based on ultrathin Si optoelectronic pixel arrays with a stretchable kirigami design. Reproduced with permission from ref 130. Copyright 2020 Springer Nature.

3D architectures (e.g., interconnected bridges, coils, and chiral structures) was also demonstrated, showing great potential for multimodal photodetection.[249] Furthermore, using folded cubic structures consisting of monolayer MoS_2, Au electrodes, and SU-8 supports, photodetectors capable of 3D angle-resolved photodetections were reported.[296] Tubular QWIPs were also developed, featuring omnidirectional detections of infrared radiations (e.g., with absorption wavelengths peaking at 3.6 and 6.5 μm) and imaging capabilities through photocurrent mappings.[293]

Additionally, architected flexible devices were also adopted to manipulate light interactions.[312,419,420] For example, a collective coupling of 3D confined optical modes for photodetections was enabled by monolithic twin microtube cavities formed through the rolling assembly of nanomembranes.[312] Nanoscale light confinements were also achieved at the hinges within folded cubic or polyhedral structures consisting of poly(methyl methacrylate) (PMMA) supported monolayer graphene.[294,421] By the use of residual-stress-induced folding assembly, flexible and morphable nano-kirigami devices were developed for light manipulation (Figure 28d).[246]

Mechanotunable 3D photonic structures, such as tunable optical filters[422] and metasurfaces,[419,423] were also enabled by mechanically-guided assembly methods, offering dynamic platforms for light manipulations. For example, through nonlinear buckling mechanics, a large-scale 3D array of

https://doi.org/10.1021/acs.chemrev.3c00335
Chem. Rev. 2023, 123, 11137−11189

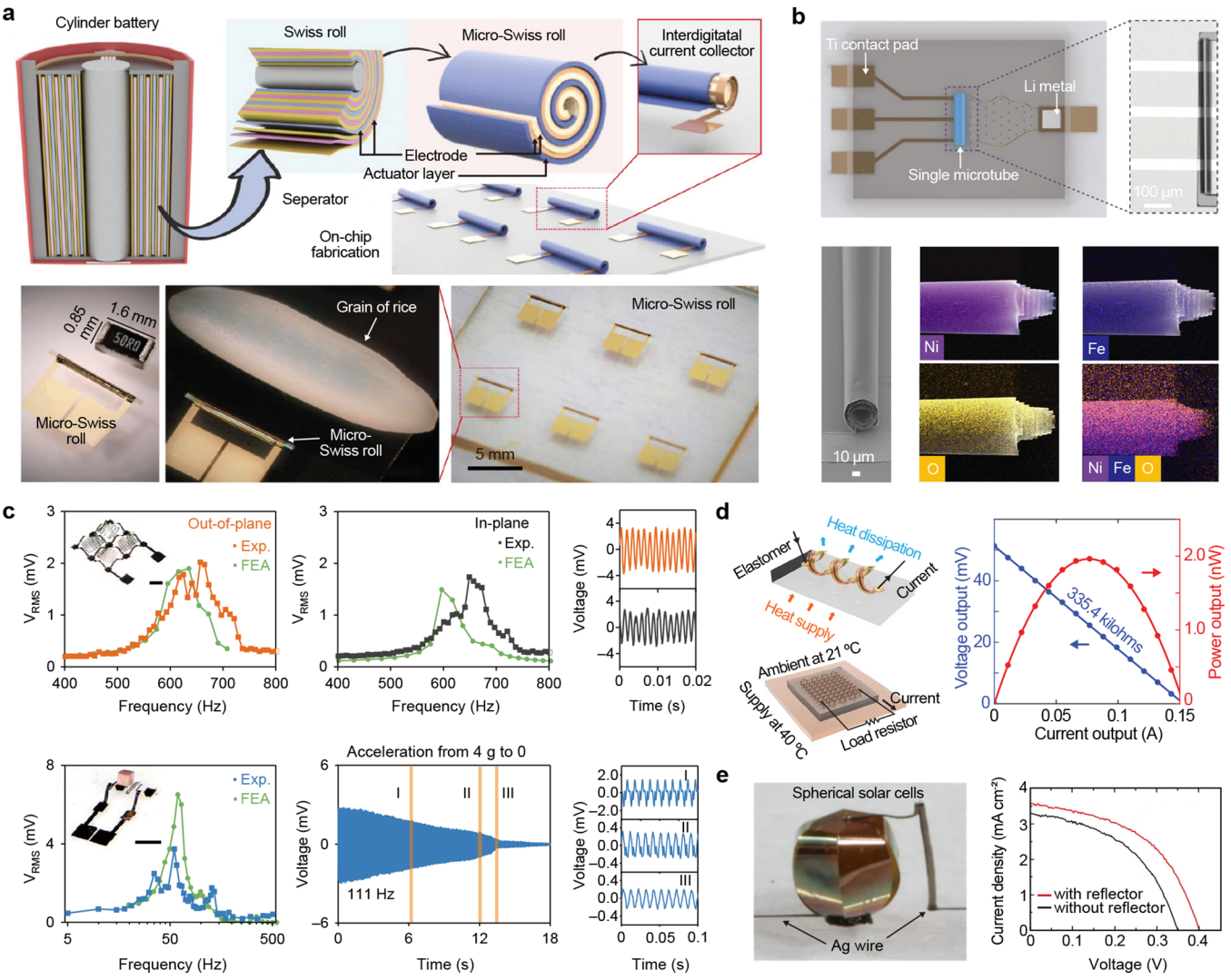

Figure 30. 3D energy devices. (a) Microbattery composed of 3D metal layer current collectors formed by a rolling assembly. Reproduced with permission from ref 314 under CC BY. Copyright 2022 Wiley. (b) A "Swiss-roll" microelectrode platform for *in situ* study of electrical conductivity, electrochemical reactions, and morphology evolution in battery electrodes. Reproduced with permission from ref 430 under CC BY. Copyright 2022 The American Association for the Advancement of Science. (c) 3D piezoelectric microdevice capable of efficiently harvesting low-frequency vibrational energies. Reproduced with permission from ref 132. Copyright 2019 Springer Nature. (d) Wearable energy harvesting system composed of 3D thermoelectric coils formed using buckling-guided assembly. Reproduced with permission from ref 289 under CC BY. Copyright 2018 The American Association for the Advancement of Science. (e) Spherical solar cells. Reproduced with permission from ref 357. Copyright 2009 National Academy of Sciences.

plasmonic nanodisks (several square centimeters) on elastomeric substrates was shown to be capable of reversibly shifting optical resonances over 600 nm within near-infrared range.[419] Nanophotonic electro-mechanical metasurfaces driven by electrostatic forces were demonstrated, featuring a tunable optical chirality in the near-infrared range with a modulation speed of more than 10 MHz.[423]

6.4.3. Eyeball Cameras. Cameras in forms of biomimetic 3D eyeballs can significantly improve the imaging performance by offering broadened field of views, reduced distortions, and decreased chromatic aberrations.[198,424] Various eyeball cameras manufactured using mechanically-guided assembly methods were reported.[100,101,129,130,187,197,246,414,425−427]

For example, paraboloid electronic eyeball cameras were fabricated through curving-induced assembly of flexible photodetector arrays on top of hemispherical surfaces, demonstrating improved uniformity of illuminations and well-performed focusing capabilities across a wide field of view, when compared with planar ones.[100] Inspired by the exceptionally wide fields of view, infinite depth of field, and high sensitivity to motions of a natural arthropod eye,[129] digital cameras in forms of apposition compound eyes were manufactured (Figure 29a), achieving a wider field of view (160°) with much fewer eye units (i.e., 180 units) than those of dragonflies and worker ants. Additionally, different superposition compound eyes (RSCEs) were designed to provide wide spectra of artificial reflections (from infrared to X-ray) with minimum chromatic aberrations, thereby enabling enhanced motion-tracking capabilities and high imaging qualities (i.e., the intensity ratio of the focused image to the background pattern can reach ∼5).[425] Notably, flexible photodetector arrays with other structural designs were also exploited to improve the conformability so as to facilitate the manufacturing of eyeball cameras.[187]

https://doi.org/10.1021/acs.chemrev.3c00335
Chem. Rev. 2023, 123, 11137−11189

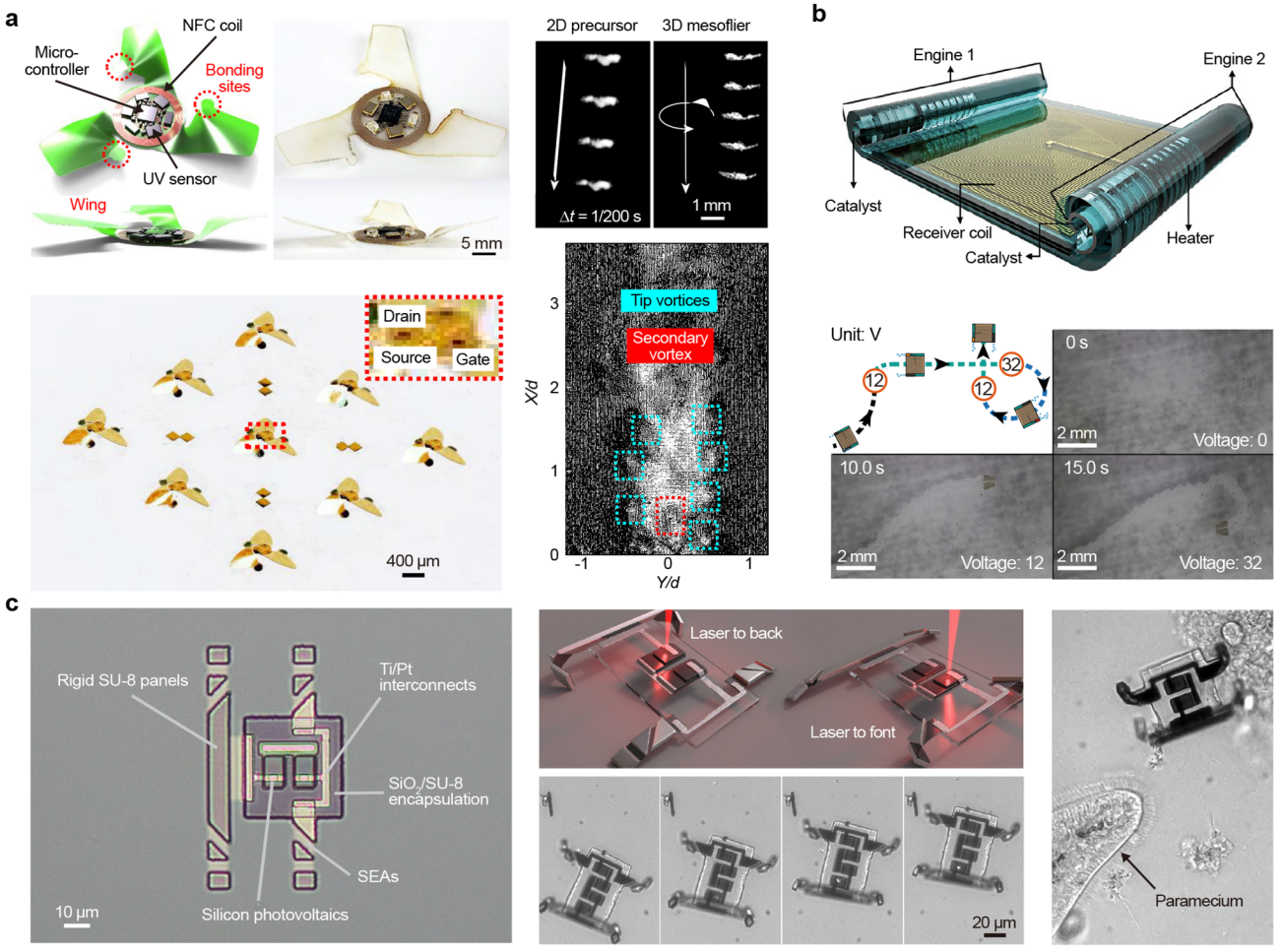

Figure 31. 3D fliers and aquatic robots. (a) Seed-inspired 3D electronic fliers with an integrated microsystem or a transistor, which exhibit stable rotational falling in the air. Reproduced with permission from ref 22. Copyright 2021 Springer Nature. (b) Wirelessly controlled swimming microrobot composed of rolled twin-jet-engines. Reproduced with permission from ref 15. Copyright 2020 Springer Nature. (c) Laser controlled microrobots consisting of 3D electrochemical actuators formed by using the rolling assembly. Reproduced with permission from ref 18. Copyright 2020 Springer Nature.

Apart from electronic compound eyes, eyeball cameras inspired by aquatic visions were reported as well.[426,427] For example, inspired by the vision of cichlid fish, miniaturized eyeball cameras (with a diameter of 11.5 mm) were developed, offering a large field of view (120°), a deep depth of field (20 cm), a low optical aberration, and a simple visual accommodation capability (Figure 29b).[426] Furthermore, a 3D eyeball camera inspired by the cuttlefish eye, consisting of a W-shaped pupil, a single ball lens, a surface-integrated flexible polarizer, and a highly integrated cylindrical silicon photodiode array that can maintain an average degree of polarization of ~78% in the visible wavelength range, was able to perform high-quality imaging under uneven illumination conditions.[427]

To improve the accommodation of cameras to the changes in the Petzval surface upon the use of different lenses, tunable hemispherical electronic eye camera systems with adjustable zooming capabilities were developed through curving-induced assembly.[101] In particular, these cameras employed deformable photodetector arrays on thin elastomeric membranes, which are capable of pneumatically controlled dynamic curvature adjustments. Additionally, origami[197] and kirigami[130] designs were also exploited for the manufacturing of hemispherical electronic eyes. For example, shape-adaptive imagers with kirigami designs were fabricated featuring high pixel fill factors (i.e., 78%), unvaried electrical performances under expansion, and focused views of objects at different distances with low aberrations. The adjustable optical focusing power of these electronic eyes ranges from 22.9 to 34.7 dioptres (dpt), surpassing the capability of the human eye (Figure 29c).[130]

6.5. Energy Devices

6.5.1. Microbatteries. Mechanically-guided 3D assembly has driven the development of various microbatteries[313−315,428−431] and supercapacitors.[291,432,433] For instance, spiral microelectrodes were prepared by residual-stress-induced rolling for lithium-ion microbatteries.[313] In detail, such spiral microbatteries featured tiny dimensions (i.e., a footprint area of around 1 mm^2), a relatively high maximum area capacity of 1053 $\mu Ah\ cm^{-2}$, an energy density of 12.6 $mWh\ cm^{-3}$, as well as a retention of 67% after 50 cycles. By the use of the rolling assembly, MnO_2-based microbatteries were prepared (Figure 30a), rendering enhanced overall performances of a footprint area of 0.75 mm^2, a reversible area capacity of 1 $mAh\ cm^{-2}$, as well as a retention of 50% after 600 cycles.[314]

Apart from microbatteries, microelectrodes were also manufactured and utilized as platforms for *in situ* character-

https://doi.org/10.1021/acs.chemrev.3c00335
Chem. Rev. 2023, 123, 11137−11189

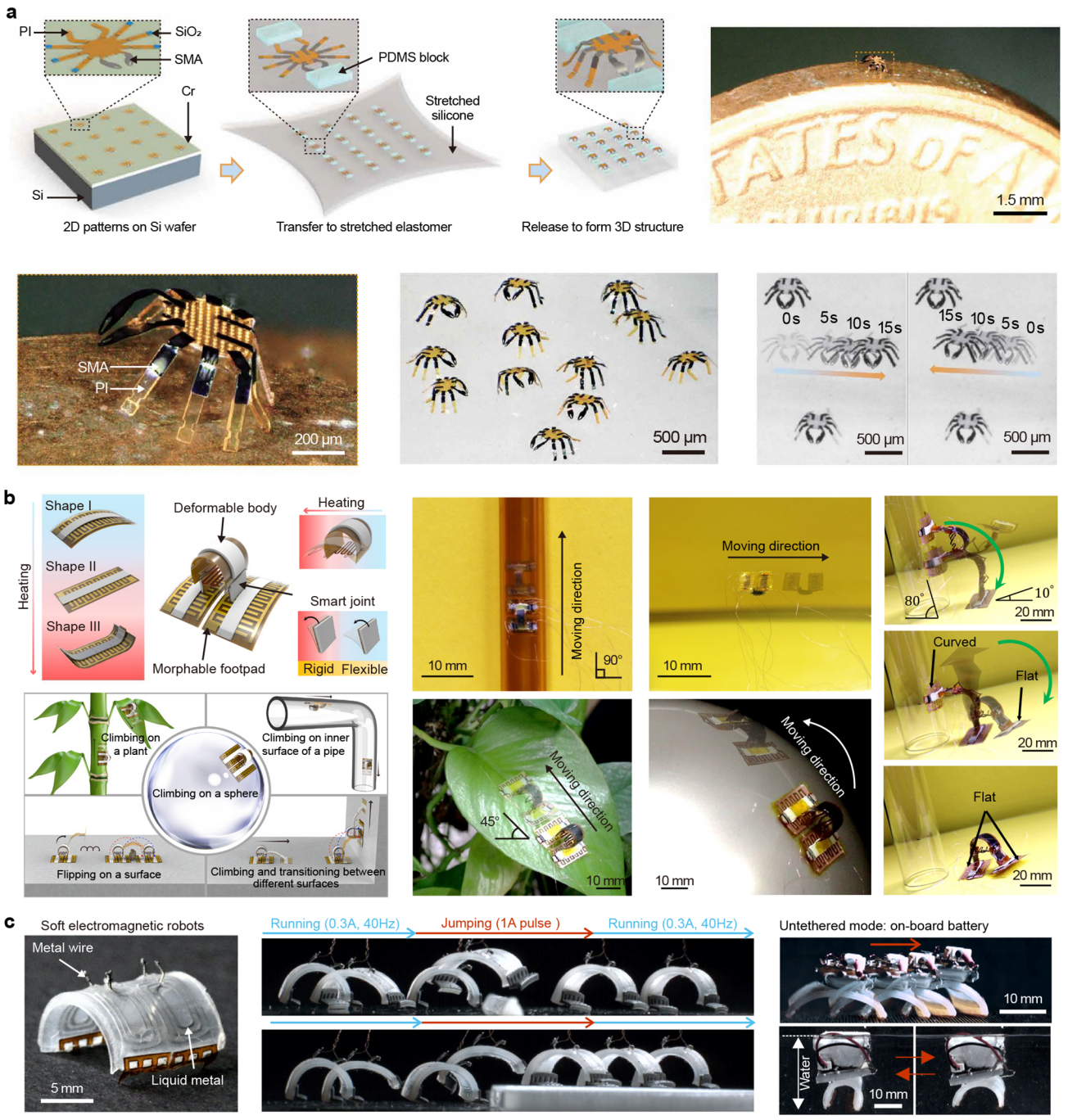

Figure 32. 3D terrestrial robots. (a) Submillimeter-scale terrestrial robots with heterogeneously integrated 3D mesostructures with a patterned SMA, a PI skeleton, and a SiO_2 shell. Reproduced with permission from ref 17. Copyright 2022 The American Association for the Advancement of Science. (b) Soft climbing microrobot capable of climbing on and transitioning between different curved surfaces. Reproduced with permission from ref 16 under CC BY. Copyright 2022 National Academy of Sciences. (c) Amphibious soft electromagnetic robot capable of walking, running, jumping, and swimming. Reproduced with permission from ref 442 under CC BY. Copyright 2022 Springer Nature.

izations of batteries (Figure 30b).[430] The elucidations of the role that Fe substitution played for conversion-type NiO battery were showcased as a model study through the monitoring of Fe_2O_3 evolution and solid electrolyte interphase layer, demonstrating great potentials of using such microelectrodes to probe electrochemistry within batteries.

Tubular supercapacitors were also fabricated by the use of mechanically-guided assembly approaches. For instance, a tubular microsupercapacitor (TMSC)[291] was demonstrated, featuring excellent overall performances of a footprint area of less than 0.8 mm^2, a capacitance of 88.6 mF cm^{-2}, an energy density of 28.69 mWh cm^{-2}, and a retention of 91.8% after 12,000 cycles.

6.5.2. Energy Harvesters. Transforming piezoelectric microsystems into 3D configurations using mechanically-guided assembly methods can enrich their operational modes[133,434,435] as well as offer improved energy harvesting performance.[132,436] For example, the integration of piezoelectric elements (i.e.,

https://doi.org/10.1021/acs.chemrev.3c00335
Chem. Rev. 2023, 123, 11137−11189

PVDF) with 3D structures of ultralow stiffnesses[437,438] allowed for energy harvesters with complex modes of vibrations, thereby achieving an enhanced energy harvesting performance (Figure 30c).[132] In particular, different vibrational modes, such as out-of-plane (vertical) and in-plane (lateral) modes, were achieved by the use of suspended 3D serpentine arrays, generating root-mean-square (RMS) voltages ranging from 1 to 2.02 mV under a frequency ranging from 600 to 700 Hz. In this work, a buckled bistable serpentine structure equipped with a proof mass was also manufactured, featuring the generation of electrical powers across a wide range of frequencies, spanning 2 orders of magnitude (from 5 to 500 Hz). Integrating thin-film thermoelectric materials (i.e., doped Si) with compliant 3D architectures allowed for efficient thermal impedance matching and increased power conversion efficiencies.[289,350,439] For example, a 3D flexible helical array (i.e., an 8 × 8 helical coils array) was prepared for thermoelectric energy harvesting (Figure 30d).[289] In particular, the open-circuit voltage generated by this thermoelectric harvester reached 51.3 mV subjected to a temperature difference of only 19 K, and the measured output power was 2 nW. In another case, a folded 3D photovoltaic (PV) device was capable of efficient light trapping, with a short-circuit current density of 3.6 mA cm^{-2} and a fill factor of 0.49 (Figure 30e).[357] Last by not least, graphene-based hydroelectric generators (GHEGs) in various 3D configurations could realize good energy harvesting performances by harnessing humidity gradients (i.e., with generated voltages of up to 1.5 V under the humidity variation of atmosphere).[229]

6.6. Robotics

3D electronic fliers hold great potential for environmental monitoring, population surveillance, and sensing applications that require volumetric coverage in 3D spaces. Inspired by wind-dispersed seeds, 3D macro-, meso-, and microscale electronic fliers were developed through buckling-guided assembly approaches, featuring controlled, rotational kinematics, and low terminal velocities.[22] Incorporations of active electronic and colorimetric materials on top of such 3D fliers allowed battery-free, wireless devices and colorimetric sensors for environmental analysis, such as measurements of particle matter (PM) pollution and pH values in the atmosphere (Figure 31a). Derived from the above, biodegradable 3D colorimetric fliers were also fabricated, allowing remote assessments of multiple environmental parameters such as pH values, heavy metal concentrations, ultraviolet exposures, humidity levels, as well as temperatures.[23] Furthermore, by integrating responsive materials (e.g., SMP) with such electronic fliers, morphable 3D mesofliers were developed, featuring large degrees of actuation deformations with a fast response time of 1.08 s.[131]

6.6.1. Electronic Fliers. 6.6.2. Aquatic Robots. Untethered aquatic robotic systems have important applications in biomedical fields, such as lab-on-a-chip devices, minimally invasive surgical interventions, among others.[318] For instance, through the rolling assembly associated with asymmetric designs of tilted head-flagellum geometries, arc-shaped microswimmers were manufactured, featuring bidirectional motions without the requirement of a reversal in the direction of the applied rotational magnetic field.[440] Additionally, by the use of morphable SMP substrates, aquatic robots were manufactured,[226] featuring remote control of switchable swimming modes through thermomechanical stimulations. Wirelessly powered flexible microjet systems with controlled locomotion modes were also developed (Figure 31b).[15] In particular, such systems can be remotely powered by inductive coupling, and their motions were driven by controlled catalytic reactions. Additionally, through the development of a novel type of voltage-driven foldable surface electrochemical actuators, a series of subhundred-micrometer robots were manufactured (Figure 31c).[18,441] Remarkably, the fabrication process was highly compatible with planar techniques, rendering the mass production of over one million robots on a 4 in. Si wafer.

6.6.3. Terrestrial Robots. Various terrestrial robots with diverse locomotion modes were developed by using mechanically-guided assembly methods. For example, submillimeter robots of various 3D geometries were developed[17] through the assembly of a patterned heterogeneous membrane consisting of a PI skeleton, SMA actuators, and a SiO_2 elastic encapsulation shell (Figure 32a). Owing to the rich diversity of structural designs, such robots could enable different locomotion modes under laser control, including crawling, walking, turning, and jumping. Soft microrobots, with a broad spectrum of architected 3D configurations and stiffness adjusting capabilities, were also manufactured through the buckling-guided assembly of LCE composites (i.e., enabling large degrees of 3D-to-3D shape morphing) (Figure 32b).[16] In particular, such soft microrobots were equipped with morphable electroadhesive footpads (Figure 32b, bottom left) and stiffness-variable smart joints, enabling different locomotion modes in a single microrobot, including climbing on complexly curved walls (e.g., wedge-shaped, cylindrical, spherical, and wavy surfaces) as well as transitioning between two distinct surfaces. Through the use of the roll assembly, electromagnetically controlled soft robots were manufactured, capable of walking, running, swimming, jumping, steering, and transporting cargos (Figure 32c).[442] In addition, origami-inspired designs were also introduced to fabricate robots through the folding assembly, rendering controlled transformations from flat sheets into functional robots.[175,443] Furthermore, insect-scale fast-moving and ultra-robust soft robots were also developed by curving-induced assembly of unimorph piezoelectric structures, exhibiting a high moving speed of 20 body lengths per second.[19]

7. CONCLUSIONS AND OUTLOOKS

During the last two decades, the field of flexible/stretchable electronics has been growing very rapidly, sparking significant interests in the contemporary society, spanning diverse industrial and research areas (e.g., IoT, daily healthcare, robotics, fundamental biology, medicine, energy, sensors, etc.). Originated by pioneer works in organic electronics[1] and structurally engineered inorganic electronics,[103] flexible/stretchable electronics well pronounce the future needs and directions of electronic devices from divergent points of views. Fruitful research works have been conducted, demonstrating plentiful 3D flexible electronic devices,[34,35,106] fabrication protocols for functional circuits on 3D curved surfaces,[102,138,201] stretchable standalone device platforms,[17,203,228] and so on. Among the various promising directions of the vibrant field, 3D flexible electronics represent a core branch, owing to their unique structure-induced functionalities, expanded design freedoms, and capabilities of better conforming to or replicating complexly shaped biological objects, when compared with planar counterparts. Compatible with well-established fabrication techniques of planar inorganic flexible electronics,[35,104,106] mechanically-guided 3D assembly methods stand as powerful tools for the manufacturing of architected 3D flexible electronics with precisely engineered structural configurations and

https://doi.org/10.1021/acs.chemrev.3c00335
Chem. Rev. 2023, 123, 11137−11189

Table 2. Summary of Representative Architected Flexible Devices Prepared through Mechanically-Guided 3D Assembly Methods

Applications	Devices	Assembly methods	Device forms	Structure-induced functionalities	Superiorities comparing to planar counterparts	Reference
Cell devices	Inter/intracellular recorders	Buckling	3D arc-shaped	Vertically directed sensing diodes with predesigned locations	High density measurements of transmembrane potential at multiple locations	325
	Single cell microgrippers	Folding	Polyhedral	Conformal cell capture enabled by folded gripper arms	Nondestructive and real-time analysis of 3D surface of cell	184, 372
Organoid devices	3D electronic frameworks	Buckling	Conformally wrapping	Compliant 3D electronic neural interface in conformal geometries	3D spatiotemporal mapping of spontaneous neural activities	127
	Shell microelectrode arrays	Folding	Polyhedral	3D conformal shells with tunable contact area between electrode and target	3D spatiotemporal recording of encapsulated organoids with large contact area	128
Electronic tissue scaffolds	Spherical cap-shaped electronic cell scaffold	Buckling	Hemispherical	Creation of biomimetic 3D microenvironments	Noninvasive real-time investigations of cell activities	138
	Tubular scaffolds	Rolling	Tubular	Biomimetic tubular structures with multilayer walls	Enhanced viability and precise multicellular layering of artificial arteries	375
In situ monitoring devices	Piezoelectric microsystems	Buckling	3D arc-shaped	3D compliant thin piezoelectric structure with high sensitivity to external forces	Enhanced signals with high reproducibility for differentiating various motion states	132
	Climbing-inspired twining electrodes	Rolling	3D helical	Twining electrode capable of self-climbing along nerves	Conformal neural interface for electrical stimulation and recording	310
	3D multifunctional membranes	Curving	Conformal curvilinear	3D conformal electronic membranes	Epicardial mapping and stimulation with a mechanically stable interface during normal cardiac cycles	191
In situ therapeutic devices	"Hookworms" microgrippers	Folding	Worms-mouthparts-shaped	Foldable sharp microtips that ensure effective latching onto the GI mucosa	Enhanced drug delivery performances enabled by controlled long-term residency	134
	Pain-blocking microfluidic devices	Rolling	3D helical	Soft, curled, nerve-clasping microfluidic channels with secure sutureless attachment to nerves	Long-term *in situ* pain relief through neural cooling	388
Surgical instruments	Instrumented catheter	Curving	Complex curvilinear	3D conformal electronic interfaces	High-density spatiotemporal mappings of multiple biological signals and surgical operations	135, 158
3D electromagnetic devices	Hemispherical/spherical ESAs	Buckling	Hemispherical	High volume occupation of the Chu-sphere	Wireless communication with enhanced Q factors and broadened working angles	301, 404
	3D magnetically charged particle optics	Rolling	Tubular	Self-rolling tubular microsized electromagnets	Fast beam manipulation	405
	Cubic magnetic sensors	Folding	Polyhedral	Spatial rearrangement of sensing elements through self-folding	Simultaneous measurements of three magnetic field components in 3D space	98
3D displays	Foldable quantum dot light-emitting	Folding	Polyhedral	3D foldable QLEDs in origami forms enabled by customized creases	3D reconfigurable displays	297
	Ultrathin inorganic light-emitting diodes	Curving	Complex curvilinear	3D arrangement of multilayer LED arrays	3D multilayer displays that can be integrated on various unusual substrates	45
3D devices for photodetection and Light manipulation	3D photodetectors	Buckling	Hemispherical	Spatial arrangement of photodetectors	Simultaneous measurements of the direction, intensity and angular divergence of incident light	217
	Nano-kirigami metasurface	Folding	Kirigami	Out-of-plane configurations of plasmonic materials	Giant intrinsic optical chirality	246
Eyeball cameras	Compound eyes cameras	Curving	Hemispherical	Bioinspired spatial arrangements of optical elements on hemispherical surfaces	Wide field of view, low levels of chromatic aberrations and deep depth of field	129
	Aquatic eyeball cameras	Curving	Hemispherical			426, 427
	Tunable hemispherical electronic eye camera	Curving	Hemispherical	Tunable ultrathin kirigami membranes consisting of optoelectronic pixels	Imaging of objects at different distances with low aberration	130
Microbatteries	Spiral microbatteries and microelectrodes	Rolling	Tubular	3D stacking of electrode materials	High loadings of electrode materials with reduced footprint area	313, 314
Energy harvesters	Piezoelectric element 3D structures	Buckling	3D arc-shaped	3D compliant piezoelectric structure with multiple vibration modes	High power output under wide range of frequencies	132
	3D flexible thermoelectric helical array	Buckling	3D helical	Enlarged temperature gradients through creations of altitude intercept	Enhanced heat exchange efficiency and output power	289

https://doi.org/10.1021/acs.chemrev.3c00335
Chem. Rev. 2023, 123, 11137−11189

Table 2. continued

Applications	Devices	Assembly methods	Device forms	Structure-induced functionalities	Superiorities comparing to planar counterparts	Reference
Robotics	Electronic fliers	Buckling	Shapes resembling wind-dispersed seeds	Rotational falling and low terminal velocities	Flying with controlled rotational kinematics and enhanced stability	22
	Aquatic robots	Rolling	Tubular	Construction of tubular jet propulsion engines	Untethered multimodal swimming in a controlled manner	15
	Wall-climbing robot	Buckling	3D arc-shaped	Reconfigurable 3D structures capable of large deformations	Multiple locomotion modes	16

functionalities.[138,300] Though the primary goal of mechanically-guided assembly methods (i.e., rolling, folding, curving and buckling) is to manufacture miniaturized flexible electronic devices from nano- to millimeter-scale, many examples have showcased that the mechanically-guided assembly methods, such as the rolling, folding and buckling, are capable of parallel manufacturing of multiple devices/systems/structures in one round.[96,119,249,444] Notably, herein, to establish a clear material−fabrication−performance−application relationship, a detailed comparison table (Table 2) summarizing the used assembly methods, device forms, structure-induced functionalities, superiorities comparing to their planar counterparts, and applications of various architected 3D flexible devices is presented. Despite significant progress summarized above, rich opportunities exist in this burgeoning area of architected 3D flexible electronics, as detailed below.

7.1. Routes to Extremes: Deformations and Dimensions

Through creative uses of the mechanics of materials and structures, mechanically-guided assembly methods transform the as-prepared planar electronic devices into deterministic 3D architectures, achieving many previously inaccessible (or hard-to-achieve) structure-induced functionalities such as the 3D integration with programmable spatial resolution, omnidirectional photoenergy harvesting, and morphological/structural evolution.

Two core aspects of mechanically-guided methods for 3D device assembly are how complicated the accessible deformations can be (i.e., complexity and diversity of deformations) and to what extent each deformation mode can reach (i.e., magnitudes of deformations). Although many basic deformation modes (i.e., bending, folding, twisting, shearing, and buckling) are already exploited in mechanically-guided assembly methods, combined deformation modes applied in desired sequences are rarely achieved due to technical challenges to implement the mechanical loadings experimentally. In addition, the magnitudes of each deformation mode are not yet pushed to extreme. For example, an extreme rolling process might result in tubular structures with ultracompact walls and supersmall diameters of only several manometers; a buckling-guided assembly with huge biaxial prestrains (e.g., 1000%) might generate a device with extreme expansion ratios. To achieve extreme deformations in mechanically-guided 3D assembly, developments of experimental platforms with powerful loading capabilities as well as artificial intelligence boosted topology optimization methods of 2D precursors and substrates are promising to explore.

The manufacturing of well-defined 3D nanostructures with unique physical and chemical properties stands as the long-term goal for nanofabrication methods, and mechanically-guided assembly methods are no exception. Although several initial trials have been conducted using mechanically-guided assembly, only 3D nanostructures with very simple geometric configurations were formed.[126,221,242] Therefore, developments of nanoscale assembly approaches that allow the manufacturing of 3D nanoarchitectures with complex geometric configurations stand as a vital direction in this field. Such fabrication capabilities with nanoscale precision are expected to give rise to architected flexible electronic devices with fundamentally new functions.

7.2. Inverse Design Methods

Powerful inverse design methods that can rapidly map target 3D geometries onto optimized 2D precursor patterns and give required loading forms/magnitudes are foundational to the widespread utility of mechanically-guided assembly methods.

https://doi.org/10.1021/acs.chemrev.3c00335
Chem. Rev. 2023, 123, 11137−11189

Very recently, by introducing microlattice designs and tuning their local stiffnesses through a tailored porosity distribution, an inverse design method assisted by machine learning algorithms was developed for the buckling-guided assembly, capable of replicating many 3D curved surfaces in biology.[300] However, the nature of the 2D-to-3D assembly and in-plane loadings set certain limitations to the range of accessible 3D geometries. Plenty of open opportunities lie in devising novel inverse design strategies with the assistance of artificial intelligence under the framework of mechanically-guided methods. For example, the two-level inverse design that involves concurrent optimization of kirigami cuts at a global level and microlattice patterns at a local level can well expand the range of inversely designed 3D geometries and is very exciting to explore.

7.3. Encapsulation Strategies

Encapsulation is the key to ensuring the secure and stable operation of flexible electronic devices. The existing encapsulation methods of flexible electronics mostly exploit polymeric materials such as PI and silicone elastomers (e.g., PDMS). These encapsulations are simple and efficient for planar flexible electronics. When turning to those emerging architected 3D flexible electronics that have certain components popping up from the substrate surface,[238,240,280] such encapsulation methods are no longer applicable. For example, to allow free out-of-plane deformations of serpentine interconnects, an encapsulation approach harnessing the excellent stretchability of soft network materials (i.e., both uni- and biaxial) can be exploited.[333,445−447] However, the reported encapsulation strategies are just the tip of the whole iceberg. Exciting opportunities lie in the developments of new encapsulation strategies that pose significantly reduced mechanical constraints to the functional 3D architectures while providing effective protection.

7.4. Applications

Flexible electronics assembled using mechanically-guided approaches have already found applications in diverse fields, including biology, medicine, sensing, energy, robotics, and so on. On the one hand, the exploration of new application scenarios and areas (e.g., catalysis, deep space exploration, and nonlinear optics) of architected 3D flexible devices stands as a mainstream research direction in the field. On the other hand, the discovery of more structure-induced functionalities is instrumental to expand the applications of architected flexible electronics. For example, the incorporation of rationally distributed local metasurfaces in a designed 3D architecture to achieve controlled coupling of electromagnetic waves into desired functional elements is worthy of investigation.

AUTHOR INFORMATION

Corresponding Author

Yihui Zhang − *Applied Mechanics Laboratory, Department of Engineering Mechanics, Tsinghua University, 100084 Beijing, People's Republic of China; Laboratory of Flexible Electronics Technology, Tsinghua University, 100084 Beijing, People's Republic of China;* orcid.org/0000-0003-0885-2067; Email: yihuizhang@tsinghua.edu.cn

Authors

Renheng Bo − *Applied Mechanics Laboratory, Department of Engineering Mechanics, Tsinghua University, 100084 Beijing, People's Republic of China; Laboratory of Flexible Electronics Technology, Tsinghua University, 100084 Beijing, People's Republic of China*

Shiwei Xu − *Applied Mechanics Laboratory, Department of Engineering Mechanics, Tsinghua University, 100084 Beijing, People's Republic of China; Laboratory of Flexible Electronics Technology, Tsinghua University, 100084 Beijing, People's Republic of China;* orcid.org/0000-0002-3047-0252

Youzhou Yang − *Applied Mechanics Laboratory, Department of Engineering Mechanics, Tsinghua University, 100084 Beijing, People's Republic of China; Laboratory of Flexible Electronics Technology, Tsinghua University, 100084 Beijing, People's Republic of China*

Complete contact information is available at: https://pubs.acs.org/10.1021/acs.chemrev.3c00335

Author Contributions

[§]R.B., S.X., and Y.Y contributed equally to this work. CRediT: **Renheng Bo** visualization, writing-original draft, writing-review & editing; **Shiwei Xu** visualization, writing-original draft; **Youzhou Yang** visualization, writing-original draft; **Yihui Zhang** supervision, writing-review & editing.

Notes

The authors declare no competing financial interest.

Biographies

Renheng Bo obtained his Ph.D. (2020) in Materials Science and Nanotechnology from Research School of Engineering at the Australian National University. He is currently a postdoctoral fellow at Tsinghua University, with research interests involving multifunctional architected flexible electronics, biomedical devices, and mechanically-guided 3D assembly.

Shiwei Xu obtained his B.S. degree in Engineering Mechanics from Huazhong University of Science and Technology, China, in 2020. He is currently pursuing his Ph.D. degree in Solid Mechanics at Tsinghua University, focusing on mechanically-guided 3D assembly for soft robotics and reconfigurable electronics, under the supervision of Prof. Yihui Zhang.

Youzhou Yang obtained both his B.S. degree in Electronic Science and Technology and M.E. in Microelectronics and Solid State Electronics from Huazhong University of Science and Technology, China, in 2018 and 2022, respectively. Under the supervision of Prof. Yihui Zhang, he is currently pursuing his Ph.D. degree in Solid Mechanics at Tsinghua University, focusing on mechanically-guided 3D assembly for magnetically controlled microscale biorobotics and organoid/tissues engineering.

Yihui Zhang obtained his Ph.D. (2011) in Solid Mechanics from the Department of Engineering Mechanics at Tsinghua University. Then he worked as a postdoctoral fellow from 2011 to 2014 and as a research assistant professor from 2014 to 2015, both at Northwestern University. He is a professor of engineering mechanics and vice director of the Laboratory of Flexible Electronics Technology at Tsinghua University. His research interests include mechanically-guided 3D assembly, unusual soft composite materials, and stretchable electronics.

ACKNOWLEDGMENTS

Y.Z. acknowledges support from the National Natural Science Foundation of China (Grant Nos. 12225206, 12050004, and 11921002), the Tsinghua National Laboratory for Information Science and Technology, a grant from the Institute for Guo Qiang, Tsinghua University (Grant No. 2021GQG1009), and

the New Cornerstone Science Foundation through the XPLORER PRIZE. R.B. gratefully acknowledges support from the National Natural Science Foundation of China (Grant No. 12102221), and China Postdoctoral Science Foundation for the fellowships (Grant Nos. 2021M691795 and 2022T150361).

LIST OF ABBREVIATIONS

PDMS	Polydimethylsiloxane
LCE	Liquid crystal elastomer
SMA	Shape memory alloy
FIB	Focused ion beam
SMP	Shape memory polymer
TFFA	Thin film-shaped flexible actuator
PI	Polyimide
PVDF	Polyvinylidene fluoride
PZT	Lead zirconium titanate
CN	Carbon nanotube
RF	Radiofrequency
FEA	Finite element analyse
QWIP	Quantum well infrared photodetector
nBSC	Nano-biosupercapacitor
QLED	Quantum dot light-emitting diode
ESA	Electrically small antenna
IoT	Internet of Things
VOC	Volatile organic compound
PEC	Photoelectrochemical
FET	Field-effect transistor
MT-SERS	Mechanical trapping and surface-enhanced Raman spectroscopy
MEA	Microelectrode array
DRG	Dorsal root ganglion
BAEP	Bioartificial endocrine pancreas
RPE	Retinal pigment epithelium
GI	Gastrointestinal
NFC	Near-field communication
NMR	Nuclear magnetic resonance
GMR	Giant magnetoresistance
EL	Electroluminescent
LMPA	Low melting point alloy
GNP	Graphene nanoplatelet
PMMA	Poly(methyl methacrylate)
RSCE	Reflecting superposition compound eye
TMSC	Tubular microsupercapacitor
RMS	Root-mean-square
PV	Photovoltaic
GHEG	Graphene-based hydroelectric generator
PM	Particle matter

REFERENCES

(1) Garnier, F.; Hajlaoui, R.; Yassar, A.; Srivastava, P. All-Polymer Field-Effect Transistor Realized by Printing Techniques. *Science* **1994**, *265*, 1684−1686.

(2) Rogers, J. A.; Someya, T.; Huang, Y. Materials and Mechanics for Stretchable Electronics. *Science* **2010**, *327*, 1603−1607.

(3) Chung, H. U.; Kim, B. H.; Lee, J. Y.; Lee, J.; Xie, Z.; Ibler, E. M.; Lee, K.; Banks, A.; Jeong, J. Y.; Kim, J.; et al. Binodal, Wireless Epidermal Electronic Systems with in-Sensor Analytics for Neonatal Intensive Care. *Science* **2019**, *363*, No. eaau0780.

(4) Chen, G.; Li, Y.; Bick, M.; Chen, J. Smart Textiles for Electricity Generation. *Chem. Rev.* **2020**, *120*, 3668−3720.

(5) Chen, G.; Xiao, X.; Zhao, X.; Tat, T.; Bick, M.; Chen, J. Electronic Textiles for Wearable Point-of-Care Systems. *Chem. Rev.* **2022**, *122*, 3259−3291.

(6) Wang, C.; Chen, X.; Wang, L.; Makihata, M.; Liu, H.-C.; Zhou, T.; Zhao, X. Bioadhesive Ultrasound for Long-Term Continuous Imaging of Diverse Organs. *Science* **2022**, *377*, 517−523.

(7) Hu, H.; Ma, Y.; Gao, X.; Song, D.; Li, M.; Huang, H.; Qian, X.; Wu, R.; Shi, K.; Ding, H.; et al. Stretchable Ultrasonic Arrays for the Three-Dimensional Mapping of the Modulus of Deep Tissue. *Nat. Biomed. Eng.* **2023**. DOI: 10.1038/s41551-023-01038-w

(8) Kim, J.-H.; Marcus, C.; Ono, R.; Sadat, D.; Mirzazadeh, A.; Jens, M.; Fernandez, S.; Zheng, S.; Durak, T.; Dagdeviren, C. A Conformable Sensory Face Mask for Decoding Biological and Environmental Signals. *Nat. Electron.* **2022**, *5*, 794−807.

(9) Jiang, S.; Liu, J.; Xiong, W.; Yang, Z.; Yin, L.; Li, K.; Huang, Y. A Snakeskin-Inspired, Soft-Hinge Kirigami Metamaterial for Self-Adaptive Conformal Electronic Armor. *Adv. Mater.* **2022**, *34*, 2204091.

(10) Awad, L. N.; Bae, J.; O'Donnell, K.; De Rossi, S. M. M.; Hendron, K.; Sloot, L. H.; Kudzia, P.; Allen, S.; Holt, K. G.; Ellis, T. D.; et al. A Soft Robotic Exosuit Improves Walking in Patients after Stroke. *Sci. Transl. Med.* **2017**, *9*, No. eaai9084.

(11) Yang, Y.; Song, Y.; Bo, X.; Min, J.; Pak, O. S.; Zhu, L.; Wang, M.; Tu, J.; Kogan, A.; Zhang, H.; et al. A Laser-Engraved Wearable Sensor for Sensitive Detection of Uric Acid and Tyrosine in Sweat. *Nat. Biotechnol.* **2020**, *38*, 217−224.

(12) Wang, M.; Yang, Y.; Min, J.; Song, Y.; Tu, J.; Mukasa, D.; Ye, C.; Xu, C.; Heflin, N.; McCune, J. S.; et al. A Wearable Electrochemical Biosensor for the Monitoring of Metabolites and Nutrients. *Nat. Biomed. Eng.* **2022**, *6*, 1225−1235.

(13) Wu, S.; Moody, K.; Kollipara, A.; Zhu, Y. Highly Sensitive, Stretchable, and Robust Strain Sensor Based on Crack Propagation and Opening. *ACS Appl. Mater. Interfaces.* **2023**, *15*, 1798−1807.

(14) Hu, H.; Zhu, X.; Wang, C.; Zhang, L.; Li, X.; Lee, S.; Huang, Z.; Chen, R.; Chen, Z.; Wang, C.; et al. Stretchable Ultrasonic Transducer Arrays for Three-Dimensional Imaging on Complex Surfaces. *Sci. Adv.* **2018**, *4*, No. eaar3979.

(15) Bandari, V. K.; Nan, Y.; Karnaushenko, D.; Hong, Y.; Sun, B.; Striggow, F.; Karnaushenko, D. D.; Becker, C.; Faghih, M.; Medina-Sánchez, M.; et al. A Flexible Microsystem Capable of Controlled Motion and Actuation by Wireless Power Transfer. *Nat. Electron.* **2020**, *3*, 172−180.

(16) Pang, W.; Xu, S.; Wu, J.; Bo, R.; Jin, T.; Xiao, Y.; Liu, Z.; Zhang, F.; Cheng, X.; Bai, K.; et al. A Soft Microrobot with Highly Deformable 3d Actuators for Climbing and Transitioning Complex Surfaces. *Proc. Natl. Acad. Sci. U.S.A.* **2022**, *119*, No. e2215028119.

(17) Han, M.; Guo, X.; Chen, X.; Liang, C.; Zhao, H.; Zhang, Q.; Bai, W.; Zhang, F.; Wei, H.; Wu, C.; et al. Submillimeter-Scale Multimaterial Terrestrial Robots. *Sci. Robot.* **2022**, *7*, No. eabn0602.

(18) Reynolds, M. F.; Cortese, A. J.; Liu, Q.; Zheng, Z.; Wang, W.; Norris, S. L.; Lee, S.; Miskin, M. Z.; Molnar, A. C.; Cohen, I.; et al. Microscopic Robots with Onboard Digital Control. *Sci. Robot.* **2022**, *7*, No. eabq2296.

(19) Wu, Y.; Yim, J. K.; Liang, J.; Shao, Z.; Qi, M.; Zhong, J.; Luo, Z.; Yan, X.; Zhang, M.; Wang, X.; et al. Insect-Scale Fast Moving and Ultrarobust Soft Robot. *Sci. Robot.* **2019**, *4*, No. eaax1594.

(20) Li, S.; Xu, J.; Li, R.; Wang, Y.; Zhang, M.; Li, J.; Yin, S.; Liu, G.; Zhang, L.; Li, B.; et al. Stretchable Electronic Facial Masks for Sonophoresis. *ACS Nano* **2022**, *16*, 5961−5974.

(21) Yu, C.-C.; Shah, A.; Amiri, N.; Marcus, C.; Nayeem, M. O. G.; Bhayadia, A. K.; Karami, A.; Dagdeviren, C. A Conformable Ultrasound Patch for Cavitation-Enhanced Transdermal Cosmeceutical Delivery. *Adv. Mater.* **2023**, *35*, 2300066.

(22) Kim, B. H.; Li, K.; Kim, J. T.; Park, Y.; Jang, H.; Wang, X.; Xie, Z.; Won, S. M.; Yoon, H. J.; Lee, G.; et al. Three-Dimensional Electronic Microfliers Inspired by Wind-Dispersed Seeds. *Nature* **2021**, *597*, 503−510.

(23) Yoon, H.-J.; Lee, G.; Kim, J.-T.; Yoo, J.-Y.; Luan, H.; Cheng, S.; Kang, S.; Huynh, H. L. T.; Kim, H.; Park, J.; et al. Biodegradable, Three-Dimensional Colorimetric Fliers for Environmental Monitoring. *Sci. Adv.* **2022**, *8*, No. eade3201.

https://doi.org/10.1021/acs.chemrev.3c00335
Chem. Rev. 2023, 123, 11137−11189

(24) Savagatrup, S.; Printz, A. D.; O'Connor, T. F.; Zaretski, A. V.; Lipomi, D. J. Molecularly Stretchable Electronics. *Chem. Mater.* **2014**, *26*, 3028−3041.
(25) Root, S. E.; Savagatrup, S.; Printz, A. D.; Rodriquez, D.; Lipomi, D. J. Mechanical Properties of Organic Semiconductors for Stretchable, Highly Flexible, and Mechanically Robust Electronics. *Chem. Rev.* **2017**, *117*, 6467−6499.
(26) Choi, S.; Han, S. I.; Kim, D.; Hyeon, T.; Kim, D. H. High-Performance Stretchable Conductive Nanocomposites: Materials, Processes, and Device Applications. *Chem. Soc. Rev.* **2019**, *48*, 1566−1596.
(27) Park, S.; Heo, S. W.; Lee, W.; Inoue, D.; Jiang, Z.; Yu, K.; Jinno, H.; Hashizume, D.; Sekino, M.; Yokota, T.; et al. Self-Powered Ultra-Flexible Electronics Via Nano-Grating-Patterned Organic Photovoltaics. *Nature* **2018**, *561*, 516−521.
(28) Wang, S.; Xu, J.; Wang, W.; Wang, G. N.; Rastak, R.; Molina-Lopez, F.; Chung, J. W.; Niu, S.; Feig, V. R.; Lopez, J.; et al. Skin Electronics from Scalable Fabrication of an Intrinsically Stretchable Transistor Array. *Nature* **2018**, *555*, 83−88.
(29) Zheng, Y.; Zhang, S.; Tok, J. B.; Bao, Z. Molecular Design of Stretchable Polymer Semiconductors: Current Progress and Future Directions. *J. Am. Chem. Soc.* **2022**, *144*, 4699−4715.
(30) Nawaz, A.; Merces, L.; Ferro, L. M. M.; Sonar, P.; Bufon, C. C. B. Impact of Planar and Vertical Organic Field-Effect Transistors on Flexible Electronics. *Adv. Mater.* **2023**, *35*, No. e2204804.
(31) Khang, D. Y.; Jiang, H.; Huang, Y.; Rogers, J. A. A Stretchable Form of Single-Crystal Silicon for High-Performance Electronics on Rubber Substrates. *Science* **2006**, *311*, 208−212.
(32) Kim, D. H.; Xiao, J.; Song, J.; Huang, Y.; Rogers, J. A. Stretchable, Curvilinear Electronics Based on Inorganic Materials. *Adv. Mater.* **2010**, *22*, 2108−2124.
(33) Rafeedi, T.; Lipomi, D. J. Multiple Pathways to Stretchable Electronics. *Science* **2022**, *378*, 1174−1175.
(34) Wang, C.; Wang, C.; Huang, Z.; Xu, S. Materials and Structures toward Soft Electronics. *Adv. Mater.* **2018**, *30*, No. 1801368.
(35) Xue, Z.; Song, H.; Rogers, J. A.; Zhang, Y.; Huang, Y. Mechanically-Guided Structural Designs in Stretchable Inorganic Electronics. *Adv. Mater.* **2020**, *32*, 1902254.
(36) Bowden, N.; Brittain, S.; Evans, A. G.; Hutchinson, J. W.; Whitesides, G. M. Spontaneous Formation of Ordered Structures in Thin Films of Metals Supported on an Elastomeric Polymer. *Nature* **1998**, *393*, 146−149.
(37) Sun, Y.; Choi, W. M.; Jiang, H.; Huang, Y. Y.; Rogers, J. A. Controlled Buckling of Semiconductor Nanoribbons for Stretchable Electronics. *Nat. Nanotechnol.* **2006**, *1*, 201−207.
(38) Sun, Y. G.; Kumar, V.; Adesida, I.; Rogers, J. A. Buckled and Wavy Ribbons of Gaas for High-Performance Electronics on Elastomeric Substrates. *Adv. Mater.* **2006**, *18*, 2857−2862.
(39) Ko, H. C.; Stoykovich, M. P.; Song, J.; Malyarchuk, V.; Choi, W. M.; Yu, C. J.; Geddes, J. B., 3rd; Xiao, J.; Wang, S.; Huang, Y.; et al. A Hemispherical Electronic Eye Camera Based on Compressible Silicon Optoelectronics. *Nature* **2008**, *454*, 748−753.
(40) Kim, D.-H.; Song, J.; Choi, W. M.; Kim, H.-S.; Kim, R.-H.; Liu, Z.; Huang, Y. Y.; Hwang, K.-C.; Zhang, Y.-w.; Rogers, J. A. Materials and Noncoplanar Mesh Designs for Integrated Circuits with Linear Elastic Responses to Extreme Mechanical Deformations. *Proc. Natl. Acad. Sci. U.S.A.* **2008**, *105*, 18675−18680.
(41) Brosteaux, D.; Axisa, F.; Gonzalez, M.; Vanfleteren, J. Design and Fabrication of Elastic Interconnections for Stretchable Electronic Circuits. *IEEE Electron Device Lett.* **2007**, *28*, 552−554.
(42) Fan, Z.; Zhang, Y.; Ma, Q.; Zhang, F.; Fu, H.; Hwang, K. C.; Huang, Y. A Finite Deformation Model of Planar Serpentine Interconnects for Stretchable Electronics. *Int. J. Solids Struct.* **2016**, *91*, 46−54.
(43) Jeong, J. W.; Yeo, W. H.; Akhtar, A.; Norton, J. J.; Kwack, Y. J.; Li, S.; Jung, S. Y.; Su, Y.; Lee, W.; Xia, J.; et al. Materials and Optimized Designs for Human-Machine Interfaces Via Epidermal Electronics. *Adv. Mater.* **2013**, *25*, 6839−6846.
(44) Kim, D.-H.; Kim, Y.-S.; Wu, J.; Liu, Z.; Song, J.; Kim, H.-S.; Huang, Y. Y.; Hwang, K.-C.; Rogers, J. A. Ultrathin Silicon Circuits with Strain-Isolation Layers and Mesh Layouts for High-Performance Electronics on Fabric, Vinyl, Leather, and Paper (Adv. Mater. 36/2009). *Adv. Mater.* **2009**, *21*, NA−NA.
(45) Kim, R. H.; Kim, D. H.; Xiao, J.; Kim, B. H.; Park, S. I.; Panilaitis, B.; Ghaffari, R.; Yao, J.; Li, M.; Liu, Z.; et al. Waterproof Alingap Optoelectronics on Stretchable Substrates with Applications in Biomedicine and Robotics. *Nat. Mater.* **2010**, *9*, 929−937.
(46) Shyu, T. C.; Damasceno, P. F.; Dodd, P. M.; Lamoureux, A.; Xu, L.; Shlian, M.; Shtein, M.; Glotzer, S. C.; Kotov, N. A. A Kirigami Approach to Engineering Elasticity in Nanocomposites through Patterned Defects. *Nat. Mater.* **2015**, *14*, 785−789.
(47) Bertoldi, K.; Vitelli, V.; Christensen, J.; van Hecke, M. Flexible Mechanical Metamaterials. *Nat. Rev. Mater.* **2017**, *2*, 17066.
(48) Blees, M. K.; Barnard, A. W.; Rose, P. A.; Roberts, S. P.; McGill, K. L.; Huang, P. Y.; Ruyack, A. R.; Kevek, J. W.; Kobrin, B.; Muller, D. A.; et al. Graphene Kirigami. *Nature* **2015**, *524*, 204−207.
(49) Coulais, C.; Sabbadini, A.; Vink, F.; van Hecke, M. Multi-Step Self-Guided Pathways for Shape-Changing Metamaterials. *Nature* **2018**, *561*, 512−515.
(50) Eidini, M. Zigzag-Base Folded Sheet Cellular Mechanical Metamaterials. *EXTREME MECH. LETT.* **2016**, *6*, 96−102.
(51) Lamoureux, A.; Lee, K.; Shlian, M.; Forrest, S. R.; Shtein, M. Dynamic Kirigami Structures for Integrated Solar Tracking. *Nat. Commun.* **2015**, *6*, 8092.
(52) Tang, Y. C.; Yin, J. Design of Cut Unit Geometry in Hierarchical Kirigami-Based Auxetic Metamaterials for High Stretchability and Compressibility. *EXTREME MECH. LETT.* **2017**, *12*, 77−85.
(53) Alcheikh, N.; Shaikh, S. F.; Hussain, M. M. Ultra-Stretchable Archimedean Interconnects for Stretchable Electronics. *EXTREME MECH. LETT.* **2018**, *24*, 6−13.
(54) Cavazos Sepulveda, A. C.; Diaz Cordero, M. S.; Carreño, A. A. A.; Nassar, J. M.; Hussain, M. M. Stretchable and Foldable Silicon-Based Electronics. *Appl. Phys. Lett.* **2017**, *110*. DOI: 10.1063/1.4979545
(55) Lv, C.; Yu, H.; Jiang, H. Archimedean Spiral Design for Extremely Stretchable Interconnects. *EXTREME MECH. LETT.* **2014**, *1*, 29−34.
(56) Mamidanna, A.; Song, Z.; Lv, C.; Lefky, C. S.; Jiang, H.; Hildreth, O. J. Printing Stretchable Spiral Interconnects Using Reactive Ink Chemistries. *ACS Appl. Mater. Interfaces* **2016**, *8*, 12594−12598.
(57) Qaiser, N.; Khan, S. M.; Hussain, M. M. In-Plane and out-of-Plane Structural Response of Spiral Interconnects for Highly Stretchable Electronics. *J. Appl. Phys.* **2018**, *124*. DOI: 10.1063/1.5031176
(58) Qaiser, N.; Khan, S. M.; Nour, M.; Rehman, M. U.; Rojas, J. P.; Hussain, M. M. Mechanical Response of Spiral Interconnect Arrays for Highly Stretchable Electronics. *Appl. Phys. Lett.* **2017**, *111*. DOI: 10.1063/1.5007111
(59) Rehman, M. U.; Rojas, J. P. Optimization of Compound Serpentine-Spiral Structure for Ultra-Stretchable Electronics. *EXTREME MECH. LETT.* **2017**, *15*, 44−50.
(60) Rojas, J. P.; Arevalo, A.; Foulds, I. G.; Hussain, M. M. Design and Characterization of Ultra-Stretchable Monolithic Silicon Fabric. *Appl. Phys. Lett.* **2014**, *105*. DOI: 10.1063/1.4898128
(61) Rojas, J. P.; Singh, D.; Conchouso, D.; Arevalo, A.; Foulds, I. G.; Hussain, M. M. Stretchable Helical Architecture Inorganic-Organic Hetero Thermoelectric Generator. *Nano Energy* **2016**, *30*, 691−699.
(62) Fan, J. A.; Yeo, W. H.; Su, Y.; Hattori, Y.; Lee, W.; Jung, S. Y.; Zhang, Y.; Liu, Z.; Cheng, H.; Falgout, L.; et al. Fractal Design Concepts for Stretchable Electronics. *Nat. Commun.* **2014**, *5*, 3266.
(63) Hattori, Y.; Falgout, L.; Lee, W.; Jung, S. Y.; Poon, E.; Lee, J. W.; Na, I.; Geisler, A.; Sadhwani, D.; Zhang, Y.; et al. Multifunctional Skin-Like Electronics for Quantitative, Clinical Monitoring of Cutaneous Wound Healing. *Adv. Healthc. Mater.* **2014**, *3*, 1597−1607.
(64) Huang, K. H.; Lin, C. T.; Chen, Y. T.; Yang, Y. J. J. Study of Fractal Electrode Designs for Buckypaper-Based Micro-Supercapacitors. *J. Appl. Phys.* **2019**, *125*. DOI: 10.1063/1.5051702

(65) Xu, L.; Gutbrod, S. R.; Ma, Y.; Petrossians, A.; Liu, Y.; Webb, R. C.; Fan, J. A.; Yang, Z.; Xu, R.; Whalen, J. J., 3rd; et al. Materials and Fractal Designs for 3d Multifunctional Integumentary Membranes with Capabilities in Cardiac Electrotherapy. *Adv. Mater.* **2015**, *27*, 1731−1737.
(66) Xu, S.; Zhang, Y.; Cho, J.; Lee, J.; Huang, X.; Jia, L.; Fan, J. A.; Su, Y.; Su, J.; Zhang, H.; et al. Stretchable Batteries with Self-Similar Serpentine Interconnects and Integrated Wireless Recharging Systems. *Nat. Commun.* **2013**, *4*, 1543.
(67) Zhang, Y. H.; Fu, H. R.; Xu, S.; Fan, J. A.; Hwang, K. C.; Jiang, J. Q.; Rogers, J. A.; Huang, Y. G. A Hierarchical Computational Model for Stretchable Interconnects with Fractal-Inspired Designs. *J. Mech. Phys. Solids* **2014**, *72*, 115−130.
(68) Kim, D. H.; Lu, N.; Ma, R.; Kim, Y. S.; Kim, R. H.; Wang, S.; Wu, J.; Won, S. M.; Tao, H.; Islam, A.; et al. Epidermal Electronics. *Science* **2011**, *333*, 838−843.
(69) Yan, W.; Noel, G.; Loke, G.; Meiklejohn, E.; Khudiyev, T.; Marion, J.; Rui, G.; Lin, J.; Cherston, J.; Sahasrabudhe, A.; et al. Single Fibre Enables Acoustic Fabrics Via Nanometre-Scale Vibrations. *Nature* **2022**, *603*, 616−623.
(70) Yang, Q.; Jin, W.; Zhang, Q.; Wei, Y.; Guo, Z.; Li, X.; Yang, Y.; Luo, Q.; Tian, H.; Ren, T.-L. Mixed-Modality Speech Recognition and Interaction Using a Wearable Artificial Throat. *Nat. Mach. Intell.* **2023**, *5*, 169−180.
(71) Byun, J.; Lee, Y.; Yoon, J.; Lee, B.; Oh, E.; Chung, S.; Lee, T.; Cho, K.-J.; Kim, J.; Hong, Y. Electronic Skins for Soft, Compact, Reversible Assembly of Wirelessly Activated Fully Soft Robots. *Sci. Robot.* **2018**, *3*, No. eaas9020.
(72) Xiong, W.; Zhu, C.; Guo, D.; Hou, C.; Yang, Z.; Xu, Z.; Qiu, L.; Yang, H.; Li, K.; Huang, Y. Bio-Inspired, Intelligent Flexible Sensing Skin for Multifunctional Flying Perception. *Nano Energy* **2021**, *90*, 106550.
(73) Yu, Y.; Li, J.; Solomon, S. A.; Min, J.; Tu, J.; Guo, W.; Xu, C.; Song, Y.; Gao, W. All-Printed Soft Human-Machine Interface for Robotic Physicochemical Sensing. *Sci. Robot.* **2022**, *7*, No. eabn0495.
(74) Liu, Y. M.; Yiu, C. K.; Song, Z.; Huang, Y.; Yao, K. M.; Wong, T.; Zhou, J. K.; Zhao, L.; Huang, X. C.; Nejad, S. K.; et al. Electronic Skin as Wireless Human-Machine Interfaces for Robotic Vr. *Sci. Adv.* **2022**, *8*. DOI: 10.1126/sciadv.abl6700
(75) Kim, K. K.; Kim, M.; Pyun, K.; Kim, J.; Min, J.; Koh, S.; Root, S. E.; Kim, J.; Nguyen, B.-N. T.; Nishio, Y.; et al. A Substrate-Less Nanomesh Receptor with Meta-Learning for Rapid Hand Task Recognition. *Nat. Electron.* **2023**, *6*, 64−75.
(76) Yoon, J.; Li, L.; Semichaevsky, A. V.; Ryu, J. H.; Johnson, H. T.; Nuzzo, R. G.; Rogers, J. A. Flexible Concentrator Photovoltaics Based on Microscale Silicon Solar Cells Embedded in Luminescent Waveguides. *Nat. Commun.* **2011**, *2*, 343.
(77) Sheng, X.; Bower, C. A.; Bonafede, S.; Wilson, J. W.; Fisher, B.; Meitl, M.; Yuen, H.; Wang, S.; Shen, L.; Banks, A. R.; et al. Printing-Based Assembly of Quadruple-Junction Four-Terminal Microscale Solar Cells and Their Use in High-Efficiency Modules. *Nat. Mater.* **2014**, *13*, 593−598.
(78) Liu, R.; Wang, Z. L.; Fukuda, K.; Someya, T. Flexible Self-Charging Power Sources. *Nat. Rev. Mater.* **2022**, *7*, 870−886.
(79) Liu, Y.; Li, J.; Song, S.; Kang, J.; Tsao, Y.; Chen, S.; Mottini, V.; McConnell, K.; Xu, W.; Zheng, Y.-Q.; et al. Morphing Electronics Enable Neuromodulation in Growing Tissue. *Nat. Biotechnol.* **2020**, *38*, 1031−1036.
(80) Hensleigh, R.; Cui, H.; Xu, Z.; Massman, J.; Yao, D.; Berrigan, J.; Zheng, X. Charge-Programmed Three-Dimensional Printing for Multi-Material Electronic Devices. *Nat. Electron.* **2020**, *3*, 216−224.
(81) Ge, Q.; Chen, Z.; Cheng, J.; Zhang, B.; Zhang, Y.-F.; Li, H.; He, X.; Yuan, C.; Liu, J.; Magdassi, S.; et al. 3d Printing of Highly Stretchable Hydrogel with Diverse Uv Curable Polymers. *Sci. Adv.* **2021**, *7*, No. eaba4261.
(82) Cheng, J.; Wang, R.; Sun, Z.; Liu, Q.; He, X.; Li, H.; Ye, H.; Yang, X.; Wei, X.; Li, Z.; et al. Centrifugal Multimaterial 3d Printing of Multifunctional Heterogeneous Objects. *Nat. Commun.* **2022**, *13*, 7931.
(83) Duraivel, S.; Laurent, D.; Rajon, D. A.; Scheutz, G. M.; Shetty, A. M.; Sumerlin, B. S.; Banks, S. A.; Bova, F. J.; Angelini, T. E. A Silicone-Based Support Material Eliminates Interfacial Instabilities in 3d Silicone Printing. *Science* **2023**, *379*, 1248−1252.
(84) Jung, W.; Jung, Y. H.; Pikhitsa, P. V.; Feng, J.; Yang, Y.; Kim, M.; Tsai, H. Y.; Tanaka, T.; Shin, J.; Kim, K. Y.; et al. Three-Dimensional Nanoprinting Via Charged Aerosol Jets. *Nature* **2021**, *592*, 54−59.
(85) Kawata, S.; Sun, H.-B.; Tanaka, T.; Takada, K. Finer Features for Functional Microdevices. *Nature* **2001**, *412*, 697−698.
(86) Meza, L. R.; Das, S.; Greer, J. R. Strong, Lightweight, and Recoverable Three-Dimensional Ceramic Nanolattices. *Science* **2014**, *345*, 1322−1326.
(87) Han, F.; Gu, S.; Klimas, A.; Zhao, N.; Zhao, Y.; Chen, S.-C. Three-Dimensional Nanofabrication Via Ultrafast Laser Patterning and Kinetically Regulated Material Assembly. *Science* **2022**, *378*, 1325−1331.
(88) Li, S.; Lerch, M. M.; Waters, J. T.; Deng, B.; Martens, R. S.; Yao, Y.; Kim, D. Y.; Bertoldi, K.; Grinthal, A.; Balazs, A. C.; et al. Self-Regulated Non-Reciprocal Motions in Single-Material Microstructures. *Nature* **2022**, *605*, 76−83.
(89) Wehner, M.; Truby, R. L.; Fitzgerald, D. J.; Mosadegh, B.; Whitesides, G. M.; Lewis, J. A.; Wood, R. J. An Integrated Design and Fabrication Strategy for Entirely Soft, Autonomous Robots. *Nature* **2016**, *536*, 451−455.
(90) Saccone, M. A.; Gallivan, R. A.; Narita, K.; Yee, D. W.; Greer, J. R. Additive Manufacturing of Micro-Architected Metals Via Hydrogel Infusion. *Nature* **2022**, *612*, 685−690.
(91) Schmidt, O. G.; Eberl, K. Thin Solid Films Roll up into Nanotubes. *Nature* **2001**, *410*, 168−168.
(92) Schmidt, O. G.; Jin-Phillipp, N. Y. Free-Standing Sige-Based Nanopipelines on Si (001) Substrates. *Appl. Phys. Lett.* **2001**, *78*, 3310−3312.
(93) Cho, J.-H.; James, T.; Gracias, D. H. Curving Nanostructures Using Extrinsic Stress. *Adv. Mater.* **2010**, *22*, 2320−2324.
(94) Armon, S.; Efrati, E.; Kupferman, R.; Sharon, E. Geometry and Mechanics in the Opening of Chiral Seed Pods. *Science* **2011**, *333*, 1726−1730.
(95) Vaccaro, P. O.; Kubota, K.; Fleischmann, T.; Saravanan, S.; Aida, T. Valley-Fold and Mountain-Fold in the Micro-Origami Technique. *Microelectron. J.* **2003**, *34*, 447−449.
(96) Leong, T.; Gu, Z.; Koh, T.; Gracias, D. H. Spatially Controlled Chemistry Using Remotely Guided Nanoliter Scale Containers. *J. Am. Chem. Soc.* **2006**, *128*, 11336−11337.
(97) Bassik, N.; Brafman, A.; Zarafshar, A. M.; Jamal, M.; Luvsanjav, D.; Selaru, F. M.; Gracias, D. H. Enzymatically Triggered Actuation of Miniaturized Tools. *J. Am. Chem. Soc.* **2010**, *132*, 16314−16317.
(98) Becker, C.; Bao, B.; Karnaushenko, D. D.; Bandari, V. K.; Rivkin, B.; Li, Z.; Faghih, M.; Karnaushenko, D.; Schmidt, O. G. A New Dimension for Magnetosensitive E-Skins: Active Matrix Integrated Micro-Origami Sensor Arrays. *Nat. Commun.* **2022**, *13*, 2121.
(99) Ko, H. C.; Shin, G.; Wang, S.; Stoykovich, M. P.; Lee, J. W.; Kim, D.-H.; Ha, J. S.; Huang, Y.; Hwang, K.-C.; Rogers, J. A. Curvilinear Electronics Formed Using Silicon Membrane Circuits and Elastomeric Transfer Elements. *Small* **2009**, *5*, 2703−2709.
(100) Jung, I.; Shin, G.; Malyarchuk, V.; Ha, J. S.; Rogers, J. A. Paraboloid Electronic Eye Cameras Using Deformable Arrays of Photodetectors in Hexagonal Mesh Layouts. *Appl. Phys. Lett.* **2010**, *96*, 021110.
(101) Jung, I.; Xiao, J.; Malyarchuk, V.; Lu, C.; Li, M.; Liu, Z.; Yoon, J.; Huang, Y.; Rogers, J. A. Dynamically Tunable Hemispherical Electronic Eye Camera System with Adjustable Zoom Capability. *Proc. Natl. Acad. Sci. U.S.A.* **2011**, *108*, 1788−1793.
(102) Huang, Y.; Wu, H.; Xiao, L.; Duan, Y.; Zhu, H.; Bian, J.; Ye, D.; Yin, Z. Assembly and Applications of 3d Conformal Electronics on Curvilinear Surfaces. *Mater. Horizons* **2019**, *6*, 642−683.
(103) Xu, S.; Yan, Z.; Jang, K.-I.; Huang, W.; Fu, H.; Kim, J.; Wei, Z.; Flavin, M.; McCracken, J.; Wang, R.; et al. Assembly of Micro/Nanomaterials into Complex, Three-Dimensional Architectures by Compressive Buckling. *Science* **2015**, *347*, 154−159.

(104) Zhang, Y.; Zhang, F.; Yan, Z.; Ma, Q.; Li, X.; Huang, Y.; Rogers, J. A. Printing, Folding and Assembly Methods for Forming 3d Mesostructures in Advanced Materials. *Nat. Rev. Mater.* **2017**, *2*, 17019.
(105) Huang, G.; Mei, Y. Assembly and Self-Assembly of Nanomembrane Materials-from 2d to 3d. *Small* **2018**, *14*, 1703665.
(106) Cheng, X.; Zhang, Y. Micro/Nanoscale 3d Assembly by Rolling, Folding, Curving, and Buckling Approaches. *Adv. Mater.* **2019**, *31*, 1901895.
(107) Karnaushenko, D.; Kang, T.; Bandari, V. K.; Zhu, F.; Schmidt, O. G. 3d Self-Assembled Microelectronic Devices: Concepts, Materials, Applications. *Adv. Mater.* **2020**, *32*, 1902994.
(108) Mei, Y.; Huang, G.; Solovev, A. A.; Urena, E. B.; Moench, I.; Ding, F.; Reindl, T.; Fu, R. K. Y.; Chu, P. K.; Schmidt, O. G. Versatile Approach for Integrative and Functionalized Tubes by Strain Engineering of Nanomembranes on Polymers. *Adv. Mater.* **2008**, *20*, 4085−4090.
(109) Huang, X. N.; Kumar, K.; Jawed, M. K.; Nasab, A. M.; Ye, Z. S.; Shan, W. L.; Majidi, C. Chasing Biomimetic Locomotion Speeds: Creating Untethered Soft Robots with Shape Memory Alloy Actuators. *Sci. Robot.* **2018**, *3*, No. eaau7557.
(110) Jamal, M.; Bassik, N.; Cho, J.-H.; Randall, C. L.; Gracias, D. H. Directed Growth of Fibroblasts into Three Dimensional Micropatterned Geometries Via Self-Assembling Scaffolds. *Biomaterials* **2010**, *31*, 1683−1690.
(111) Py, C.; Reverdy, P.; Doppler, L.; Bico, J.; Roman, B.; Baroud, C. Capillary Origami. *Phys. Fluids* **2007**, *19*, 091104.
(112) Py, C.; Reverdy, P.; Doppler, L.; Bico, J.; Roman, B.; Baroud, C. N. Capillary Origami: Spontaneous Wrapping of a Droplet with an Elastic Sheet. *Phys. Rev. Lett.* **2007**, *98*, 156103.
(113) Cho, J.-H.; Gracias, D. H. Self-Assembly of Lithographically Patterned Nanoparticles. *Nano Lett.* **2009**, *9*, 4049−4052.
(114) Cho, J.-H.; Azam, A.; Gracias, D. H. Three Dimensional Nanofabrication Using Surface Forces. *Langmuir* **2010**, *26*, 16534−16539.
(115) Gladman, A. S.; Matsumoto, E. A.; Nuzzo, R. G.; Mahadevan, L.; Lewis, J. A. Biomimetic 4d Printing. *Nat. Mater.* **2016**, *15*, 413.
(116) Aharoni, H.; Xia, Y.; Zhang, X.; Kamien, R. D.; Yang, S. Universal Inverse Design of Surfaces with Thin Nematic Elastomer Sheets. *Proc. Natl. Acad. Sci. U.S.A.* **2018**, *115*, 7206−7211.
(117) Hu, W.; Lum, G. Z.; Mastrangeli, M.; Sitti, M. Small-Scale Soft-Bodied Robot with Multimodal Locomotion. *Nature* **2018**, *554*, 81−85.
(118) Wang, C.; Sim, K.; Chen, J.; Kim, H.; Rao, Z.; Li, Y.; Chen, W.; Song, J.; Verduzco, R.; Yu, C. Soft Ultrathin Electronics Innervated Adaptive Fully Soft Robots. *Adv. Mater.* **2018**, *30*, No. 1706695.
(119) Xu, B.; Tian, Z.; Wang, J.; Han, H.; Lee, T.; Mei, Y. Stimuli-Responsive and on-Chip Nanomembrane Micro-Rolls for Enhanced Macroscopic Visual Hydrogen Detection. *Sci. Adv.* **2018**, *4*, No. eaap8203.
(120) Zhang, Y.; Yan, Z.; Nan, K.; Xiao, D.; Liu, Y.; Luan, H.; Fu, H.; Wang, X.; Yang, Q.; Wang, J.; et al. A Mechanically Driven Form of Kirigami as a Route to 3d Mesostructures in Micro/Nanomembranes. *Proc. Natl. Acad. Sci. U.S.A.* **2015**, *112*, 11757−11764.
(121) Yan, Z.; Zhang, F.; Liu, F.; Han, M.; Ou, D.; Liu, Y.; Lin, Q.; Guo, X.; Fu, H.; Xie, Z.; et al. Mechanical Assembly of Complex, 3d Mesostructures from Releasable Multilayers of Advanced Materials. *Sci. Adv.* **2016**, *2*, No. e1601014.
(122) Liu, Q.; Wang, W.; Reynolds, M. F.; Cao, M. C.; Miskin, M. Z.; Arias, T. A.; Muller, D. A.; McEuen, P. L.; Cohen, I. Micrometer-Sized Electrically Programmable Shape-Memory Actuators for Low-Power Microrobotics. *Sci. Robot.* **2021**, *6*, No. eabe6663.
(123) Wang, W.; Liu, Q.; Tanasijevic, I.; Reynolds, M. F.; Cortese, A. J.; Miskin, M. Z.; Cao, M. C.; Muller, D. A.; Molnar, A. C.; Lauga, E.; et al. Cilia Metasurfaces for Electronically Programmable Microfluidic Manipulation. *Nature* **2022**, *605*, 681−686.
(124) Fu, H.; Nan, K.; Bai, W.; Huang, W.; Bai, K.; Lu, L.; Zhou, C.; Liu, Y.; Liu, F.; Wang, J.; et al. Morphable 3d Mesostructures and Microelectronic Devices by Multistable Buckling Mechanics. *Nat. Mater.* **2018**, *17*, 268−276.
(125) Cools, J.; Jin, Q.; Yoon, E.; Burbano, D. A.; Luo, Z.; Cuypers, D.; Callewaert, G.; Braeken, D.; Gracias, D. H. A Micropatterned Multielectrode Shell for 3d Spatiotemporal Recording from Live Cells. *Adv. Sci.* **2018**, *5*, 1700731.
(126) Gao, H.; Yang, F.; Sattari, K.; Du, X.; Fu, T.; Fu, S.; Liu, X.; Lin, J.; Sun, Y.; Yao, J. Bioinspired Two-in-One Nanotransistor Sensor for the Simultaneous Measurements of Electrical and Mechanical Cellular Responses. *Sci. Adv.* **2022**, *8*, No. eabn2485.
(127) Park, Y.; Franz, C. K.; Ryu, H.; Luan, H.; Cotton, K. Y.; Kim, J. U.; Chung, T. S.; Zhao, S.; Vazquez-Guardado, A.; Yang, D. S.; et al. Three-Dimensional, Multifunctional Neural Interfaces for Cortical Spheroids and Engineered Assembloids. *Sci. Adv.* **2021**, *7*, No. eabf9153.
(128) Huang, Q.; Tang, B.; Romero, J. C.; Yang, Y.; Elsayed, S. K.; Pahapale, G.; Lee, T.-J.; Morales Pantoja, I. E.; Han, F.; Berlinicke, C.; et al. Shell Microelectrode Arrays (Meas) for Brain Organoids. *Sci. Adv.* **2022**, *8*, No. eabq5031.
(129) Song, Y. M.; Xie, Y.; Malyarchuk, V.; Xiao, J.; Jung, I.; Choi, K.-J.; Liu, Z.; Park, H.; Lu, C.; Kim, R.-H.; et al. Digital Cameras with Designs Inspired by the Arthropod Eye. *Nature* **2013**, *497*, 95−99.
(130) Rao, Z.; Lu, Y.; Li, Z.; Sim, K.; Ma, Z.; Xiao, J.; Yu, C. Curvy, Shape-Adaptive Imagers Based on Printed Optoelectronic Pixels with a Kirigami Design. *Nat. Electron.* **2021**, *4*, 513−521.
(131) Ji, Z.; Zhao, J.; Song, H.; Xu, S.; Pang, W.; Hu, X.; Zhang, F.; Jin, T.; Shuai, Y.; Lan, Y.; et al. Morphable Three-Dimensional Electronic Mesofliers Capable of on-Demand Unfolding. *Sci. China Mater.* **2022**, *65*, 2309−2318.
(132) Han, M.; Wang, H.; Yang, Y.; Liang, C.; Bai, W.; Yan, Z.; Li, H.; Xue, Y.; Wang, X.; Akar, B.; et al. Three-Dimensional Piezoelectric Polymer Microsystems for Vibrational Energy Harvesting, Robotic Interfaces and Biomedical Implants. *Nat. Electron.* **2019**, *2*, 26−35.
(133) Won, S. M.; Wang, H.; Kim, B. H.; Lee, K.; Jang, H.; Kwon, K.; Han, M.; Crawford, K. E.; Li, H.; Lee, Y.; et al. Multimodal Sensing with a Three-Dimensional Piezoresistive Structure. *ACS Nano* **2019**, *13*, 10972−10979.
(134) Ghosh, A.; Li, L.; Xu, L.; Dash, R. P.; Gupta, N.; Lam, J.; Jin, Q.; Akshintala, V.; Pahapale, G.; Liu, W.; et al. Gastrointestinal-Resident, Shape-Changing Microdevices Extend Drug Release in Vivo. *Sci. Adv.* **2020**, *6*, No. eabb4133.
(135) Han, M.; Chen, L.; Aras, K.; Liang, C.; Chen, X.; Zhao, H.; Li, K.; Faye, N. R.; Sun, B.; Kim, J. H.; et al. Catheter-Integrated Soft Multilayer Electronic Arrays for Multiplexed Sensing and Actuation During Cardiac Surgery. *Nat. Biomed. Eng.* **2020**, *4*, 997−1009.
(136) Prinz, V. Y.; Seleznev, V. A.; Gutakovsky, A. K.; Chehovskiy, A. V.; Preobrazhenskii, V. V.; Putyato, M. A.; Gavrilova, T. A. Free-Standing and Overgrown Ingaas/Gaas Nanotubes, Nanohelices and Their Arrays. *Physica E* **2000**, *6*, 828−831.
(137) Zhang, L.; Ruh, E.; Gruetzmacher, D.; Dong, L.; Bell, D. J.; Nelson, B. J.; Schoenenberger, C. Anomalous Coiling of Sige/Si and Sige/Si/Cr Helical Nanobelts. *Nano Lett.* **2006**, *6*, 1311−1317.
(138) Cheng, X.; Fan, Z.; Yao, S.; Jin, T.; Lv, Z.; Lan, Y.; Bo, R.; Chen, Y.; Zhang, F.; Shen, Z.; et al. Programming 3d Curved Mesosurfaces Using Microlattice Designs. *Science* **2023**, *379*, 1225−1232.
(139) Bai, K.; Cheng, X.; Xue, Z.; Song, H.; Sang, L.; Zhang, F.; Liu, F.; Luo, X.; Huang, W.; Huang, Y.; et al. Geometrically Reconfigurable 3d Mesostructures and Electromagnetic Devices through a Rational Bottom-up Design Strategy. *Sci. Adv.* **2020**, *6*, No. eabb7417.
(140) Taylor, J. M.; Luan, H.; Lewis, J. A.; Rogers, J. A.; Nuzzo, R. G.; Braun, P. V. Biomimetic and Biologically Compliant Soft Architectures Via 3d and 4d Assembly Methods: A Perspective. *Adv. Mater.* **2022**, *34*, No. 2108391.
(141) Xu, B.; Zhang, B.; Wang, L.; Huang, G.; Mei, Y. Tubular Micro/Nanomachines: From the Basics to Recent Advances. *Adv. Funct. Mater.* **2018**, *28*, 1705872.
(142) Bell, D. J.; Dong, L. X.; Nelson, B. J.; Golling, M.; Zhang, L.; Grutzmacher, D. Fabrication and Characterization of Three-Dimensional Ingaas/Gaas Nanosprings. *Nano Lett.* **2006**, *6*, 725−729.
(143) Songmuang, R.; Rastelli, A.; Mendach, S.; Schmidt, O. G. Siox/Si Radial Superlattices and Microtube Optical Ring Resonators. *Appl. Phys. Lett.* **2007**, *90*, 091905.

https://doi.org/10.1021/acs.chemrev.3c00335
Chem. Rev. 2023, 123, 11137−11189

(144) Chun, I. S.; Li, X. Controlled Assembly and Dispersion of Strain-Induced Ingaas/Gaas Nanotubes. *IEEE Trans. Nanotechnol.* **2008**, *7*, 493−495.
(145) Zhang, L.; Abbott, J. J.; Dong, L.; Peyer, K. E.; Kratochvil, B. E.; Zhang, H.; Bergeles, C.; Nelson, B. J. Characterizing the Swimming Properties of Artificial Bacterial Flagella. *Nano Lett.* **2009**, *9*, 3663−3667.
(146) Chun, I. S.; Challa, A.; Derickson, B.; Hsia, K. J.; Li, X. Geometry Effect on the Strain-Induced Self-Rolling of Semiconductor Membranes. *Nano Lett.* **2010**, *10*, 3927−3932.
(147) Jamal, M.; Zarafshar, A. M.; Gracias, D. H. Differentially Photo-Crosslinked Polymers Enable Self-Assembling Microfluidics. *Nat. Commun.* **2011**, *2*, 527.
(148) Mönch, I.; Makarov, D.; Koseva, R.; Baraban, L.; Karnaushenko, D.; Kaiser, C.; Arndt, K.-F.; Schmidt, O. G. Rolled-up Magnetic Sensor: Nanomembrane Architecture for in-Flow Detection of Magnetic Objects. *ACS Nano* **2011**, *5*, 7436−7442.
(149) Smith, E. J.; Schulze, S.; Kiravittaya, S.; Mei, Y.; Sanchez, S.; Schmidt, O. G. Lab-in-a-Tube: Detection of Individual Mouse Cells for Analysis in Flexible Split-Wall Microtube Resonator Sensors. *Nano Lett.* **2011**, *11*, 4037−4042.
(150) Huang, W.; Yu, X.; Froeter, P.; Xu, R.; Ferreira, P.; Li, X. On-Chip Inductors with Self-Rolled-up Sinx Nanomembrane Tubes: A Novel Design Platform for Extreme Miniaturization. *Nano Lett.* **2012**, *12*, 6283−6288.
(151) Grimm, D.; Bufon, C. C. B.; Deneke, C.; Atkinson, P.; Thurmer, D. J.; Schaeffel, F.; Gorantla, S.; Bachmatiuk, A.; Schmidt, O. G. Rolled-up Nanomembranes as Compact 3d Architectures for Field Effect Transistors and Fluidic Sensing Applications. *Nano Lett.* **2013**, *13*, 213−218.
(152) Martinez-Cisneros, C. S.; Sanchez, S.; Xi, W.; Schmidt, O. G. Ultracompact Three-Dimensional Tubular Conductivity Microsensors for Ionic and Biosensing Applications. *Nano Lett.* **2014**, *14*, 2219−2224.
(153) Sharma, R.; Bufon, C. C. B.; Grimm, D.; Sommer, R.; Wollatz, A.; Schadewald, J.; Thurmer, D. J.; Siles, P. F.; Bauer, M.; Schmidt, O. G. Large-Area Rolled-up Nanomembrane Capacitor Arrays for Electrostatic Energy Storage. *Adv. Electron. Mater.* **2014**, *4*, 1301631.
(154) Magdanz, V.; Medina-Sanchez, M.; Chen, Y.; Guix, M.; Schmidt, O. G. How to Improve Spermbot Performance. *Adv. Funct. Mater.* **2015**, *25*, 2763−2770.
(155) Yu, X.; Huang, W.; Li, M.; Comberiate, T. M.; Gong, S.; Schutt-Aine, J. E.; Li, X. Ultra-Small, High-Frequency, and Substrate-Immune Microtube Inductors Transformed from 2d to 3d. *Sci. Rep.* **2015**, *5*, 9661.
(156) Deng, J.; Lu, X.; Liu, L.; Zhang, L.; Schmidt, O. G. Introducing Rolled-up Nanotechnology for Advanced Energy Storage Devices. *Adv. Electron. Mater.* **2016**, *6*, 1600797.
(157) Jalil, A. R.; Chang, H.; Bandari, V. K.; Robaschik, P.; Zhang, J.; Siles, P. F.; Li, G.; Buerger, D.; Grimm, D.; Liu, X.; et al. Fully Integrated Organic Nanocrystal Diode as High Performance Room Temperature No2 Sensor. *Adv. Mater.* **2016**, *28*, 2971−2977.
(158) Zhao, Z.; Kuang, X.; Yuan, C.; Qi, H. J.; Fang, D. Hydrophilic/Hydrophobic Composite Shape-Shifting Structures. *ACS Appl. Mater. Interfaces* **2018**, *10*, 19932−19939.
(159) Deng, T.; Zhang, Z.; Liu, Y.; Wang, Y.; Su, F.; Li, S.; Zhang, Y.; Li, H.; Chen, H.; Zhao, Z.; et al. Three-Dimensional Graphene Field-Effect Transistors as High-Performance Photodetectors. *Nano Lett.* **2019**, *19*, 1494−1503.
(160) Huang, H. W.; Uslu, F. E.; Katsamba, P.; Lauga, E.; Sakar, M. S.; Nelson, B. J. Adaptive Locomotion of Artificial Microswimmers. *Sci. Adv.* **2019**, *5*, No. eaau1532.
(161) Huang, X.; Kumar, K.; Jawed, M. K.; Mohammadi Nasab, A.; Ye, Z.; Shan, W.; Majidi, C. Highly Dynamic Shape Memory Alloy Actuator for Fast Moving Soft Robots. *Adv. Mater. Technol.* **2019**, *4*, 1800540.
(162) Tian, Z.; Xu, B.; Wan, G.; Han, X.; Di, Z.; Chen, Z.; Mei, Y. Gaussian-Preserved, Non-Volatile Shape Morphing in Three-Dimensional Microstructures for Dual-Functional Electronic Devices. *Nat. Commun.* **2021**, *12*. DOI: 10.1038/s41467-020-20843-4
(163) Li, X.; Cao, C.; Liu, C.; He, W.; Wu, K.; Wang, Y.; Xu, B.; Tian, Z.; Song, E.; Cui, J.; et al. Self-Rolling of Vanadium Dioxide Nanomembranes for Enhanced Multi-Level Solar Modulation. *Nat. Commun.* **2022**, *13*, 7819.
(164) Zhang, F.; Li, D.; Wang, C.; Liu, Z.; Yang, M.; Cui, Z.; Yi, J.; Wang, M.; Jiang, Y.; Lv, Z.; et al. Shape Morphing of Plastic Films. *Nat. Commun.* **2022**, *13*, 7294.
(165) In, H. J.; Lee, H.; Nichol, A. J.; Kim, S. G.; Barbastathis, G. Carbon Nanotube-Based Magnetic Actuation of Origami Membranes. *J. Vac. Sci. Technol. B* **2008**, *26*, 2509−2512.
(166) Bassik, N.; Stern, G. M.; Gracias, D. H. Microassembly Based on Hands Free Origami with Bidirectional Curvature. *Appl. Phys. Lett.* **2009**, *95*, 091901.
(167) Leong, T. G.; Randall, C. L.; Benson, B. R.; Bassik, N.; Stern, G. M.; Gracias, D. H. Tetherless Thermobiochemically Actuated Microgrippers. *Proc. Natl. Acad. Sci. U.S.A.* **2009**, *106*, 703−708.
(168) Li, H.; Guo, X.; Nuzzo, R. G.; Hsia, K. J. Capillary Induced Self-Assembly of Thin Foils into 3d Structures. *J. Mech. Phys. Solids* **2010**, *58*, 2033−2042.
(169) Randhawa, J. S.; Gurbani, S. S.; Keung, M. D.; Demers, D. P.; Leahy-Hoppa, M. R.; Gracias, D. H. Three-Dimensional Surface Current Loops in Terahertz Responsive Microarrays. *Appl. Phys. Lett.* **2010**, *96*, 191108.
(170) Azam, A.; Laflin, K. E.; Jamal, M.; Fernandes, R.; Gracias, D. H. Self-Folding Micropatterned Polymeric Containers. *Biomed. Microdevices* **2011**, *13*, 51−58.
(171) Cho, J.-H.; Keung, M. D.; Verellen, N.; Lagae, L.; Moshchalkov, V. V.; Van Dorpe, P.; Gracias, D. H. Nanoscale Origami for 3d Optics. *Small* **2011**, *7*, 1943−1948.
(172) Pandey, S.; Ewing, M.; Kunas, A.; Nguyen, N.; Gracias, D. H.; Menon, G. Algorithmic Design of Self-Folding Polyhedra. *Proc. Natl. Acad. Sci. U.S.A.* **2011**, *108*, 19885−19890.
(173) Randall, C. L.; Kalinin, Y. V.; Jamal, M.; Manohar, T.; Gracias, D. H. Three-Dimensional Microwell Arrays for Cell Culture. *Lab Chip* **2011**, *11*, 127−131.
(174) Felton, S. M.; Tolley, M. T.; Shin, B.; Onal, C. D.; Demaine, E. D.; Rus, D.; Wood, R. J. Self-Folding with Shape Memory Composites. *Soft Matter* **2013**, *9*, 7688.
(175) Felton, S.; Tolley, M.; Demaine, E.; Rus, D.; Wood, R. A Method for Building Self-Folding Machines. *Science* **2014**, *345*, 644−646.
(176) Legrain, A.; Janson, T. G.; Berenschot, J. W.; Abelmann, L.; Tas, N. R. Controllable Elastocapillary Folding of Three-Dimensional Micro-Objects by through-Wafer Filling. *J. Appl. Phys.* **2014**, *115*, 214905.
(177) Cui, A.; Liu, Z.; Li, J.; Shen, T. H.; Xia, X.; Li, Z.; Gong, Z.; Li, H.; Wang, B.; Li, J.; et al. Directly Patterned Substrate-Free Plasmonic "Nanograter" Structures with Unusual Fano Resonances. *Light-Sci. Appl.* **2015**, *4*, No. e308.
(178) Na, J.-H.; Evans, A. A.; Bae, J.; Chiappelli, M. C.; Santangelo, C. D.; Lang, R. J.; Hull, T. C.; Hayward, R. C. Programming Reversibly Self-Folding Origami with Micropatterned Photo-Crosslinkable Polymer Trilayers. *Adv. Mater.* **2015**, *27*, 79−85.
(179) Anacleto, P.; Gultepe, E.; Gomes, S.; Mendes, P. M.; Gracias, D. H. Self-Folding Microcube Antennas for Wireless Power Transfer in Dispersive Media. *Technology* **2016**, *4*, 120−129.
(180) Mao, Y.; Pan, Y.; Zhang, W.; Zhu, R.; Xu, J.; Wu, W. Multi-Direction-Tunable Three-Dimensional Meta-Atoms for Reversible Switching between Midwave and Long-Wave Infrared Regimes. *Nano Lett.* **2016**, *16*, 7025−7029.
(181) Pandey, S.; Macias, N. J.; Ciobanu, C.; Yoon, C.; Teuscher, C.; Gracias, D. H. Assembly of a 3d Cellular Computer Using Folded E-Blocks. *Micromachines* **2016**, *7*, 78.
(182) Jin, Q.; Li, M.; Polat, B.; Paidi, S. K.; Dai, A.; Zhang, A.; Pagaduan, J. V.; Barman, I.; Gracias, D. H. Mechanical Trap Surface-Enhanced Raman Spectroscopy for Three-Dimensional Surface

Molecular Imaging of Single Live Cells. *Angew. Chem., Int. Ed.* **2017**, *56*, 3822−3826.
(183) Cui, J. Z.; Huang, T. Y.; Luo, Z. C.; Testa, P.; Gu, H. R.; Chen, X. Z.; Nelson, B. J.; Heyderman, L. J. Nanomagnetic Encoding of Shape-Morphing Micromachines. *Nature* **2019**, *575*, 164−168.
(184) Jin, Q.; Yang, Y.; Jackson, J. A.; Yoon, C.; Gracias, D. H. Untethered Single Cell Grippers for Active Biopsy. *Nano Lett.* **2020**, *20*, 5383−5390.
(185) Li, C.; Xue, Y.; Han, M.; Palmer, L. C.; Rogers, J. A.; Huang, Y.; Stupp, S. I. Synergistic Photoactuation of Bilayered Spiropyran Hydrogels for Predictable Origami-Like Shape Change. *Matter* **2021**, *4*, 1377−1390.
(186) Xu, X.; Davanco, M.; Qi, X.; Forrest, S. R. Direct Transfer Patterning on Three Dimensionally Deformed Surfaces at Micrometer Resolutions and Its Application to Hemispherical Focal Plane Detector Arrays. *Org. Electron.* **2008**, *9*, 1122−1127.
(187) Shin, G.; Jung, I.; Malyarchuk, V.; Song, J.; Wang, S.; Ko, H. C.; Huang, Y.; Ha, J. S.; Rogers, J. A. Micromechanics and Advanced Designs for Curved Photodetector Arrays in Hemispherical Electronic-Eye Cameras. *Small* **2010**, *6*, 851−856.
(188) Kim, D.-H.; Lu, N.; Ghaffari, R.; Kim, Y.-S.; Lee, S. P.; Xu, L.; Wu, J.; Kim, R.-H.; Song, J.; Liu, Z.; et al. Materials for Multifunctional Balloon Catheters with Capabilities in Cardiac Electrophysiological Mapping and Ablation Therapy. *Nat. Mater.* **2011**, *10*, 316−323.
(189) Kim, J.; Lee, M.; Shim, H. J.; Ghaffari, R.; Cho, H. R.; Son, D.; Jung, Y. H.; Soh, M.; Choi, C.; Jung, S.; et al. Stretchable Silicon Nanoribbon Electronics for Skin Prosthesis. *Nat. Commun.* **2014**, *5*, 5747.
(190) Park, H.; Cho, H.; Kim, J.; Bang, J. W.; Seo, S.; Rahmawan, Y.; Lee, D. Y.; Suh, K.-Y. Multiscale Transfer Printing into Recessed Microwells and on Curved Surfaces Via Hierarchical Perfluoropolyether Stamps. *Small* **2014**, *10*, 52−59.
(191) Xu, L.; Gutbrod, S. R.; Bonifas, A. P.; Su, Y.; Sulkin, M. S.; Lu, N.; Chung, H. J.; Jang, K. I.; Liu, Z.; Ying, M.; et al. 3d Multifunctional Integumentary Membranes for Spatiotemporal Cardiac Measurements and Stimulation across the Entire Epicardium. *Nat. Commun.* **2014**, *5*, 3329.
(192) Zhang, Y.; Huang, Y.; Rogers, J. A. Mechanics of Stretchable Batteries and Supercapacitors. *Curr. Opin Solid St M* **2015**, *19*, 190−199.
(193) Park, J.; Choi, S.; Janardhan, A. H.; Lee, S.-Y.; Raut, S.; Soares, J.; Shin, K.; Yang, S.; Lee, C.; Kang, K.-W.; et al. Electromechanical Cardioplasty Using a Wrapped Elasto-Conductive Epicardial Mesh. *Sci. Transl. Med.* **2016**, *8*, 344ra386.
(194) Choi, C.; Choi, M. K.; Liu, S.; Kim, M. S.; Park, O. K.; Im, C.; Kim, J.; Qin, X.; Lee, G. J.; Cho, K. W.; et al. Human Eye-Inspired Soft Optoelectronic Device Using High-Density Mos2-Graphene Curved Image Sensor Array. *Nat. Commun.* **2017**, *8*, 1664.
(195) Le Borgne, B.; De Sagazan, O.; Crand, S.; Jacques, E.; Harnois, M. Conformal Electronics Wrapped around Daily Life Objects Using an Original Method: Water Transfer Printing. *ACS Appl. Mater. Interfaces* **2017**, *9*, 29424−29429.
(196) Saada, G.; Layani, M.; Chernevousky, A.; Magdassi, S. Hydroprinting Conductive Patterns onto 3d Structures. *Adv. Mater. Technol.* **2017**, *2*, 1600289.
(197) Zhang, K.; Jung, Y. H.; Mikael, S.; Seo, J.-H.; Kim, M.; Mi, H.; Zhou, H.; Xia, Z.; Zhou, W.; Gong, S.; et al. Origami Silicon Optoelectronics for Hemispherical Electronic Eye Systems. *Nat. Commun.* **2017**, *8*, 1782.
(198) Lee, G. J.; Choi, C.; Kim, D.-H.; Song, Y. M. Bioinspired Artificial Eyes: Optic Components, Digital Cameras, and Visual Prostheses. *Adv. Funct. Mater.* **2018**, *28*, 1705202.
(199) Ershad, F.; Sim, K.; Thukral, A.; Zhang, Y. S.; Yu, C. Emerging Soft Bioelectronics for Cardiac Health Diagnosis and Treatment. *APL Mater.* **2019**, *7*, 031301.
(200) Fan, D.; Lee, B.; Coburn, C.; Forrest, S. R. From 2d to 3d: Strain- and Elongation-Free Topological Transformations of Optoelectronic Circuits. *Proc. Natl. Acad. Sci. U.S.A.* **2019**, *116*, 3968−3973.
(201) Sim, K.; Chen, S.; Li, Z.; Rao, Z.; Liu, J.; Lu, Y.; Jang, S.; Ershad, F.; Chen, J.; Xiao, J.; et al. Three-Dimensional Curvy Electronics Created Using Conformal Additive Stamp Printing. *Nat. Electron.* **2019**, *2*, 471−479.
(202) Tian, L.; Zimmerman, B.; Akhtar, A.; Yu, K. J.; Moore, M.; Wu, J.; Larsen, R. J.; Lee, J. W.; Li, J.; Liu, Y.; et al. Large-Area Mri-Compatible Epidermal Electronic Interfaces for Prosthetic Control and Cognitive Monitoring. *Nat. Biomed. Eng.* **2019**, *3*, 194−205.
(203) Choi, J.; Han, C.; Cho, S.; Kim, K.; Ahn, J.; Del Orbe, D.; Cho, I.; Zhao, Z. J.; Oh, Y. S.; Hong, H.; et al. Customizable, Conformal, and Stretchable 3d Electronics Via Predistorted Pattern Generation and Thermoforming. *Sci. Adv.* **2021**, *7*. DOI: 10.1126/sciadv.abj0694
(204) Liu, J.; Jiang, S.; Xiong, W.; Zhu, C.; Li, K.; Huang, Y. Self-Healing Kirigami Assembly Strategy for Conformal Electronics. *Adv. Funct. Mater.* **2022**. DOI: 10.1002/adfm.202109214
(205) Liu, X.; Cao, Y.; Zheng, K.; Zhang, Y.; Wang, Z.; Chen, Y.; Chen, Y.; Ma, Y.; Feng, X. Liquid Droplet Stamp Transfer Printing. *Adv. Funct. Mater.* **2021**, *31*. DOI: 10.1002/adfm.202105407
(206) Jiang, S.; Liu, J.; Xiong, W.; Yang, Z.; Yin, L.; Li, K.; Huang, Y. A Snakeskin-Inspired, Soft-Hinge Kirigami Metamaterial for Self-Adaptive Conformal Electronic Armor. *Adv. Mater.* **2022**, *34*, No. 2204091.
(207) Zabow, G. Reflow Transfer for Conformal Three-Dimensional Microprinting. *Science* **2022**, *378*, 894−898.
(208) Liu, S.; He, J.; Rao, Y.; Dai, Z.; Ye, H.; Tanir, J. C.; Li, Y.; Lu, N. Conformability of Flexible Sheets on Spherical Surfaces. *Sci. Adv.* **2023**, *9*, No. eadf2709.
(209) Liu, Y.; Yan, Z.; Lin, Q.; Guo, X.; Han, M.; Nan, K.; Hwang, K. C.; Huang, Y.; Zhang, Y.; Rogers, J. A. Guided Formation of 3d Helical Mesostructures by Mechanical Buckling: Analytical Modeling and Experimental Validation. *Adv. Funct. Mater.* **2016**, *26*, 2909−2918.
(210) Yan, Z.; Zhang, F.; Wang, J.; Liu, F.; Guo, X.; Nan, K.; Lin, Q.; Gao, M.; Xiao, D.; Shi, Y.; et al. Controlled Mechanical Buckling for Origami-Inspired Construction of 3d Microstructures in Advanced Materials. *Adv. Funct. Mater.* **2016**, *26*, 2629−2639.
(211) McCracken, J. M.; Xu, S.; Badea, A.; Jang, K. I.; Yan, Z.; Wetzel, D. J.; Nan, K.; Lin, Q.; Han, M.; Anderson, M. A.; et al. Deterministic Integration of Biological and Soft Materials onto 3d Microscale Cellular Frameworks. *Adv. Biosyst.* **2017**, *1*, 1700068.
(212) Nan, K.; Luan, H.; Yan, Z.; Ning, X.; Wang, Y.; Wang, A.; Wang, J.; Han, M.; Chang, M.; Li, K.; et al. Engineered Elastomer Substrates for Guided Assembly of Complex 3d Mesostructures by Spatially Nonuniform Compressive Buckling. *Adv. Funct. Mater.* **2017**, *27*, 1604281.
(213) Shi, Y.; Zhang, F.; Nan, K.; Wang, X.; Wang, J.; Zhang, Y.; Zhang, Y.; Luan, H.; Hwang, K.-C.; Huang, Y.; et al. Plasticity-Induced Origami for Assembly of Three Dimensional Metallic Structures Guided by Compressive Buckling. *Extreme Mech. Lett.* **2017**, *11*, 105−110.
(214) Yan, Z.; Han, M.; Shi, Y.; Badea, A.; Yang, Y.; Kulkarni, A.; Hanson, E.; Kandel, M. E.; Wen, X.; Zhang, F.; et al. Three-Dimensional Mesostructures as High-Temperature Growth Templates, Electronic Cellular Scaffolds, and Self-Propelled Microrobots. *Proc. Natl. Acad. Sci. U.S.A.* **2017**, *114*, e9455−e9464.
(215) Fan, Z.; Hwang, K.-C.; Rogers, J. A.; Huang, Y.; Zhang, Y. A Double Perturbation Method of Postbuckling Analysis in 2d Curved Beams for Assembly of 3d Ribbon-Shaped Structures. *J. Mech. Phys. Solids* **2018**, *111*, 215−238.
(216) Guo, X.; Wang, X.; Ou, D.; Ye, J.; Pang, W.; Huang, Y.; Rogers, J. A.; Zhang, Y. Controlled Mechanical Assembly of Complex 3d Mesostructures and Strain Sensors by Tensile Buckling. *npj Flex. Electron.* **2018**, *2*, 14.
(217) Lee, W.; Liu, Y.; Lee, Y.; Sharma, B. K.; Shinde, S. M.; Kim, S. D.; Nan, K.; Yan, Z.; Han, M.; Huang, Y.; et al. Two-Dimensional Materials in Functional Three-Dimensional Architectures with Applications in Photodetection and Imaging. *Nat. Commun.* **2018**, *9*, 1417.
(218) Ling, Y.; Zhuang, X.; Xu, Z.; Xie, Y.; Zhu, X.; Xu, Y.; Sun, B.; Lin, J.; Zhang, Y.; Yan, Z. Mechanically Assembled, Three-Dimensional

Hierarchical Structures of Cellular Graphene with Programmed Geometries and Outstanding Electromechanical Properties. *ACS Nano* **2018**, *12*, 12456−12463.
(219) Ning, X.; Yu, X.; Wang, H.; Sun, R.; Corman, R. E.; Li, H.; Lee, C. M.; Xue, Y.; Chempakasseril, A.; Yao, Y.; et al. Mechanically Active Materials in Three-Dimensional Mesostructures. *Sci. Adv.* **2018**, *4*, No. eaat8313.
(220) Zhang, F.; Liu, F.; Zhang, Y. Analyses of Mechanically-Assembled 3d Spiral Mesostructures with Applications as Tunable Inductors. *Sci. China Technol. Sci.* **2019**, *62*, 243−251.
(221) Liu, W.; Zou, Q.; Zheng, C.; Jin, C. Metal-Assisted Transfer Strategy for Construction of 2d and 3d Nanostructures on an Elastic Substrate. *ACS Nano* **2019**, *13*, 440−448.
(222) Liu, Y.; Wang, X.; Xu, Y.; Xue, Z.; Zhang, Y.; Ning, X.; Cheng, X.; Xue, Y.; Lu, D.; Zhang, Q.; et al. Harnessing the Interface Mechanics of Hard Films and Soft Substrates for 3d Assembly by Controlled Buckling. *Proc. Natl. Acad. Sci. U.S.A.* **2019**, *116*, 15368−15377.
(223) Liu, Y.; Xu, Z.; Hwang, K. C.; Huang, Y.; Zhang, Y. Postbuckling Analyses of Frame Mesostructures Consisting of Straight Ribbons for Mechanically Guided Three-Dimensional Assembly. *Proc.R.Soc.A* **2019**, *475*, 20190012.
(224) Luan, H.; Cheng, X.; Wang, A.; Zhao, S.; Bai, K.; Wang, H.; Pang, W.; Xie, Z.; Li, K.; Zhang, F.; et al. Design and Fabrication of Heterogeneous, Deformable Substrates for the Mechanically Guided 3d Assembly. *ACS Appl. Mater. Interfaces* **2019**, *11*, 3482−3492.
(225) Pang, W.; Cheng, X.; Zhao, H.; Guo, X.; Ji, Z.; Li, G.; Liang, Y.; Xue, Z.; Song, H.; Zhang, F.; et al. Electro-Mechanically Controlled Assembly of Reconfigurable 3d Mesostructures and Electronic Devices Based on Dielectric Elastomer Platforms. *Natl. Sci. Rev.* **2020**, *7*, 342−354.
(226) Park, J. K.; Nan, K.; Luan, H.; Zheng, N.; Zhao, S.; Zhang, H.; Cheng, X.; Wang, H.; Li, K.; Xie, T.; et al. Remotely Triggered Assembly of 3d Mesostructures through Shape-Memory Effects. *Adv. Mater.* **2019**, *31*, No. 1905715.
(227) Park, Y.; Luan, H.; Kwon, K.; Zhao, S.; Franklin, D.; Wang, H.; Zhao, H.; Bai, W.; Kim, J. U.; Lu, W.; et al. Transformable, Freestanding 3d Mesostructures Based on Transient Materials and Mechanical Interlocking. *Adv. Funct. Mater.* **2019**, *29*, 1903181.
(228) Wang, X.; Guo, X.; Ye, J.; Zheng, N.; Kohli, P.; Choi, D.; Zhang, Y.; Xie, Z.; Zhang, Q.; Luan, H.; et al. Freestanding 3d Mesostructures, Functional Devices, and Shape-Programmable Systems Based on Mechanically Induced Assembly with Shape Memory Polymers. *Adv. Mater.* **2019**, *31*, No. 1805615.
(229) Yang, C.; Huang, Y.; Cheng, H.; Jiang, L.; Qu, L. Rollable, Stretchable, and Reconfigurable Graphene Hygroelectric Generators. *Adv. Mater.* **2019**, *31*, No. 1805705.
(230) Zhang, C.; Deng, H.; Xie, Y.; Zhang, C.; Su, J. W.; Lin, J. Stimulus Responsive 3d Assembly for Spatially Resolved Bifunctional Sensors. *Small* **2019**, *15*, No. 1904224.
(231) Zhang, Y.; Wang, F.; Ma, Y.; Feng, X. Buckling Configurations of Stiff Thin Films Tuned by Micro-Patterns on Soft Substrate. *Int. J. Solids Struct.* **2019**, *161*, 55−63.
(232) Zhao, H.; Li, K.; Han, M.; Zhu, F.; Vazquez-Guardado, A.; Guo, P.; Xie, Z.; Park, Y.; Chen, L.; Wang, X.; et al. Buckling and Twisting of Advanced Materials into Morphable 3d Mesostructures. *Proc. Natl. Acad. Sci. U.S.A.* **2019**, *116*, 13239−13248.
(233) Lim, S.; Luan, H.; Zhao, S.; Lee, Y.; Zhang, Y.; Huang, Y.; Rogers, J. A.; Ahn, J.-H. Assembly of Foldable 3d Microstructures Using Graphene Hinges. *Adv. Mater.* **2020**, *32*, 2001303.
(234) Li, Y.; Luo, C.; Yu, K.; Wang, X. Remotely Controlled, Reversible, on-Demand Assembly and Reconfiguration of 3d Mesostructures Via Liquid Crystal Elastomer Platforms. *ACS Appl. Mater. Interfaces* **2021**, *13*, 8929−8939.
(235) Li, Y.; Yu, H.; Yu, K.; Guo, X.; Wang, X. Reconfigurable Three-Dimensional Mesotructures of Spatially Programmed Liquid Crystal Elastomers and Their Ferromagnetic Composites. *Adv. Funct. Mater.* **2021**, *31*, 2100338.
(236) Luan, H.; Zhang, Q.; Liu, T.-L.; Wang, X.; Zhao, S.; Wang, H.; Yao, S.; Xue, Y.; Kwak, J. W.; Bai, W.; et al. Complex 3d Microfluidic Architectures Formed by Mechanically Guided Compressive Buckling. *Sci. Adv.* **2021**, *7*, No. eabj3686.
(237) Miao, L.; Song, Y.; Ren, Z.; Xu, C.; Wan, J.; Wang, H.; Guo, H.; Xiang, Z.; Han, M.; Zhang, H. 3d Temporary-Magnetized Soft Robotic Structures for Enhanced Energy Harvesting. *Adv. Mater.* **2021**, *33*, No. 2102691.
(238) Zhang, F.; Li, S.; Shen, Z.; Cheng, X.; Xue, Z.; Zhang, H.; Song, H.; Bai, K.; Yan, D.; Wang, H.; et al. Rapidly Deployable and Morphable 3d Mesostructures with Applications in Multimodal Biomedical Devices. *Proc. Natl. Acad. Sci. U.S.A.* **2021**, *118*. DOI: 10.1073/pnas.2026414118
(239) Li, R.; Zhang, C.; Li, J.; Zhang, Y.; Liu, S.; Hu, Y.; Jiang, S.; Chen, C.; Xin, C.; Tao, Y.; et al. Magnetically Encoded 3d Mesostructure with High-Order Shape Morphing and High-Frequency Actuation. *Natl. Sci. Rev.* **2022**, *9*, nwac163.
(240) Xue, Z.; Jin, T.; Xu, S.; Bai, K.; He, Q.; Zhang, F.; Cheng, X.; Ji, Z.; Pang, W.; Shen, Z.; et al. Assembly of Complex 3d Structures and Electronics on Curved Surfaces. *Sci. Adv.* **2022**, *8*, No. eabm6922.
(241) Zhao, H.; Cheng, X.; Wu, C.; Liu, T. L.; Zhao, Q.; Li, S.; Ni, X.; Yao, S.; Han, M.; Huang, Y.; et al. Mechanically Guided Hierarchical Assembly of 3d Mesostructures. *Adv. Mater.* **2022**, *34*, No. 2109416.
(242) Ahn, J.; Ha, J. H.; Jeong, Y.; Jung, Y.; Choi, J.; Gu, J.; Hwang, S. H.; Kang, M.; Ko, J.; Cho, S.; et al. Nanoscale Three-Dimensional Fabrication Based on Mechanically Guided Assembly. *Nat. Commun.* **2023**, *14*, 833.
(243) Pang, W.; Liu, L.; Xu, S.; Shuai, Y.; Zhao, J.; Zhang, Y.; Electroadhesion-Mediated Interface Delamination for Assembly of Reconfigurable 3d Mesostructures. *J. Appl. Mech.* **2023**, *90*. DOI: 10.1115/1.4056861
(244) Shuai, Y.; Zhao, J.; Bo, R.; Lan, Y.; Lv, Z.; Zhang, Y. A Wrinkling-Assisted Strategy for Controlled Interface Delamination in Mechanically-Guided 3d Assembly. *J. Mech. Phys. Solids* **2023**, *173*, 105203.
(245) Ling, Y.; Pang, W.; Li, X.; Goswami, S.; Xu, Z.; Stroman, D.; Liu, Y.; Fei, Q.; Xu, Y.; Zhao, G.; et al. Laser-Induced Graphene for Electrothermally Controlled, Mechanically Guided, 3d Assembly and Human-Soft Actuators Interaction. *Adv. Mater.* **2020**, *32*, No. 1908475.
(246) Liu, Z.; Du, H.; Li, J.; Lu, L.; Li, Z.-Y.; Fang, N. X. Nano-Kirigami with Giant Optical Chirality. *Sci. Adv.* **2018**, *4*, No. eaat4436.
(247) Jiang, J.; Zhang, S.; Wang, B.; Ding, H.; Wu, Z. Hydroprinted Liquid-Alloy-Based Morphing Electronics for Fast-Growing/Tender Plants: From Physiology Monitoring to Habit Manipulation. *Small* **2020**, *16*, 2003833.
(248) Liu, Y.; Zheng, M.; O'Connor, B.; Dong, J.; Zhu, Y. Curvilinear Soft Electronics by Micromolding of Metal Nanowires in Capillaries. *Sci. Adv.* **2022**, *8*, No. eadd6996.
(249) Kim, B. H.; Lee, J.; Won, S. M.; Xie, Z.; Chang, J. K.; Yu, Y.; Cho, Y. K.; Jang, H.; Jeong, J. Y.; Lee, Y.; et al. Three-Dimensional Silicon Electronic Systems Fabricated by Compressive Buckling Process. *ACS Nano* **2018**, *12*, 4164−4171.
(250) Luo, G.; Fu, H.; Cheng, X.; Bai, K.; Shi, L.; He, X.; Rogers, J. A.; Huang, Y.; Zhang, Y. Mechanics of Bistable Cross-Shaped Structures through Loading-Path Controlled 3d Assembly. *J. Mech. Phys. Solids* **2019**, *129*, 261−277.
(251) Rogers, J. A.; Lagally, M. G.; Nuzzo, R. G. Synthesis, Assembly and Applications of Semiconductor Nanomembranes. *Nature* **2011**, *477*, 45−53.
(252) Khang, D. Y.; Rogers, J. A.; Lee, H. H. Mechanical Buckling: Mechanics, Metrology, and Stretchable Electronics. *Adv. Funct. Mater.* **2009**, *19*, 1526−1536.
(253) Jiang, H.; Sun, Y.; Rogers, J. A.; Huang, Y. Mechanics of Precisely Controlled Thin Film Buckling on Elastomeric Substrate. *Appl. Phys. Lett.* **2007**, *90*. DOI: 10.1063/1.2719027
(254) Wang, S.; Song, J.; Kim, D.-H.; Huang, Y.; Rogers, J. A. Local Versus Global Buckling of Thin Films on Elastomeric Substrates. *Appl. Phys. Lett.* **2008**, *93*. DOI: 10.1063/1.2956402
(255) Yan, Z. G.; Wang, B. L.; Wang, K. F. Stretchability and Compressibility of a Novel Layout Design for Flexible Electronics

Based on Bended Wrinkle Geometries. *Compos. B. Eng.* **2019**, *166*, 65−73.
(256) Li, Z. W.; Wang, Y.; Xiao, J. L. Mechanics of Curvilinear Electronics and Optoelectronics. *Curr. Opin Solid St M* **2015**, *19*, 171−189.
(257) Cheng, H. Y.; Zhang, Y. H.; Hwang, K. C.; Rogers, J. A.; Huang, Y. G. Buckling of a Stiff Thin Film on a Pre-Strained Bi-Layer Substrate. *Int. J. Solids Struct.* **2014**, *51*, 3113−3118.
(258) Jiang, H.; Sun, Y.; Rogers, J. A.; Huang, Y. Post-Buckling Analysis for the Precisely Controlled Buckling of Thin Film Encapsulated by Elastomeric Substrates. *Int. J. Solids Struct.* **2008**, *45*, 2014−2023.
(259) Song, J.; Jiang, H.; Liu, Z. J.; Khang, D. Y.; Huang, Y.; Rogers, J. A.; Lu, C.; Koh, C. G. Buckling of a Stiff Thin Film on a Compliant Substrate in Large Deformation. *Int. J. Solids Struct.* **2008**, *45*, 3107−3121.
(260) Yoder, M. A.; Yan, Z.; Han, M.; Rogers, J. A.; Nuzzo, R. G. Semiconductor Nanomembrane Materials for High-Performance Soft Electronic Devices. *J. Am. Chem. Soc.* **2018**, *140*, 9001−9019.
(261) Cheng, H.; Song, J. A Simply Analytic Study of Buckled Thin Films on Compliant Substrates. *J. Appl. Mech.* **2014**, *81*. DOI: 10.1115/1.4025306
(262) Wang, A.; Avila, R.; Ma, Y. J. Mechanics Design for Buckling of Thin Ribbons on an Elastomeric Substrate without Material Failure. *J. Appl. Mech.* **2017**, *84*. DOI: 10.1115/1.4037149
(263) Song, J.; Huang, Y.; Xiao, J.; Wang, S.; Hwang, K. C.; Ko, H. C.; Kim, D. H.; Stoykovich, M. P.; Rogers, J. A. Mechanics of Noncoplanar Mesh Design for Stretchable Electronic Circuits. *J. Appl. Phys.* **2009**, *105*. DOI: 10.1063/1.3148245
(264) Wang, Y.; Li, Z. W.; Xiao, J. L. Stretchable Thin Film Materials: Fabrication, Application, and Mechanics. *J. Electron. Packag.* **2016**, *138*. DOI: 10.1115/1.4032984
(265) Sun, Y. G.; Rogers, J. A. Structural Forms of Single Crystal Semiconductor Nanoribbons for High-Performance Stretchable Electronics. *J. Mater. Chem.* **2007**, *17*, 832−840.
(266) Jiang, H. Q.; Khang, D. Y.; Fei, H. Y.; Kim, H.; Huang, Y. G.; Xiao, J. L.; Rogers, J. A. Finite Width Effect of Thin-Films Buckling on Compliant Substrate: Experimental and Theoretical Studies. *J. Mech. Phys. Solids* **2008**, *56*, 2585−2598.
(267) Zhang, Q. T.; Yin, H. Spontaneous Buckling-Driven Periodic Delamination of Thin Films on Soft Substrates under Large Compression. *J. Mech. Phys. Solids* **2018**, *118*, 40−57.
(268) Song, J.; Jiang, H.; Huang, Y.; Rogers, J. A. Mechanics of Stretchable Inorganic Electronic Materials. *J. Vac. Sci. Technol. A* **2009**, *27*, 1107−1125.
(269) Choi, W. M.; Song, J.; Khang, D. Y.; Jiang, H.; Huang, Y. Y.; Rogers, J. A. Biaxially Stretchable "Wavy" Silicon Nanomembranes. *Nano Lett.* **2007**, *7*, 1655−1663.
(270) Li, G.; Zhang, M.; Liu, S.; Yuan, M.; Wu, J.; Yu, M.; Teng, L.; Xu, Z.; Guo, J.; Li, G.; et al. Three-Dimensional Flexible Electronics Using Solidified Liquid Metal with Regulated Plasticity. *Nat. Electron.* **2023**, *6*, 154.
(271) Song, J.; Feng, X.; Huang, Y. Mechanics and Thermal Management of Stretchable Inorganic Electronics. *Natl. Sci. Rev.* **2016**, *3*, 128−143.
(272) Jiang, H.; Khang, D. Y.; Song, J.; Sun, Y.; Huang, Y.; Rogers, J. A. Finite Deformation Mechanics in Buckled Thin Films on Compliant Supports. *Proc. Natl. Acad. Sci. U.S.A.* **2007**, *104*, 15607−15612.
(273) Ma, Y.; Xue, Y.; Jang, K. I.; Feng, X.; Rogers, J. A.; Huang, Y. Wrinkling of a Stiff Thin Film Bonded to a Pre-Strained, Compliant Substrate with Finite Thickness. *Proc.R.Soc.A* **2016**, *472*, 20160339.
(274) Li, R.; Li, M.; Su, Y. W.; Song, J. Z.; Ni, X. Q. An Analytical Mechanics Model for the Island-Bridge Structure of Stretchable Electronics. *Soft Matter* **2013**, *9*, 8476−8482.
(275) Wang, S. D.; Xiao, J. L.; Song, J. Z.; Ko, H. C.; Hwang, K. C.; Huang, Y. G.; Rogers, J. A. Mechanics of Curvilinear Electronics. *Soft Matter* **2010**, *6*, 5757−5763.
(276) Chen, C.; Tao, W.; Liu, Z. J.; Zhang, Y. W.; Song, J. Controlled Buckling of Thin Film on Elastomeric Substrate in Large Deformation. *Theor. Appl. Mech. Lett.* **2011**, *1*, 021001.
(277) Zhang, Y.; Wang, S.; Li, X.; Fan, J. A.; Xu, S.; Song, Y. M.; Choi, K.-J.; Yeo, W.-H.; Lee, W.; Nazaar, S. N.; et al. Experimental and Theoretical Studies of Serpentine Microstructures Bonded to Prestrained Elastomers for Stretchable Electronics. *Adv. Funct. Mater.* **2014**, *24*, 2028−2037.
(278) Kim, D. H.; Liu, Z.; Kim, Y. S.; Wu, J.; Song, J.; Kim, H. S.; Huang, Y.; Hwang, K. C.; Zhang, Y.; Rogers, J. A. Optimized Structural Designs for Stretchable Silicon Integrated Circuits. *Small* **2009**, *5*, 2841−2847.
(279) Li, K.; Cheng, X.; Zhu, F.; Li, L. Z.; Xie, Z. Q.; Luan, H. W.; Wang, Z. H.; Ji, Z. Y.; Wang, H. L.; Liu, F.; et al. A Generic Soft Encapsulation Strategy for Stretchable Electronics. *Adv. Funct. Mater.* **2019**, *29*. DOI: 10.1002/adfm.201806630
(280) Jang, K. I.; Li, K.; Chung, H. U.; Xu, S.; Jung, H. N.; Yang, Y.; Kwak, J. W.; Jung, H. H.; Song, J.; Yang, C.; et al. Self-Assembled Three Dimensional Network Designs for Soft Electronics. *Nat. Commun.* **2017**, *8*, 15894.
(281) Lee, J.; Ihle, S. J.; Pellegrino, G. S.; Kim, H.; Yea, J.; Jeon, C.-Y.; Son, H.-C.; Jin, C.; Eberli, D.; Schmid, F.; et al. Stretchable and Suturable Fibre Sensors for Wireless Monitoring of Connective Tissue Strain. *Nat. Electron.* **2021**, *4*, 291−301.
(282) Wang, B.; Bao, S.; Vinnikova, S.; Ghanta, P.; Wang, S. Buckling Analysis in Stretchable Electronics. *npj Flex. Electron.* **2017**, *1*. DOI: 10.1038/s41528-017-0004-y
(283) Nan, K.; Wang, H.; Ning, X.; Miller, K. A.; Wei, C.; Liu, Y.; Li, H.; Xue, Y.; Xie, Z.; Luan, H.; et al. Soft Three-Dimensional Microscale Vibratory Platforms for Characterization of Nano-Thin Polymer Films. *ACS Nano* **2019**, *13*, 449−457.
(284) Liu, F.; Cheng, X.; Zhang, F.; Chen, Y.; Song, H.; Huang, Y.; Zhang, Y. Design and Assembly of Reconfigurable 3d Radio-Frequency Antennas Based on Mechanically Triggered Switches. *Adv. Electron. Mater.* **2019**, *5*, 1900256.
(285) Qi, D.; Liu, Z.; Liu, Y.; Leow, W. R.; Zhu, B.; Yang, H.; Yu, J.; Wang, W.; Wang, H.; Yin, S.; et al. Suspended Wavy Graphene Microribbons for Highly Stretchable Microsupercapacitors. *Adv. Mater.* **2015**, *27*, 5559−5566.
(286) Kwon, K.; Kim, J. U.; Won, S. M.; Zhao, J.; Avila, R.; Wang, H.; Chun, K. S.; Jang, H.; Lee, K. H.; Kim, J. H.; et al. A Battery-Less Wireless Implant for the Continuous Monitoring of Vascular Pressure, Flow Rate and Temperature. *Nat. Biomed. Eng.* **2023**. DOI: 10.1038/s41551-023-01022-4
(287) Zhao, H.; Kim, Y.; Wang, H.; Ning, X.; Xu, C.; Suh, J.; Han, M.; Pagan-Diaz, G. J.; Lu, W.; Li, H.; et al. Compliant 3d Frameworks Instrumented with Strain Sensors for Characterization of Millimeter-Scale Engineered Muscle Tissues. *Proc. Natl. Acad. Sci. U.S.A.* **2021**, *118*. DOI: 10.1073/pnas.2100077118
(288) Medina-Sánchez, M.; Magdanz, V.; Guix, M.; Fomin, V. M.; Schmidt, O. G. Swimming Microrobots: Soft, Reconfigurable, and Smart. *Adv. Funct. Mater.* **2018**, *28*, 1707228.
(289) Nan, K.; Kang, S. D.; Li, K.; Yu, K. J.; Zhu, F.; Wang, J.; Dunn, A. C.; Zhou, C.; Xie, Z.; Agne, M. T.; et al. Compliant and Stretchable Thermoelectric Coils for Energy Harvesting in Miniature Flexible Devices. *Sci. Adv.* **2018**, *4*, No. eaau5849.
(290) Deng, J.; Ji, H.; Yan, C.; Zhang, J.; Si, W.; Baunack, S.; Oswald, S.; Mei, Y.; Schmidt, O. G. Naturally Rolled-up C/Si/C Trilayer Nanomembranes as Stable Anodes for Lithium-Ion Batteries with Remarkable Cycling Performance. *Angew. Chem., Int. Ed.* **2013**, *52*, 2326−2330.
(291) Gabler, F.; Karnaushenko, D. D.; Karnaushenko, D.; Schmidt, O. G. Magnetic Origami Creates High Performance Micro Devices. *Nat. Commun.* **2019**, *10*, 3013.
(292) Lee, Y.; Bandari, V. K.; Li, Z.; Medina-Sánchez, M.; Maitz, M. F.; Karnaushenko, D.; Tsurkan, M. V.; Karnaushenko, D. D.; Schmidt, O. G. Nano-Biosupercapacitors Enable Autarkic Sensor Operation in Blood. *Nat. Commun.* **2021**, *12*, 4967.

(293) Wang, H.; Zhen, H.; Li, S.; Jing, Y.; Huang, G.; Mei, Y.; Lu, W. Self-Rolling and Light-Trapping in Flexible Quantum Well-Embedded Nanomembranes for Wide-Angle Infrared Photodetectors. *Sci. Adv.* **2016**, *2*, No. e1600027.
(294) Joung, D.; Nemilentsau, A.; Agarwal, K.; Dai, C.; Liu, C.; Su, Q.; Li, J.; Low, T.; Koester, S. J.; Cho, J. H. Self-Assembled Three-Dimensional Graphene-Based Polyhedrons Inducing Volumetric Light Confinement. *Nano Lett.* **2017**, *17*, 1987−1994.
(295) Malachowski, K.; Jamal, M.; Jin, Q.; Polat, B.; Morris, C. J.; Gracias, D. H. Self-Folding Single Cell Grippers. *Nano Lett.* **2014**, *14*, 4164−4170.
(296) Xu, W.; Li, T.; Qin, Z.; Huang, Q.; Gao, H.; Kang, K.; Park, J.; Buehler, M. J.; Khurgin, J. B.; Gracias, D. H. Reversible Mos_2 Origami with Spatially Resolved and Reconfigurable Photosensitivity. *Nano Lett.* **2019**, *19*, 7941−7949.
(297) Kim, D. C.; Yun, H.; Kim, J.; Seung, H.; Yu, W. S.; Koo, J. H.; Yang, J.; Kim, J. H.; Hyeon, T.; Kim, D.-H. Three-Dimensional Foldable Quantum Dot Light-Emitting Diodes. *Nat. Electron.* **2021**, *4*, 671−680.
(298) Bao, N.; Liu, Q.; Reynolds, M. F.; Figueras, M.; Smith, E.; Wang, W.; Cao, M. C.; Muller, D. A.; Mavrikakis, M.; Cohen, I.; et al. Gas-Phase Microactuation Using Kinetically Controlled Surface States of Ultrathin Catalytic Sheets. *Proc. Natl. Acad. Sci. U.S.A.* **2023**, *120*, No. e2221740120.
(299) Adams, J. J.; Duoss, E. B.; Malkowski, T. F.; Motala, M. J.; Ahn, B. Y.; Nuzzo, R. G.; Bernhard, J. T.; Lewis, J. A. Conformal Printing of Electrically Small Antennas on Three-Dimensional Surfaces. *Adv. Funct. Mater.* **2011**, *23*, 1335−1340.
(300) Fan, Z.; Yang, Y.; Zhang, F.; Xu, Z.; Zhao, H.; Wang, T.; Song, H.; Huang, Y.; Rogers, J. A.; Zhang, Y. Inverse Design Strategies for 3d Surfaces Formed by Mechanically Guided Assembly. *Adv. Mater.* **2020**, *32*, No. e1908424.
(301) Liu, F.; Chen, Y.; Song, H.; Zhang, F.; Fan, Z.; Liu, Y.; Feng, X.; Rogers, J. A.; Huang, Y.; Zhang, Y. High Performance, Tunable Electrically Small Antennas through Mechanically Guided 3d Assembly. *Small* **2019**, *15*, No. 1804055.
(302) Hao, X. P.; Li, C. Y.; Zhang, C. W.; Du, M.; Ying, Z.; Zheng, Q.; Wu, Z. L. Self-Shaping Soft Electronics Based on Patterned Hydrogel with Stencil-Printed Liquid Metal. *Adv. Funct. Mater.* **2021**, *31*. DOI: 10.1002/adfm.202105481
(303) Gultepe, E.; Randhawa, J. S.; Kadam, S.; Yamanaka, S.; Selaru, F. M.; Shin, E. J.; Kalloo, A. N.; Gracias, D. H. Biopsy with Thermally-Responsive Untethered Microtools. *Adv. Mater.* **2013**, *25*, 514−519.
(304) Hiendlmeier, L.; Zurita, F.; Vogel, J.; Del Duca, F.; Al Boustani, G.; Peng, H.; Kopic, I.; Nikic, M.; Teshima, T.; Wolfrum, B. 4d Printed Soft and Stretchable Self-Folding Cuff Electrodes for Small-Nerve Interfacing. *Adv. Mater.* **2023**, *35*, No. e2210206.
(305) Ryu, H.; Park, Y.; Luan, H.; Dalgin, G.; Jeffris, K.; Yoon, H. J.; Chung, T. S.; Kim, J. U.; Kwak, S. S.; Lee, G.; et al. Transparent, Compliant 3d Mesostructures for Precise Evaluation of Mechanical Characteristics of Organoids. *Adv. Mater.* **2021**, *33*, No. 2100026.
(306) Du, X.; Cui, H.; Sun, B.; Wang, J.; Zhao, Q.; Xia, K.; Wu, T.; Humayun, M. S. Photothermally Triggered Shape-Adaptable 3d Flexible Electronics. *Adv. Mater. Technol.* **2017**, *2*, 1700120.
(307) Wang, J.; Zhao, Q.; Wang, Y.; Zeng, Q.; Wu, T.; Du, X. Self-Unfolding Flexible Microelectrode Arrays Based on Shape Memory Polymers. *Adv. Mater. Technol.* **2019**, *4*, 1900566.
(308) Wang, H.; Wang, Y.; Tee, B. C.; Kim, K.; Lopez, J.; Cai, W.; Bao, Z. Shape-Controlled, Self-Wrapped Carbon Nanotube 3d Electronics. *Adv. Sci.* **2015**, *2*, 1500103.
(309) Kalmykov, A.; Huang, C.; Bliley, J.; Shiwarski, D.; Tashman, J.; Abdullah, A.; Rastogi, S. K.; Shukla, S.; Mataev, E.; Feinberg, A. W.; et al. Organ-on-E-Chip: Three-Dimensional Self-Rolled Biosensor Array for Electrical Interrogations of Human Electrogenic Spheroids. *Sci. Adv.* **2019**, *5*, No. eaax0729.
(310) Zhang, Y. C.; Zheng, N.; Cao, Y.; Wang, F. L.; Wang, P.; Ma, Y. J.; Lu, B. W.; Hou, G. H.; Fang, Z. Z.; Liang, Z. W.; et al. Climbing-Inspired Twining Electrodes Using Shape Memory for Peripheral Nerve Stimulation and Recording. *Sci. Adv.* **2019**, *5*. DOI: 10.1126/sciadv.aaw1066
(311) Zhu, Y.; Birla, M.; Oldham, K. R.; Filipov, E. T. Elastically and Plastically Foldable Electrothermal Micro-Origami for Controllable and Rapid Shape Morphing. *Adv. Funct. Mater.* **2020**, *30*, 2003741.
(312) Wang, X.; Wang, Z.; Dong, H.; Saggau, C. N.; Tang, H.; Tang, M.; Liu, L.; Baunack, S.; Bai, L.; Liu, J.; et al. Collective Coupling of 3d Confined Optical Modes in Monolithic Twin Microtube Cavities Formed by Nanomembrane Origami. *Nano Lett.* **2022**, *22*, 6692−6699.
(313) Tang, H.; Karnaushenko, D. D.; Neu, V.; Gabler, F.; Wang, S.; Liu, L.; Li, Y.; Wang, J.; Zhu, M.; Schmidt, O. G. Stress-Actuated Spiral Microelectrode for High-Performance Lithium-Ion Microbatteries. *Small* **2020**, *16*, No. 2002410.
(314) Qu, Z.; Zhu, M.; Yin, Y.; Huang, Y.; Tang, H.; Ge, J.; Li, Y.; Karnaushenko, D. D.; Karnaushenko, D.; Schmidt, O. G. A Sub-Square-Millimeter Microbattery with Milliampere-Hour-Level Footprint Capacity. *Adv. Energy Mater.* **2022**, *12*. DOI: 10.1002/aenm.202200714
(315) Si, W.; Monch, I.; Yan, C.; Deng, J.; Li, S.; Lin, G.; Han, L.; Mei, Y.; Schmidt, O. G. A Single Rolled-up Si Tube Battery for the Study of Electrochemical Kinetics, Electrical Conductivity, and Structural Integrity. *Adv. Mater.* **2014**, *26*, 7973−7978.
(316) Xu, W.; Paidi, S. K.; Qin, Z.; Huang, Q.; Yu, C.-H.; Pagaduan, J. V.; Buehler, M. J.; Barman, I.; Gracias, D. H. Self-Folding Hybrid Graphene Skin for 3d Biosensing. *Nano Lett.* **2019**, *19*, 1409−1417.
(317) Ghosh, A.; Liu, W.; Li, L.; Pahapale, G. J.; Choi, S. Y.; Xu, L.; Huang, Q.; Zhang, R.; Zhong, Z.; Selaru, F. M.; et al. Autonomous Untethered Microinjectors for Gastrointestinal Delivery of Insulin. *ACS Nano* **2022**, *16*, 16211−16220.
(318) Ghosh, A.; Liu, Y.; Artemov, D.; Gracias, D. H. Magnetic Resonance Guided Navigation of Untethered Microgrippers. *Adv. Healthc. Mater.* **2021**, *10*, No. 2000869.
(319) Melzer, M.; Kaltenbrunner, M.; Makarov, D.; Karnaushenko, D.; Karnaushenko, D.; Sekitani, T.; Someya, T.; Schmidt, O. G. Imperceptible Magnetoelectronics. *Nat. Commun.* **2015**, *6*, 6080.
(320) Lee, Y.-K.; Xi, Z.; Lee, Y.-J.; Kim, Y.-H.; Hao, Y.; Choi, H.; Lee, M.-G.; Joo, Y.-C.; Kim, C.; Lien, J.-M.; et al. Computational Wrapping: A Universal Method to Wrap 3d-Curved Surfaces with Nonstretchable Materials for Conformal Devices. *Sci. Adv.* **2020**, *6*, No. eaax6212.
(321) Chen, I. T.; Poblete, F. R.; Bagal, A.; Zhu, Y.; Chang, C. H. Anelasticity in Thin-Shell Nanolattices. *Proc. Natl. Acad. Sci. U. S. A.* **2022**, *119*, No. e2201589119.
(322) Huang, W.; Zhou, J.; Froeter, P. J.; Walsh, K.; Liu, S.; Kraman, M. D.; Li, M.; Michaels, J. A.; Sievers, D. J.; Gong, S.; et al. Three-Dimensional Radio-Frequency Transformers Based on a Self-Rolled-up Membrane Platform. *Nat. Electron.* **2018**, *1*, 305−313.
(323) Lee, H.; Choi, T. K.; Lee, Y. B.; Cho, H. R.; Ghaffari, R.; Wang, L.; Choi, H. J.; Chung, T. D.; Lu, N.; Hyeon, T.; et al. A Graphene-Based Electrochemical Device with Thermoresponsive Microneedles for Diabetes Monitoring and Therapy. *Nat. Nanotechnol.* **2016**, *11*, 566−572.
(324) Zhang, C.; Chen, J.; Gao, J.; Tan, G.; Bai, S.; Weng, K.; Chen, H. M.; Ding, X.; Cheng, H.; Yang, Y.; et al. Laser Processing of Crumpled Porous Graphene/Mxene Nanocomposites for a Standalone Gas Sensing System. *Nano Lett.* **2023**, *23*, 3435−3443.
(325) Gu, Y.; Wang, C.; Kim, N.; Zhang, J.; Wang, T. M.; Stowe, J.; Nasiri, R.; Li, J.; Zhang, D.; Yang, A.; et al. Three-Dimensional Transistor Arrays for Intra- and Inter-Cellular Recording. *Nat. Nanotechnol.* **2022**, *17*, 292−300.
(326) Liu, Y.; Li, X.; Yang, H.; Zhang, P.; Wang, P.; Sun, Y.; Yang, F.; Liu, W.; Li, Y.; Tian, Y.; et al. Skin-Interfaced Superhydrophobic Insensible Sweat Sensors for Evaluating Body Thermoregulation and Skin Barrier Functions. *ACS Nano* **2023**, *17*, 5588−5599.
(327) Shirzaei Sani, E.; Xu, C.; Wang, C.; Song, Y.; Min, J.; Tu, J.; Solomon, S. A.; Li, J.; Banks, J. L.; Armstrong, D. G.; et al. A Stretchable Wireless Wearable Bioelectronic System for Multiplexed Monitoring and Combination Treatment of Infected Chronic Wounds. *Sci. Adv.* **2023**, *9*, No. eadf7388.

(328) Akbar, F.; Rivkin, B.; Aziz, A.; Becker, C.; Karnaushenko, D. D.; Medina-Sánchez, M.; Karnaushenko, D.; Schmidt, O. G. Self-Sufficient Self-Oscillating Microsystem Driven by Low Power at Low Reynolds Numbers. *Sci. Adv.* **2021**, *7*, No. eabj0767.
(329) Wu, S.; Hong, Y.; Zhao, Y.; Yin, J.; Zhu, Y. Caterpillar-Inspired Soft Crawling Robot with Distributed Programmable Thermal Actuation. *Sci. Adv.* **2023**, *9*, No. eadf8014.
(330) Wang, Y.; Adam, M. L.; Zhao, Y.; Zheng, W.; Gao, L.; Yin, Z.; Zhao, H. Machine Learning-Enhanced Flexible Mechanical Sensing. *Nano-Micro Lett.* **2023**, *15*, 55.
(331) Hoang, A. T.; Hu, L.; Katiyar, A. K.; Ahn, J.-H. Two-Dimensional Layered Materials and Heterostructures for Flexible Electronics. *Matter* **2022**, *5*, 4116−4132.
(332) Sim, K.; Rao, Z.; Zou, Z.; Ershad, F.; Lei, J.; Thukral, A.; Chen, J.; Huang, Q.-A.; Xiao, J.; Yu, C. Metal Oxide Semiconductor Nanomembrane-Based Soft Unnoticeable Multifunctional Electronics for Wearable Human-Machine Interfaces. *Sci. Adv.* **2019**, *5*, No. eaav9653.
(333) Song, H.; Luo, G.; Ji, Z.; Bo, R.; Xue, Z.; Yan, D.; Zhang, F.; Bai, K.; Liu, J.; Cheng, X.; et al. Highly-Integrated, Miniaturized, Stretchable Electronic Systems Based on Stacked Multilayer Network Materials. *Sci. Adv.* **2022**, *8*, No. eabm3785.
(334) Lee, G.; Zarei, M.; Wei, Q.; Zhu, Y.; Lee, S. G. Surface Wrinkling for Flexible and Stretchable Sensors. *Small* **2022**, *18*, No. 2203491.
(335) Yang, R.; Zhang, W.; Tiwari, N.; Yan, H.; Li, T.; Cheng, H. Multimodal Sensors with Decoupled Sensing Mechanisms. *Adv. Sci.* **2022**, *9*, No. 2202470.
(336) Wang, Y.; Xu, C.; Yu, X.; Zhang, H.; Han, M. Multilayer Flexible Electronics: Manufacturing Approaches and Applications. *Mater. Today Phys.* **2022**, *23*, 100647.
(337) Shi, J.; Dai, Y.; Cheng, Y.; Xie, S.; Li, G.; Liu, Y.; Wang, J.; Zhang, R.; Bai, N.; Cai, M.; et al. Embedment of Sensing Elements for Robust, Highly Sensitive, and Cross-Talk-Free Iontronic Skins for Robotics Applications. *Sci. Adv.* **2023**, *9*, No. eadf8831.
(338) Hwangbo, S.; Hu, L.; Hoang, A. T.; Choi, J. Y.; Ahn, J. H. Wafer-Scale Monolithic Integration of Full-Colour Micro-Led Display Using Mos(2) Transistor. *Nat. Nanotechnol.* **2022**, *17*, 500−506.
(339) Wazir, N.; Liu, R.; Ding, C.; Wang, X.; Ye, X.; Lingling, X.; Lu, T.; Wei, L.; Zou, B. Vertically Stacked Mose2/Moo2 Nanolayered Photodetectors with Tunable Photoresponses. *ACS Appl. Nano Mater.* **2020**, *3*, 7543−7553.
(340) Bo, R.; Nasiri, N.; Chen, H.; Caputo, D.; Fu, L.; Tricoli, A. Low-Voltage High-Performance Uv Photodetectors: An Interplay between Grain Boundaries and Debye Length. *ACS Appl. Mater. Interfaces.* **2017**, *9*, 2606−2615.
(341) Nasiri, N.; Bo, R.; Wang, F.; Fu, L.; Tricoli, A. Ultraporous Electron-Depleted Zno Nanoparticle Networks for Highly Sensitive Portable Visible-Blind Uv Photodetectors. *Adv. Mater.* **2015**, *27*, 4336−4343.
(342) Chen, H.; Bo, R.; Shrestha, A.; Xin, B.; Nasiri, N.; Zhou, J.; Di Bernardo, I.; Dodd, A.; Saunders, M.; Lipton-Duffin, J.; et al. Nio-Zno Nanoheterojunction Networks for Room-Temperature Volatile Organic Compounds Sensing. *Adv. Opt. Mater.* **2018**, *6*, 1800677.
(343) Nasiri, N.; Bo, R.; Chen, H.; White, T. P.; Fu, L.; Tricoli, A. Structural Engineering of Nano-Grain Boundaries for Low-Voltage Uv-Photodetectors with Gigantic Photo- to Dark-Current Ratios. *Adv. Opt. Mater.* **2016**, *4*, 1787−1795.
(344) Bo, R.; Taheri, M.; Liu, B.; Ricco, R.; Chen, H.; Amenitsch, H.; Fusco, Z.; Tsuzuki, T.; Yu, G.; Ameloot, R.; et al. Hierarchical Metal-Organic Framework Films with Controllable Meso/Macroporosity. *Adv. Sci.* **2020**, *7*, 2002368.
(345) Nasiri, N.; Bo, R.; Hung, T. F.; Roy, V. A. L.; Fu, L.; Tricoli, A. Tunable Band-Selective Uv-Photodetectors by 3d Self-Assembly of Heterogeneous Nanoparticle Networks. *Adv. Funct. Mater.* **2016**, *26*, 7359−7366.
(346) Fusco, Z.; Rahmani, M.; Bo, R.; Verre, R.; Motta, N.; Käll, M.; Neshev, D.; Tricoli, A. Nanostructured Dielectric Fractals on Resonant Plasmonic Metasurfaces for Selective and Sensitive Optical Sensing of Volatile Compounds. *Adv. Mater.* **2018**, *30*, 1800931.
(347) Chen, H.; Zhang, M.; Bo, R.; Barugkin, C.; Zheng, J.; Ma, Q.; Huang, S.; Ho-Baillie, A. W. Y.; Catchpole, K. R.; Tricoli, A. Superior Self-Powered Room-Temperature Chemical Sensing with Light-Activated Inorganic Halides Perovskites. *Small* **2018**, *14*, 1702571.
(348) Chen, H.; Zhang, M.; Fu, X.; Fusco, Z.; Bo, R.; Xing, B.; Nguyen, H. T.; Barugkin, C.; Zheng, J.; Lau, C. F. J.; et al. Light-Activated Inorganic Cspbbr2i Perovskite for Room-Temperature Self-Powered Chemical Sensing. *Phys. Chem. Chem. Phys.* **2019**, *21*, 24187−24193.
(349) Yang, L.; Liu, C.; Yuan, W.; Meng, C.; Dutta, A.; Chen, X.; Guo, L.; Niu, G.; Cheng, H. Fully Stretchable, Porous Mxene-Graphene Foam Nanocomposites for Energy Harvesting and Self-Powered Sensing. *Nano Energy* **2022**, *103*, 107807.
(350) Han, W. B.; Heo, S.-Y.; Kim, D.; Yang, S. M.; Ko, G.-J.; Lee, G. J.; Kim, D.-J.; Rajaram, K.; Lee, J. H.; Shin, J.-W.; et al. Zebra-Inspired Stretchable, Biodegradable Radiation Modulator for All-Day Sustainable Energy Harvesters. *Sci. Adv.* **2023**, *9*, No. eadf5883.
(351) Ko, J. H.; Kim, S. H.; Kim, M. S.; Heo, S. Y.; Yoo, Y. J.; Kim, Y. J.; Lee, H.; Song, Y. M. Lithography-Free, Large-Area Spatially Segmented Disordered Structure for Light Harvesting in Photovoltaic Modules. *ACS Appl. Mater. Interfaces.* **2022**, *14*, 44419−44428.
(352) Tran-Phu, T.; Fusco, Z.; Di Bernardo, I.; Lipton-Duffin, J.; Toe, C. Y.; Daiyan, R.; Gengenbach, T.; Lin, C.-H.; Bo, R.; Nguyen, H. T.; et al. Understanding the Role of Vanadium Vacancies in Bivo4 for Efficient Photoelectrochemical Water Oxidation. *Chem. Mater.* **2021**, *33*, 3553−3565.
(353) Tran-Phu, T.; Chen, H.; Bo, R.; Di Bernardo, I.; Fusco, Z.; Simonov, A. N.; Tricoli, A. High-Temperature One-Step Synthesis of Efficient Nanostructured Bismuth Vanadate Photoanodes for Water Oxidation. *Energy Technol.* **2019**, *7*, 1801052.
(354) Bo, R.; Zhang, F.; Bu, S.; Nasiri, N.; Di Bernardo, I.; Tran-Phu, T.; Shrestha, A.; Chen, H.; Taheri, M.; Qi, S.; et al. One-Step Synthesis of Porous Transparent Conductive Oxides by Hierarchical Self-Assembly of Aluminum-Doped Zno Nanoparticles. *ACS Appl. Mater. Interfaces.* **2020**, *12*, 9589−9599.
(355) Cheng, X.; Zhang, F.; Bo, R.; Shen, Z.; Pang, W.; Jin, T.; Song, H.; Xue, Z.; Zhang, Y. An Anti-Fatigue Design Strategy for 3d Ribbon-Shaped Flexible Electronics. *Adv. Mater.* **2021**, *33*, 2102684.
(356) Chen, H.; Zhang, M.; Xing, B.; Fu, X.; Bo, R.; Mulmudi, H. K.; Huang, S.; Ho-Baillie, A. W. Y.; Catchpole, K. R.; Tricoli, A. Superior Self-Charged and -Powered Chemical Sensing with High Performance for No2 Detection at Room Temperature. *Adv. Opt. Mater.* **2020**, *8*, 1901863.
(357) Guo, X.; Li, H.; Yeop Ahn, B.; Duoss, E. B.; Hsia, K. J.; Lewis, J. A.; Nuzzo, R. G. Two- and Three-Dimensional Folding of Thin Film Single-Crystalline Silicon for Photovoltaic Power Applications. *Proc. Natl. Acad. Sci. U.S.A.* **2009**, *106*, 20149−20154.
(358) Ling, Y.; Pang, W.; Liu, J.; Page, M.; Xu, Y.; Zhao, G.; Stalla, D.; Xie, J.; Zhang, Y.; Yan, Z. Bioinspired Elastomer Composites with Programmed Mechanical and Electrical Anisotropies. *Nat. Commun.* **2022**, *13*, 524.
(359) Xu, J.; Wu, H.-C.; Zhu, C.; Ehrlich, A.; Shaw, L.; Nikolka, M.; Wang, S.; Molina-Lopez, F.; Gu, X.; Luo, S.; et al. Multi-Scale Ordering in Highly Stretchable Polymer Semiconducting Films. *Nat. Mater.* **2019**, *18*, 594−601.
(360) Bai, Y.; Wang, H.; Xue, Y.; Pan, Y.; Kim, J.-T.; Ni, X.; Liu, T.-L.; Yang, Y.; Han, M.; Huang, Y.; et al. A Dynamically Reprogrammable Surface with Self-Evolving Shape Morphing. *Nature* **2022**, *609*, 701−708.
(361) Liu, Y.; He, K.; Chen, G.; Leow, W. R.; Chen, X. Nature-Inspired Structural Materials for Flexible Electronic Devices. *Chem. Rev.* **2017**, *117*, 12893−12941.
(362) Park, Y.; Chung, T. S.; Lee, G.; Rogers, J. A. Materials Chemistry of Neural Interface Technologies and Recent Advances in Three-Dimensional Systems. *Chem. Rev.* **2022**, *122*, 5277−5316.
(363) Min, J.; Tu, J.; Xu, C.; Lukas, H.; Shin, S.; Yang, Y.; Solomon, S. A.; Mukasa, D.; Gao, W. Skin-Interfaced Wearable Sweat Sensors for Precision Medicine. *Chem. Rev.* **2023**, *123*, 5049.

https://doi.org/10.1021/acs.chemrev.3c00335
Chem. Rev. 2023, 123, 11137−11189

(364) Choi, S.; Lee, H.; Ghaffari, R.; Hyeon, T.; Kim, D.-H. Recent Advances in Flexible and Stretchable Bio-Electronic Devices Integrated with Nanomaterials. *Adv. Mater.* **2016**, *28*, 4203−4218.
(365) Li, J.; Esteban-Fernandez de Avila, B.; Gao, W.; Zhang, L.; Wang, J. Micro/Nanorobots for Biomedicine: Delivery, Surgery, Sensing, and Detoxification. *Sci. Robot.* **2017**, *2*, No. eaam6431.
(366) Ning, X.; Wang, X.; Zhang, Y.; Yu, X.; Choi, D.; Zheng, N.; Kim, D. S.; Huang, Y.; Zhang, Y.; Rogers, J. A. Assembly of Advanced Materials into 3d Functional Structures by Methods Inspired by Origami and Kirigami: A Review. *Adv. Mater. Interfaces* **2018**, *5*, 1800284.
(367) Cohen-Karni, T.; Qing, Q.; Li, Q.; Fang, Y.; Lieber, C. M. Graphene and Nanowire Transistors for Cellular Interfaces and Electrical Recording. *Nano Lett.* **2010**, *10*, 1098−1102.
(368) Tian, B.; Cohen-Karni, T.; Qing, Q.; Duan, X.; Xie, P.; Lieber, C. M. Three-Dimensional, Flexible Nanoscale Field-Effect Transistors as Localized Bioprobes. *Science* **2010**, *329*, 830−834.
(369) Huang, G.; Mei, Y.; Thurmer, D. J.; Coric, E.; Schmidt, O. G. Rolled-up Transparent Microtubes as Two-Dimensionally Confined Culture Scaffolds of Individual Yeast Cells. *Lab Chip* **2009**, *9*, 263−268.
(370) Xi, W.; Schmidt, C. K.; Sanchez, S.; Gracias, D. H.; Carazo-Salas, R. E.; Jackson, S. P.; Schmidt, O. G. Rolled-up Functionalized Nanomembranes as Three-Dimensional Cavities for Single Cell Studies. *Nano Lett.* **2014**, *14*, 4197−4204.
(371) Duan, X.; Gao, R.; Xie, P.; Cohen-Karni, T.; Qing, Q.; Choe, H. S.; Tian, B.; Jiang, X.; Lieber, C. M. Intracellular Recordings of Action Potentials by an Extracellular Nanoscale Field-Effect Transistor. *Nat. Nanotechnol.* **2012**, *7*, 174−179.
(372) Fusco, Z.; Bo, R.; Wang, Y.; Motta, N.; Chen, H.; Tricoli, A. Self-Assembly of Au Nano-Islands with Tuneable Organized Disorder for Highly Sensitive Sers. *J. Mater. Chem. C* **2019**, *7*, 6308−6316.
(373) Egunov, A. I.; Dou, Z.; Karnaushenko, D. D.; Hebenstreit, F.; Kretschmann, N.; Akgün, K.; Ziemssen, T.; Karnaushenko, D.; Medina-Sánchez, M.; Schmidt, O. G. Impedimetric Microfluidic Sensor-in-a-Tube for Label-Free Immune Cell Analysis. *Small* **2021**, *17*, 2002549.
(374) Jin, Q.; Bhatta, A.; Pagaduan, J. V.; Chen, X.; West-Foyle, H.; Liu, J.; Hou, A.; Berkowitz, D.; Kuo, S. C.; Askin, F. B.; et al. Biomimetic Human Small Muscular Pulmonary Arteries. *Sci. Adv.* **2020**, *6*, No. eaaz2598.
(375) Herzer, R.; Gebert, A.; Hempel, U.; Hebenstreit, F.; Oswald, S.; Damm, C.; Schmidt, O. G.; Medina-Sánchez, M. Rolled-up Metal Oxide Microscaffolds to Study Early Bone Formation at Single Cell Resolution. *Small* **2021**, *17*, 2005527.
(376) Park, J.; Kalinin, Y. V.; Kadam, S.; Randall, C. L.; Gracias, D. H. Design for a Lithographically Patterned Bioartificial Endocrine Pancreas. *Artif. Organs* **2013**, *37*, 1059−1067.
(377) Kim, S. J.; Cho, K. W.; Cho, H. R.; Wang, L.; Park, S. Y.; Lee, S. E.; Hyeon, T.; Lu, N.; Choi, S. H.; Kim, D.-H. Stretchable and Transparent Biointerface Using Cell-Sheet-Graphene Hybrid for Electrophysiology and Therapy of Skeletal Muscle. *Adv. Funct. Mater.* **2016**, *26*, 3207−3217.
(378) Kwak, J. W.; Han, M.; Xie, Z.; Chung, H. U.; Lee, J. Y.; Avila, R.; Yohay, J.; Chen, X.; Liang, C.; Patel, M.; et al. Wireless Sensors for Continuous, Multimodal Measurements at the Skin Interface with Lower Limb Prostheses. *Sci. Transl. Med.* **2020**, *12*, No. eabc4327.
(379) Guan, Y.-S.; Ershad, F.; Rao, Z.; Ke, Z.; da Costa, E. C.; Xiang, Q.; Lu, Y.; Wang, X.; Mei, J.; Vanderslice, P.; et al. Elastic Electronics Based on Micromesh-Structured Rubbery Semiconductor Films. *Nat. Electron.* **2022**, *5*, 881−892.
(380) Kim, B.; Soepriatna, A. H.; Park, W.; Moon, H.; Cox, A.; Zhao, J.; Gupta, N. S.; Park, C. H.; Kim, K.; Jeon, Y.; et al. Rapid Custom Prototyping of Soft Poroelastic Biosensor for Simultaneous Epicardial Recording and Imaging. *Nat. Commun.* **2021**, *12*, 3710.
(381) Wang, Y.; Li, X.; Fan, S.; Feng, X.; Cao, K.; Ge, Q.; Gao, L.; Lu, Y. Three-Dimensional Stretchable Microelectronics by Projection Microstereolithography (Pμsl). *ACS Appl. Mater. Interfaces.* **2021**, *13*, 8901−8908.
(382) Bang, J.; Ahn, J.; Zhang, J.; Ko, T. H.; Park, B.; Lee, Y. M.; Jung, B. K.; Lee, S. Y.; Ok, J.; Kim, B. H.; et al. Stretchable and Directly Patternable Double-Layer Structure Electrodes with Complete Coverage. *ACS Nano* **2022**, *16*, 12134−12144.
(383) Kang, M.; Jeong, H.; Park, S.-W.; Hong, J.; Lee, H.; Chae, Y.; Yang, S.; Ahn, J.-H. Wireless Graphene-Based Thermal Patch for Obtaining Temperature Distribution and Performing Thermography. *Sci. Adv.* **2022**, *8*, No. eabm6693.
(384) Dutta, A.; Cheng, H. Pathway of Transient Electronics Towards Connected Biomedical Applications. *Nanoscale* **2023**, *15*, 4236−4249.
(385) Xu, H.; Medina-Sanchez, M.; Magdanz, V.; Schwarz, L.; Hebenstreit, F.; Schmidt, O. G. Sperm-Hybrid Micromotor for Targeted Drug Delivery. *ACS Nano* **2018**, *12*, 327−337.
(386) Wu, Z.; Chen, Y.; Mukasa, D.; Pak, O. S.; Gao, W. Medical Micro/Nanorobots in Complex Media. *Chem. Soc. Rev.* **2020**, *49*, 8088−8112.
(387) Park, W.; Nguyen, V. P.; Jeon, Y.; Kim, B.; Li, Y.; Yi, J.; Kim, H.; Leem, J. W.; Kim, Y. L.; Kim, D. R.; et al. Biodegradable Silicon Nanoneedles for Ocular Drug Delivery. *Sci. Adv.* **2022**, *8*, No. eabn1772.
(388) Reeder, J. T.; Xie, Z.; Yang, Q.; Seo, M.-H.; Yan, Y.; Deng, Y.; Jinkins, K. R.; Krishnan, S. R.; Liu, C.; McKay, S.; et al. Soft, Bioresorbable Coolers for Reversible Conduction Block of Peripheral Nerves. *Science* **2022**, *377*, 109−115.
(389) Song, E.; Li, J.; Won, S. M.; Bai, W.; Rogers, J. A. Materials for Flexible Bioelectronic Systems as Chronic Neural Interfaces. *Nat. Mater.* **2020**, *19*, 590−603.
(390) Kim, K.; Kim, H. J.; Zhang, H.; Park, W.; Meyer, D.; Kim, M. K.; Kim, B.; Park, H.; Xu, B.; Kollbaum, P.; et al. All-Printed Stretchable Corneal Sensor on Soft Contact Lenses for Noninvasive and Painless Ocular Electrodiagnosis. *Nat. Commun.* **2021**, *12*, 1544.
(391) Theocharidis, G.; Yuk, H.; Roh, H.; Wang, L.; Mezghani, I.; Wu, J.; Kafanas, A.; Contreras, M.; Sumpio, B.; Li, Z.; et al. A Strain-Programmed Patch for the Healing of Diabetic Wounds. *Nat. Biomed. Eng.* **2022**, *6*, 1118−1133.
(392) Zhang, J.; Kim, K.; Kim, H. J.; Meyer, D.; Park, W.; Lee, S. A.; Dai, Y.; Kim, B.; Moon, H.; Shah, J. V.; et al. Smart Soft Contact Lenses for Continuous 24-h Monitoring of Intraocular Pressure in Glaucoma Care. *Nat. Commun.* **2022**, *13*, 5518.
(393) Kim, S.; Oh, Y. S.; Lee, K.; Kim, S.; Maeng, W.-Y.; Kim, K. S.; Kim, G.-B.; Cho, S.; Han, H.; Park, H.; et al. Battery-Free, Wireless, Cuff-Type, Multimodal Physical Sensor for Continuous Temperature and Strain Monitoring of Nerve. *Small* **2023**, *19*, 2206839.
(394) Barbot, A.; Tan, H.; Power, M.; Seichepine, F.; Yang, G.-Z. Floating Magnetic Microrobots for Fiber Functionalization. *Sci. Robot.* **2019**, *4*, No. eaax8336.
(395) Rivkin, B.; Becker, C.; Singh, B.; Aziz, A.; Akbar, F.; Egunov, A.; Karnaushenko, D. D.; Naumann, R.; Schäfer, R.; Medina-Sánchez, M.; et al. Electronically Integrated Microcatheters Based on Self-Assembling Polymer Films. *Sci. Adv.* **2021**, *7*, No. eabl5408.
(396) Heng, W.; Solomon, S.; Gao, W. Flexible Electronics and Devices as Human-Machine Interfaces for Medical Robotics. *Adv. Mater.* **2022**, *34*, No. 2107902.
(397) Chang, T.; Akin, S.; Kim, M. K.; Murray, L.; Kim, B.; Cho, S.; Huh, S.; Teke, S.; Couetil, L.; Jun, M. B.; et al. A Programmable Dual-Regime Spray for Large-Scale and Custom-Designed Electronic Textiles. *Adv. Mater.* **2022**, *34*, No. 2108021.
(398) Zhou, C.; Yang, Y.; Wang, J.; Wu, Q.; Gu, Z.; Zhou, Y.; Liu, X.; Yang, Y.; Tang, H.; Ling, Q.; et al. Ferromagnetic Soft Catheter Robots for Minimally Invasive Bioprinting. *Nat. Commun.* **2021**, *12*, 5072.
(399) Yang, Y.; Wang, J.; Wang, L.; Wu, Q.; Ling, L.; Yang, Y.; Ning, S.; Xie, Y.; Cao, Q.; Li, L.; et al. Magnetic Soft Robotic Bladder for Assisted Urination. *Sci. Adv.* **2022**, *8*, No. eabq1456.
(400) Wang, L.; Kim, Y.; Guo, C. F.; Zhao, X. Hard-Magnetic Elastica. *J. Mech. Phys. Solids* **2020**, *142*, 104045.
(401) Wang, L.; Zheng, D.; Harker, P.; Patel, A. B.; Guo, C. F.; Zhao, X. Evolutionary Design of Magnetic Soft Continuum Robots. *Proc. Natl. Acad. Sci. U. S. A.* **2021**, *118*, No. e2021922118.
(402) Shao, L.-H.; Qu, X.; Wang, T.; Cui, Z.; Liu, Y.; Zhu, Y. Interfacial Shear Stress Transfer between Elastoplastic Fiber and Elastic Matrix. *J. Mech. Phys. Solids* **2023**, *173*, 105218.

(403) Zhang, L.; Zhang, Z.; Weisbecker, H.; Yin, H.; Liu, Y.; Han, T.; Guo, Z.; Berry, M.; Yang, B.; Guo, X.; et al. 3d Morphable Systems Via Deterministic Microfolding for Vibrational Sensing, Robotic Implants, and Reconfigurable Telecommunication. *Sci. Adv.* **2022**, *8*, No. eade0838.
(404) Chen, X.; Jian, W.; Wang, Z.; Ai, J.; Kang, Y.; Sun, P.; Wang, Z.; Ma, Y.; Wang, H.; Chen, Y.; et al. Wrap-Like Transfer Printing for Three-Dimensional Curvy Electronics. *Sci. Adv.* **2023**, *9*, No. eadi0357.
(405) Huber, R.; Kern, F.; Karnaushenko, D. D.; Eisner, E.; Lepucki, P.; Thampi, A.; Mirhajivarzaneh, A.; Becker, C.; Kang, T.; Baunack, S.; et al. Tailoring Electron Beams with High-Frequency Self-Assembled Magnetic Charged Particle Micro Optics. *Nat. Commun.* **2022**, *13*, 3220.
(406) Becker, C.; Karnaushenko, D.; Kang, T.; Karnaushenko, D. D.; Faghih, M.; Mirhajivarzaneh, A.; Schmidt, O. G. Self-Assembly of Highly Sensitive 3d Magnetic Field Vector Angular Encoders. *Sci. Adv.* **2019**, *5*, No. eaay7459.
(407) Huang, W.; Yang, Z.; Kraman, M. D.; Wang, Q.; Ou, Z.; Rojo, M. M.; Yalamarthy, A. S.; Chen, V.; Lian, F.; Ni, J. H.; et al. Monolithic Mtesla-Level Magnetic Induction by Self-Rolled-up Membrane Technology. *Sci. Adv.* **2020**, *6*, No. eaay4508.
(408) Lepucki, P.; Egunov, A. I.; Rosenkranz, M.; Huber, R.; Mirhajivarzaneh, A.; Karnaushenko, D. D.; Dioguardi, A. P.; Karnaushenko, D.; Büchner, B.; Schmidt, O. G.; et al. Self-Assembled Rolled-up Microcoils for Nl Microfluidics Nmr Spectroscopy. *Adv. Mater. Technol.* **2021**, *6*, 2000679.
(409) Bermúdez Ureña, E.; Mei, Y.; Coric, E.; Makarov, D.; Albrecht, M.; Schmidt, O. G. Fabrication of Ferromagnetic Rolled-up Microtubes for Magnetic Sensors on Fluids. *J. Phys. D: Appl. Phys.* **2009**, *42*, 055001.
(410) Kim, T.; Price, J. S.; Grede, A.; Lee, S.; Choi, G.; Guan, W.; Jackson, T. N.; Giebink, N. C. Kirigami-Inspired 3d Organic Light-Emitting Diode (Oled) Lighting Concepts. *Adv. Mater. Technol.* **2018**, *3*, 1800067.
(411) Ju, H.; Park, H.; Kim, N.; Lim, J.; Jung, D.; Lee, J. A Locally Actuatable Soft Robotic Film for Actively Reconfiguring Shapes of Flexible Electronics. *Soft Robot.* **2022**, *9*, 767−775.
(412) Lee, Y.; Kim, B. J.; Hu, L.; Hong, J.; Ahn, J.-H. Morphable 3d Structure for Stretchable Display. *Mater. Today* **2022**, *53*, 51−57.
(413) Oh, S.; Lee, S.; Byun, S. H.; Lee, S.; Kim, C. Y.; Yea, J.; Chung, S.; Li, S.; Jang, K. I.; Kang, J.; et al. 3d Shape-Morphing Display Enabled by Electrothermally Responsive, Stiffness-Tunable Liquid Metal Platform with Stretchable Electroluminescent Device. *Adv. Funct. Mater.* **2023**. DOI: 10.1002/adfm.202214766
(414) Deng, Y.; Liu, W.; Cheung, Y. K.; Li, Y.; Hong, W.; Yu, H. Curved Display Based on Programming Origami Tessellations. *Microsyst. Nanoeng.* **2021**, *7*, 101.
(415) Song, J. K.; Kim, J.; Yoon, J.; Koo, J. H.; Jung, H.; Kang, K.; Sunwoo, S. H.; Yoo, S.; Chang, H.; Jo, J.; et al. Stretchable Colour-Sensitive Quantum Dot Nanocomposites for Shape-Tunable Multiplexed Phototransistor Arrays. *Nat. Nanotechnol.* **2022**, *17*, 849−856.
(416) Zhang, Q.; Xu, M.; Zhou, L.; Liu, S.; Wang, W.; Zhang, L.; Xie, W.; Yu, C. A Flexible Organic Mechanoluminophore Device. *Nat. Commun.* **2023**, *14*, 1257.
(417) Nasiri, N.; Bo, R.; Fu, L.; Tricoli, A. Three-Dimensional Nano-Heterojunction Networks: A Highly Performing Structure for Fast Visible-Blind Uv Photodetectors. *Nanoscale* **2017**, *9*, 2059−2067.
(418) Kang, J.; Yoo, Y. J.; Ko, J. H.; Mahmud, A. A.; Song, Y. M. Trilayered Gires-Tournois Resonator with Ultrasensitive Slow-Light Condition for Colorimetric Detection of Bioparticles. *Nanomaterials* **2023**, *13*, 319.
(419) Gao, L.; Zhang, Y.; Zhang, H.; Doshay, S.; Xie, X.; Luo, H.; Shah, D.; Shi, Y.; Xu, S.; Fang, H.; et al. Optics and Nonlinear Buckling Mechanics in Large-Area, Highly Stretchable Arrays of Plasmonic Nanostructures. *ACS Nano* **2015**, *9*, 5968−5975.
(420) Li, T.; Hantusch, M.; Qu, J.; Bandari, V. K.; Knupfer, M.; Zhu, F.; Schmidt, O. G. On-Chip Integrated Process-Programmable Sub-10 Nm Thick Molecular Devices Switching between Photomultiplication and Memristive Behaviour. *Nat. Commun.* **2022**, *13*, 2875.
(421) Wang, Y.; Zhou, W.; Cao, K.; Hu, X.; Gao, L.; Lu, Y. Architectured Graphene and Its Composites: Manufacturing and Structural Applications. *Compos. Part A Appl. Sci. Manuf.* **2021**, *140*, 106177.
(422) Ko, J. H.; Yoo, Y. J.; Lee, Y.; Jeong, H.-H.; Song, Y. M. A Review of Tunable Photonics: Optically Active Materials and Applications from Visible to Terahertz. *iScience* **2022**, *25*, 104727.
(423) Chen, S.; Liu, Z.; Du, H.; Tang, C.; Ji, C.-Y.; Quan, B.; Pan, R.; Yang, L.; Li, X.; Gu, C.; et al. Electromechanically Reconfigurable Optical Nano-Kirigami. *Nat. Commun.* **2021**, *12*, 1299.
(424) Liao, F.; Zhou, Z.; Kim, B. J.; Chen, J.; Wang, J.; Wan, T.; Zhou, Y.; Hoang, A. T.; Wang, C.; Kang, J.; et al. Bioinspired in-Sensor Visual Adaptation for Accurate Perception. *Nat. Electron.* **2022**, *5*, 84−91.
(425) Huang, C. C.; Wu, X.; Liu, H.; Aldalali, B.; Rogers, J. A.; Jiang, H. Large-Field-of-View Wide-Spectrum Artificial Reflecting Superposition Compound Eyes. *Small* **2014**, *10*, 3050−3057.
(426) Kim, M.; Lee, G. J.; Choi, C.; Kim, M. S.; Lee, M.; Liu, S.; Cho, K. W.; Kim, H. M.; Cho, H.; Choi, M. K.; et al. An Aquatic-Vision-Inspired Camera Based on a Monocentric Lens and a Silicon Nanorod Photodiode Array. *Nat. Electron.* **2020**, *3*, 546−553.
(427) Kim, M.; Chang, S.; Kim, M.; Yeo, J.-E.; Kim, M. S.; Lee, G. J.; Kim, D.-H.; Song, Y. M. Cuttlefish Eye-Inspired Artificial Vision for High-Quality Imaging under Uneven Illumination Conditions. *Sci. Robot.* **2023**, *8*, No. eade4698.
(428) Singh, D.; Kutbee, A. T.; Ghoneim, M. T.; Hussain, A. M.; Hussain, M. M. Strain-Induced Rolled Thin Films for Lightweight Tubular Thermoelectric Generators. *Adv. Mater. Technol.* **2018**, *3*, 1700192.
(429) Li, Y.; Qu, J.; Li, F.; Qu, Z.; Tang, H.; Liu, L.; Zhu, M.; Schmidt, O. G. Advanced Architecture Designs Towards High-Performance 3d Microbatteries. *Nano Matter. Sci.* **2021**, *3*, 140−153.
(430) Liu, L.; Huang, S.; Shi, W.; Sun, X.; Pang, J.; Lu, Q.; Yang, Y.; Xi, L.; Deng, L.; Oswald, S.; et al. Single "Swiss-Roll" Microelectrode Elucidates the Critical Role of Iron Substitution in Conversion-Type Oxides. *Sci. Adv.* **2022**, *8*, No. eadd6596.
(431) Liu, B.; Bo, R.; Taheri, M.; Di Bernardo, I.; Motta, N.; Chen, H.; Tsuzuki, T.; Yu, G.; Tricoli, A. Metal-Organic Frameworks/Conducting Polymer Hydrogel Integrated Three-Dimensional Free-Standing Monoliths as Ultrahigh Loading Li-S Battery Electrodes. *Nano Lett.* **2019**, *19*, 4391−4399.
(432) Li, F.; Wang, J.; Liu, L.; Qu, J.; Li, Y.; Bandari, V. K.; Karnaushenko, D.; Becker, C.; Faghih, M.; Kang, T.; et al. Self-Assembled Flexible and Integratable 3d Microtubular Asymmetric Supercapacitors. *Adv. Sci.* **2019**, *6*, 1901051.
(433) Gao, L.; Wang, Y.; Hu, X.; Zhou, W.; Cao, K.; Wang, Y.; Wang, W.; Lu, Y. Cellular Carbon-Film-Based Flexible Sensor and Waterproof Supercapacitors. *ACS Appl. Mater. Interfaces.* **2019**, *11*, 26288−26297.
(434) Shi, J.; Wang, L.; Dai, Z.; Zhao, L.; Du, M.; Li, H.; Fang, Y. Multiscale Hierarchical Design of a Flexible Piezoresistive Pressure Sensor with High Sensitivity and Wide Linearity Range. *Small* **2018**, *14*, 1800819.
(435) Xu, H.; Gao, L.; Wang, Y.; Cao, K.; Hu, X.; Wang, L.; Mu, M.; Liu, M.; Zhang, H.; Wang, W.; et al. Flexible Waterproof Piezoresistive Pressure Sensors with Wide Linear Working Range Based on Conductive Fabrics. *Nano-Micro Lett.* **2020**, *12*, 159.
(436) Zhao, J.; Li, W.; Guo, X.; Wang, H.; Rogers, J. A.; Huang, Y. Theoretical Modeling of Tunable Vibrations of Three-Dimensional Serpentine Structures for Simultaneous Measurement of Adherent Cell Mass and Modulus. *MRS Bull.* **2021**, *46*, 107−114.
(437) Zhao, J.; Zhang, F.; Guo, X.; Huang, Y.; Zhang, Y.; Wang, H. Torsional Deformation Dominated Buckling of Serpentine Structures to Form Three-Dimensional Architectures with Ultra-Low Rigidity. *J. Mech. Phys. Solids* **2021**, *155*, 104568.
(438) Zhao, J. Postbuckling Analysis of Ultra-Low Rigidity Serpentine Structures. *J. Appl. Mech.* **2022**, *89*. DOI: 10.1115/1.4053397
(439) Yang, L.; Wang, Z.; Wang, H.; Jin, B.; Meng, C.; Chen, X.; Li, R.; Wang, H.; Xin, M.; Zhao, Z.; et al. Self-Healing, Reconfigurable, Thermal-Switching, Transformative Electronics for Health Monitoring. *Adv. Mater.* **2023**, *35*, No. 2207742.

(440) Mohanty, S.; Jin, Q.; Furtado, G. P.; Ghosh, A.; Pahapale, G.; Khalil, I. S. M.; Gracias, D. H.; Misra, S. Bidirectional Propulsion of Arc-Shaped Microswimmers Driven by Precessing Magnetic Fields. *Adv. Intell. Syst.* **2020**, *2*, 2000064.
(441) Miskin, M. Z.; Cortese, A. J.; Dorsey, K.; Esposito, E. P.; Reynolds, M. F.; Liu, Q.; Cao, M.; Muller, D. A.; McEuen, P. L.; Cohen, I. Electronically Integrated, Mass-Manufactured, Microscopic Robots. *Nature* **2020**, *584*, 557−561.
(442) Mao, G.; Schiller, D.; Danninger, D.; Hailegnaw, B.; Hartmann, F.; Stockinger, T.; Drack, M.; Arnold, N.; Kaltenbrunner, M. Ultrafast Small-Scale Soft Electromagnetic Robots. *Nat. Commun.* **2022**, *13*, 4456.
(443) Yi, S.; Wang, L.; Chen, Z.; Wang, J.; Song, X.; Liu, P.; Zhang, Y.; Luo, Q.; Peng, L.; Wu, Z.; et al. High-Throughput Fabrication of Soft Magneto-Origami Machines. *Nat. Commun.* **2022**, *13*, 4177.
(444) Liu, Q.; Shen, Z.; Liu, Z.; Shuai, Y.; Lv, Z.; Jin, T.; Cheng, X.; Zhang, Y. Probability-Based Analyses of the Snap-through in Cage-Shaped Mesostructures under out-of-Plane Compressions. *Acta Mech. Solida Sin* **2023**, *36*, 569−581.
(445) Yan, D.; Chang, J.; Zhang, H.; Liu, J.; Song, H.; Xue, Z.; Zhang, F.; Zhang, Y. Soft Three-Dimensional Network Materials with Rational Bio-Mimetic Designs. *Nat. Commun.* **2020**, *11*, 1180.
(446) Ma, Q.; Cheng, H.; Jang, K. I.; Luan, H.; Hwang, K. C.; Rogers, J. A.; Huang, Y.; Zhang, Y. A Nonlinear Mechanics Model of Bio-Inspired Hierarchical Lattice Materials Consisting of Horseshoe Microstructures. *J. Mech. Phys. Solids* **2016**, *90*, 179−202.
(447) Liu, J.; Yan, D.; Zhang, Y. Mechanics of Unusual Soft Network Materials with Rotatable Structural Nodes. *J. Mech. Phys. Solids* **2021**, *146*, 104210.

https://doi.org/10.1021/acs.chemrev.3c00335
Chem. Rev. 2023, 123, 11137−11189